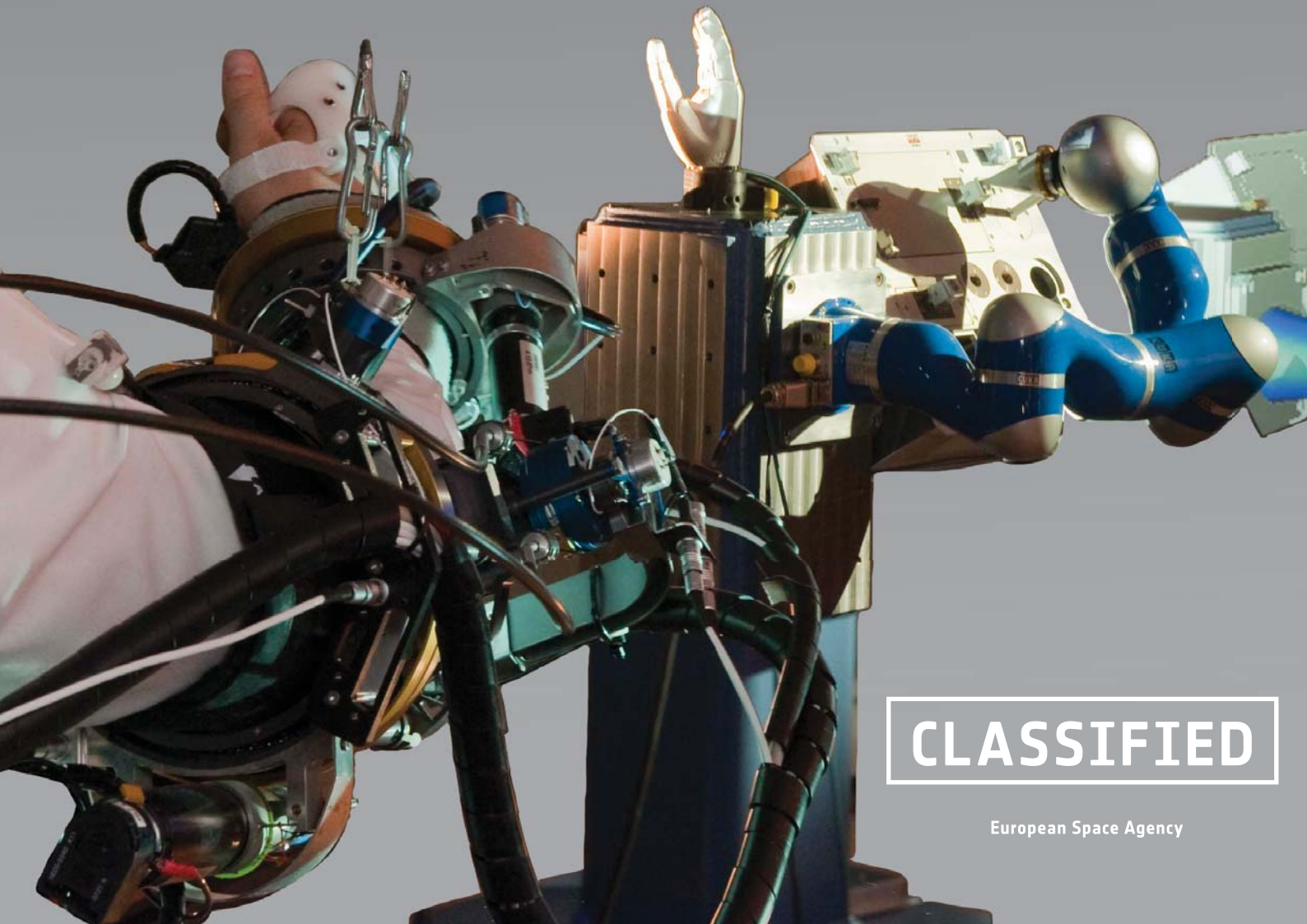


→ **THE DEVELOPMENT OF AN
EFFICIENT GRASP MASTER
FOR SPACE ROBOTICS
TELEOPERATION**

MSc Thesis - F.P.J. van der Hulst



CLASSIFIED

The Development of an Efficient Grasp Master for Space Robotics Teleoperation

Frank P. J. van der Hulst

This document and the information contained is confidential in nature and proprietary to ESA. This information shall not be disclosed by any means. Circulation is limited to the members of the graduation committee, who signed a non-disclosure agreement (NDA).

The Development of an Efficient Grasp Master for Space Robotics Teleoperation

MSc Thesis

by

Frank P. J. van der Hulst

Biomechanical Engineering Department (BmechE),
Faculty of Mechanical, Maritime and Materials Engineering,
Delft University of Technology

July 10, 2012

Graduation committee:

Prof. Dr. F. C. T. van der Helm
Biomechanical Engineering Department (BmechE),
Faculty of Mechanical, Maritime and Materials Engineering,
Delft University of Technology

Dr. Ing. A. Schiele
Biomechanical Engineering Department (BmechE),
Faculty of Mechanical, Maritime and Materials Engineering,
Delft University of Technology
& Telerobotics and Haptics Laboratory,
ESA/ESTEC European Space Agency

Prof. Ir. R.H. Munnig Schmidt
Mechatronic Systems Design,
Precision and Microsystems Engineering Department (PME),
Faculty of Mechanical, Maritime and Materials Engineering,
Delft University of Technology

EUROPEAN SPACE AGENCY
NON-DISCLOSURE AGREEMENT

The following information to be provided by ESA in the frame of activities related to technical collaboration, exchange of information, briefings, tender actions, contract negotiations, etc.

An Efficient Grasp Master for Space Robotics Teleoperation

is commercial in confidence in nature and proprietary to ESA.

The party receiving such information (hereinafter called the "Receiver"), identified as (firm name, address):

commits itself as follows:

1. For the purpose of carrying out work in the frame of the above activities, the Receiver agrees that all information whether patented or not, graphics, technological information whether written or not, and technical data owned or developed by ESA, shall be treated as sensitive and commercial in confidence.
2. The Receiver hereto further agrees:
 - a) not to make any claims or attempts to claim any right on or into Proprietary information disclosed in the execution of said activities;
 - b) that such Proprietary information be used only for the specific purpose of work related to said activities;
 - c) not to disclose information or provide copies to any legal or natural person or entity other than the Receiver, and to keep the circulation restricted to those persons directly involved in said activities after prior authorisation in writing from ESA;
 - d) to consult and involve ESA in case any follow-on claims of intellectual property rights result from said activities.

Read and agreed

Date.....

Signed on behalf of Receiver

Abstract

This thesis reports on the development of an efficient grasp master for space robotics teleoperation. This master device will complement the X-Arm-2 [1] in both its function and philosophy. It should provide the hand and fingers with sensing and feedback functions, enabling bilateral teleoperation of various types of robotic end-effectors to perform a wide range of tasks. Just as the X-Arm-2, the hand master should be easy to use by various operators without requiring adjustments.

Up to this point in time, some tens of grasp masters have been reported in literature. Analysis of the state of the art shows issues that limit the use of these devices in combination with haptic arm masters. Two important factors in this are device placement w.r.t. the operator and structural complexity. Common issues from device placement are arm coverage by actuators and arm workspace limitation by external transmissions or fixed-base designs. Common issues involved with structural complexity result from the use of extensive structures to provide accurate control over force magnitude and direction on possibly multiple positions per finger. In practice these designs are expensive in terms of mass, volume and number of components, leading to bulky designs that are uncomfortable and subject to mechanical losses.

Because of the previous reasons, the device efficiency, defined as the user- and device performance achieved with respect to the resources expended, appears to be generally too low.

It is the goal of this work to present on the development of an efficiency grasp master device that can be used by various operators in space robotics teleoperation without requiring device adjustments. Subgoals involve achieving a structurally simple design with a minimal amount of degrees of freedom (DOFs) that provides sufficient feedback during bilateral control. For the reduction of DOFs, control and feedback functions have been separated. Furthermore, the device has been designed to allow operating different slaves various kinematic structures and different control architectures.

By following a human-centric design approach, considering relevant space operation tasks, required operator grasp types, and psychophysical effects, a reduction of the required number of DOFs of a possible master was achieved. In combination with the separation of control and feedback channels this can constitute an efficient device concept and was elaborated into a detailed prototype design in this work.

As a tool in the design of device geometry and workspace verification, an adaptable kinematic human hand model was constructed. This model is based on human functional anatomy and is adaptable to various real human hand sizes. This was achieved by exploiting body proportions to derive finger segment

lengths from the hand length.

A partial hand model validation, involving index- and middle finger validation using a group of subjects, indicates that the use of body proportions offers a good estimate of finger length from a given hand length. Model estimated fingertip positions over a motion trajectory remain within reasonable limits when compared with experimental data for this subject group.

The developed hand model was applied in the verification of grasp master workspace. This showed robustness against hand size variation from the 5th female- till 95th male percentile.

Verification by analysis and simulation showed that key human factors- and performance requirements can be met. For the verification of device efficiency w.r.t different existing grasp masters, the use of device efficiency indicators was proposed and demonstrated. This indicates that the detailed prototype design is relatively efficient w.r.t. other compared devices based on slave controllability, slave observability, and the quality of the reflected force.

The proposed prototype design will be manufactured to enable further verification by testing and validation of real user interaction.

Thesis Outline

This thesis starts with an introduction to bilateral teleoperation in this chapter (Section. 1.1) and its application in space robotics (Section. 1.2). An overview of the state of the art (Section. 1.3) of haptic grasp master devices reveals the problem that existing hand haptic devices in general are expensive in terms of resources and/or show limited device and user performance, indicating that the efficiency of existing devices is generally too low (Section. 1.4). The goal of this thesis (Section. 1.5) is to develop an efficient generic grasp master device that can be used by operators with varying hand sizes in space robotics teleoperation without requiring device adjustments. This goal is achieved (Section. 1.6) by following a human-centric design approach based on separation of control and feedback functions. The thesis is concluded by the development of a device prototype design and its verification by analysis and simulation.

A realistic human hand model, easily adaptable to different hand sizes, was constructed as a tool for the design and verification of ergonomic geometry, workspace, and robustness against hand-size variation. The kinematic model was published in: *A Functional Anatomy Based Kinematic Human Hand Model with Simple Size Adaptation (IEEE/ICRA 2012)* (Chapter. 2).

The development of the grasp master device by using a human-centric design approach is described in: *An Efficient Grasp Master for Space Robotics Teleoperation* (Chapter. 3). This summarizes the relevant operation background, formulates the device concept, and reports the detailed prototype design and its verification.

The conclusions on the achieved results and the planned continuation of this development have been included in Chapter. 4.

All references have been combined inside a single bibliography at the end of this thesis. For this reason, the lists of references of the papers in Chapter. 2 and 3 have been removed and the numbering of references in these papers has been updated to correspond to the full bibliography of the thesis. The references from Annex. C have not been combined into the overall bibliography.

Additional technical details on the prototype design have been included in Annex. A. The CAD drawings of the custom mechanical components of the proposed prototype design are contained in Annex. B. The initial literature survey of development guidelines on the design of a simple grasp master for space robotics teleoperation is given in Annex. C, this is technically not part of this thesis.

Contents

Abstract	vii
Thesis Outline	ix
Contents	xi
1 Introduction	1
1.1 Bilateral Teleoperation	1
1.2 Space Robotics Teleoperation	2
1.3 State of the Art - Grasp Masters	4
1.3.1 Arm Coverage	4
1.3.2 External Actuators	4
1.3.3 Fixed Base	5
1.3.4 Mechanisms with a Remote Centre of Motion	5
1.3.5 Devices with Passive Joints	6
1.3.6 Compact Design	6
1.3.7 Commercial Devices	7
1.4 Problem Statement	8
1.4.1 Device Placement w.r.t. the User	8
1.4.2 Structural Complexity	9
1.4.3 Device Efficiency	9
1.5 Goal	9
1.6 Approach	10
2 A Functional Anatomy Based Kinematic Human Hand Model with Simple Size Adaptation	13
<i>Published in IEEE/ICRA 2012</i>	
3 From Concept to Detailed Design and Verification: An Efficient Grasp Master for Space Robotics Teleoperation	23
4 Conclusions	41
Bibliography	43
Annexes	49
A Design Details: Human Factors, Modelling, and Simulation	49

A.1	Human Factors Details	50
A.1.1	Finger Force Range	50
A.1.2	Finger Force JND	50
A.1.3	Finger Joint Range	51
A.2	Hand Model Joint Limits	53
A.3	Torque Propagation Modelling	55
A.4	Lower Lever Interaction Force Simulation	57
A.5	Motor Thermal Behaviour Simulation	59
B	Prototype CAD Drawings	61
C	Literature Survey	83

Chapter 1

Introduction

With the recent arrival of NASA's Robonaut 2 [2] on board of the International Space Station (ISS), the first humanoid robot in space is a fact, emphasising that the field of space robotics is more alive than ever. The availability of advanced robotic systems in space comes with the need for appropriate means of control. ESA's joint cooperation with DLR, NASA and Roscosmos in the METERON project [3] is addressing those needs and includes the technological validation of telepresence in a space environment. Within this framework, the haptic human arm exoskeleton X-Arm-2 [1], developed in the ESA/ESTEC Telerobotics and Haptics Laboratory, is planned to be upmassed to the ISS.

This thesis reports on the development of an efficient grasp master for space robotics teleoperation that should complement the X-Arm-2 to form a full haptic arm & hand master system, enabling bilateral teleoperation of robotic manipulators and their end-effectors.

1.1 Bilateral Teleoperation

Teleoperation allows to perform tasks distant from human presence. More specifically, robots can be teleoperated when human flexibility is required to perform tasks on remote or dangerous locations. Classic examples are tasks in a nuclear-, (deep) sea-, or space environment.

In a typical teleoperation system the operator interacts with a master device sensing the input from the operator and a slave device controlled accordingly to execute a task. In addition, in bilateral teleoperation, the environment sensed by the slave device is reflected to the human operator via a haptic master device delivering a 'sense of touch' by means of feedback. This extension of the operator's controlling and perceptual capacities to a remote site renders the operator effectively present and therefore is referred to as 'telepresence'.

The generic grasp master device developed within the context of this work is intended to link the operator with a variety of robotic end-effectors. This could be any end-effector such as a simple two-jaw gripper, multi fingered grasper or dexterous five-finger hand. The diversity of available slave devices underlines the importance of a generic solution that allows interaction with dissimilar slaves. The bilateral teleoperation system, in its most general form, is conceptually shown in Fig. 1.1.

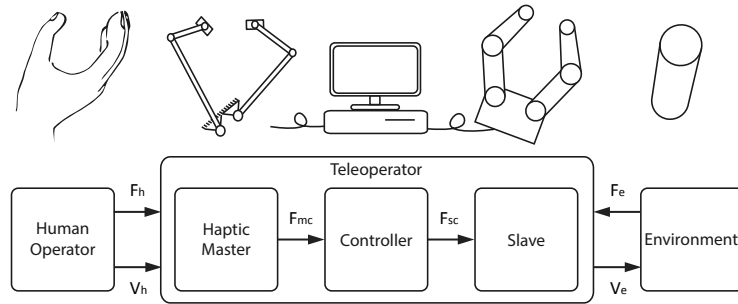


Figure 1.1: General bilateral teleoperation system

1.2 Space Robotics Teleoperation

Space robotics teleoperation is promising for its many practical applications such as operation of robotic systems for planetary investigation, satellite servicing and extravehicular activity (EVA).

As reported in [4], EVA is activity performed in an unpressurised space environment such as on the outside of the ISS (Fig. 1.2). Applications of EVA include among others: inspection, maintenance, repair, assembly and experimentation. While these are all activities invaluable in operating and maintaining the ISS space station, EVA comes with many inconveniences. The preparation, execution and the after works are cost and time intensive processes that are executed over multiple days or weeks. During EVA the pressurized space suit highly limits the astronaut's sensory perception, mobility, dexterity, strength and endurance. In addition to this, EVA imposes risks and hazards among which exposure to radiation and damage of the protective space suit due to micro meteoroids, debris and equipment.

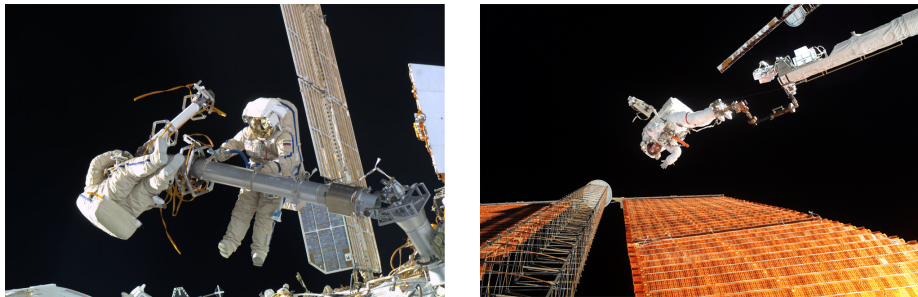


Figure 1.2: Extravehicular activity at the ISS - photos: ESA/NASA

Considering the limited and dangerous nature of EVA, assistance of, or substitution by robotic systems is desirable. Two versatile robotic platforms designed for this purpose are ESA's Eurobot [5] and NASA's Robonaut 2 [2] (Fig. 1.3). Eurobot is a non-anthropomorphic robot that is able to translate along the standard EVA interfaces and is designed to perform similar tasks as an astronaut using a limited set of specific purpose end-effectors and a general purpose robot hand. Also Robonaut 2 has been designed to be able to use the hand rails and to perform the same tasks as an astronaut. In contrast to the Eurobot, it has

a human form and two dexterous hands that allow holding and operating tools designed for humans. Robonaut 2 has been sent to the ISS in 2011 as part of the STS-133 Space Shuttle mission.

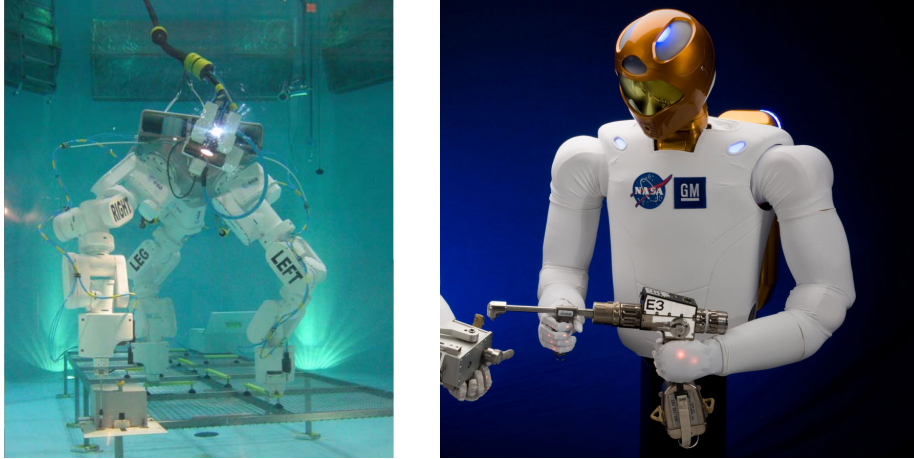


Figure 1.3: Left: ESA Eurobot water prototype moving via ISS hand rail [5]. Right: NASA Robonaut 2 holding an EVA torque tool [2]

The ongoing research into space robotic systems by ESA and NASA and even the availability of a humanoid robot in the ISS underlines the relevance of this field. With this comes the need for teleoperation enabling systems. The X-Arm-2 (Fig. 1.4) has been developed for this purpose and allows bilateral control of space robots with force-feedback [1]. This fully actuated force-reflecting human arm exoskeleton was designed via an ergonomic and human-centric approach to achieve a body-grounded design that does not require adjustments to varying operators.

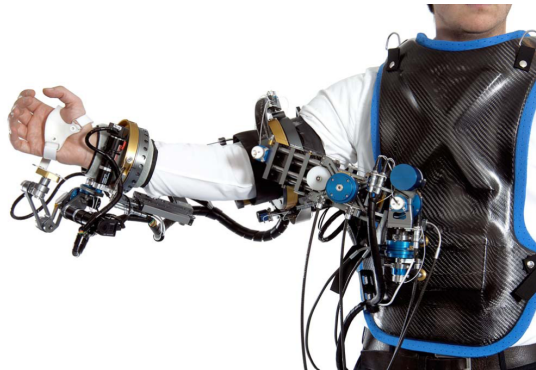


Figure 1.4: Haptic arm master X-Arm-2 [1]

While the X-Arm-2 does support the palm with sensing and actuated degrees of freedom (DOFs), the fingers are not supported yet. The current grasp master development described in this thesis will complement the X-Arm-2 in its function and philosophy. It should provide the fingers with sensing and feedback func-

tions, enabling bilateral teleoperation of various types of robotic end-effectors to perform a wide range of tasks. Just as the X-Arm-2 the grasp master should be easy to use by varying operators without requiring adjustments.

1.3 State of the Art - Grasp Masters

Some tens of grasp master devices have been reported in literature for purposes of rehabilitation, assistance, virtual reality and teleoperation. Most are experimental prototypes, while few have been commercialised and are available for purchase, albeit for high costs.

Analysis of the existing devices reveals a range of issues that might limit their use in practical applications. Common device features and their implications in terms of advantages and drawbacks are summarized in the following sections. This is illustrated by selected devices with these features. The literature survey in Annex. C gives a more detailed overview of 24 compared devices and their characteristics. These constituted a rather complete set of device existing at the time of writing this thesis.

1.3.1 Arm Coverage

Half of all 24 compared devices do not only cover the fingers and hand, but the wrist and (parts of) the arm as well. Common reasons for arm coverage are placement of actuators or other components. Hereby compatibility with arm masters is severely limited or impossible since these generally are situated around the arm. Two exemplary devices with arm coverage are presented in [6] and [7] (Fig. 1.5) where electronics and an actuator have been located on the arm respectively.

Other devices covering the wrist are: [8], [9], [10], and [11]. Other devices covering the arm as well are: [12], [13], [14], [15], [16], [17], [18], [19], and [20].

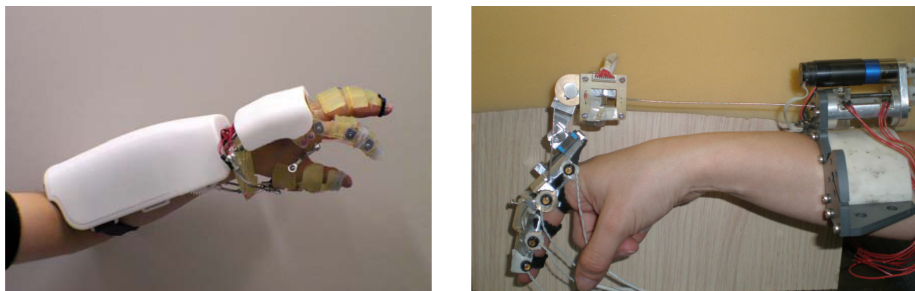


Figure 1.5: Arm covering hand masters. [6] (left) [7] (right)

1.3.2 External Actuators

To reduce size and mass placed on the hand, fingers and arm, actuators can be located on an external setup. In [21] and [19] relatively small and light device designs have been achieved and cable transmissions have been used to locate the actuators away from the hand and arm (Fig. 1.6). While this can

increase comfort, arm master compatibility and power density at the actuated joints as shown in [22], such designs are prone to suffer from mechanical losses, reduced backdrivability and backlash from the longer and more complicated transmissions. Furthermore, external connections interfere with the arm master or might limit the workspace of the arm.

Other devices that reside on the hand and have externally placed actuators are: [10], [23], and [24].

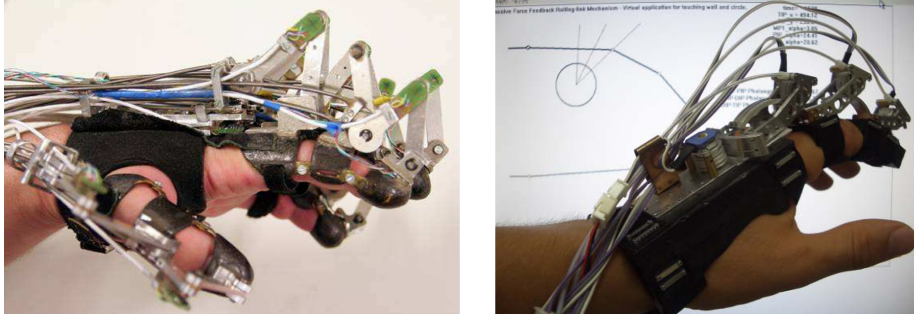


Figure 1.6: Hand masters with external actuators [21] (left) [19] (right)

1.3.3 Fixed Base

Fixed base devices such as those mounted externally in [25] or 'table-top' in [26] (Fig. 1.7) can be large and heavy while avoiding aforementioned problems of arm coverage, reduced comfort and more complicated transmissions. The main drawback is the fixed base itself that makes those devices unsuitable as mobile wearable solution. Also the workspace of the human arm is limited by that of the device.

Other devices having a fixed base are: [15] and [27].



Figure 1.7: Fixed base hand masters [25] (left) [26] (right)

1.3.4 Mechanisms with a Remote Centre of Motion

A part of the devices has been designed with extensive mechanisms to support a large range of motion while not compromising accurate control over force mag-

nitude and direction. By its kinematic structure, the device in [9] for example is able to exert force in any desired direction to the tip of the thumb and index finger (Fig. 1.8 (left)). This functionality relies on a structure that gives joints a remote centre of motion to bend around a flexing finger without colliding. Comparable functionality was implemented in devices in [8], [23], [16] and [28], of which the latter two are shown in Fig. 1.8 (middle and right respectively).

Drawbacks of devices with such extensive mechanisms are their large size, high mass and mechanical complexity. The many links and joints make them susceptible for unwanted mechanical effects such as friction and excessive backlash. Moreover, bulky devices might limit arm master compatibility by obstructing wrist motion. When inspecting the devices shown in Fig. 1.8 and imagining operation combined with the X-Arm-2 in Fig. 1.4, it can be seen that the systems do not fit together or are prone to collide when making wrist movements. In addition, the high mass and resulting inertia of bulky devices may lead to low comfort, user fatigue and altered perception.

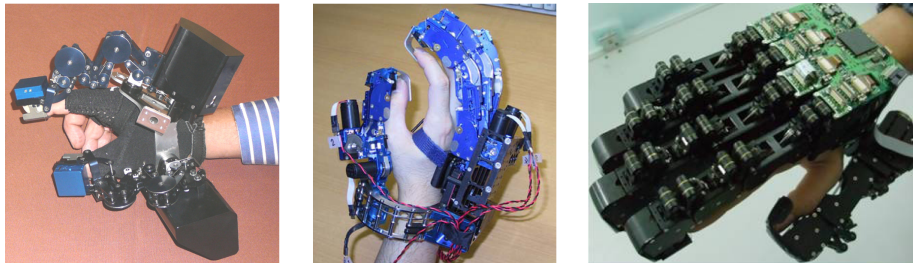


Figure 1.8: Hand masters having mechanisms with a remote center or rotation [9] (left) [8] (middle) [28] (right)

1.3.5 Devices with Passive Joints

The devices in [17] and [27] (Fig. 1.9) contain passive joints to allow the use of a single actuator per finger, while force direction is kept reasonably perpendicular to the point of contact. With this, the number of required actuators is kept low, but mechanisms with multiple links and joints are required and increase mass, size, structural complexity and undesired mechanical effects. Furthermore, for hands of different sizes, the force feedback will deviate from the intended perpendicular direction.

1.3.6 Compact Design

As shown before, the devices in Fig. 1.9, Fig. 1.7 (right) and Fig. 1.8 (left) only support a two finger pinch grasp. While this is just a part of the hand grasping functionality, large and complex structures with multiple joints and actuators are used. This poses the question whether really such extensive designs are required to support such little hand functionality.

The Rutgers Master as presented in [29] (Fig. 1.10) stands out for its small size, low mass and yet support of 4 fingers. The structure is under-actuated and optimized for dexterity and perpendicular feedback to the fingertip. It is especially striking to realize that this device provides a DOF of feedback to each

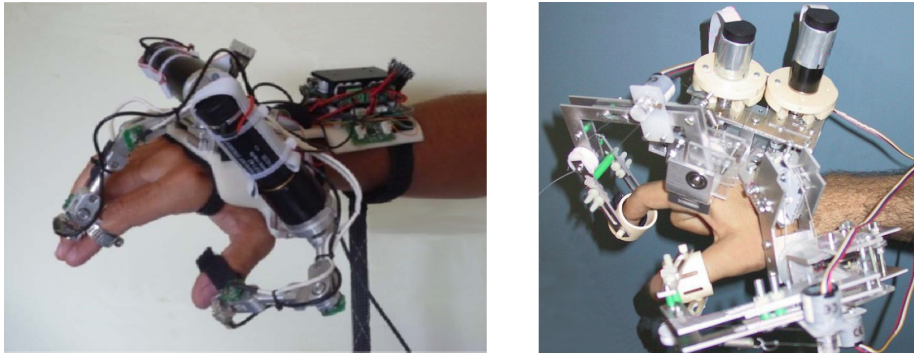


Figure 1.9: Pinch grasping masters [17] (left) [27] (right)

of 4 fingertips, while the devices introduced before in Fig. 1.9 require so much more bulky and complex designs to provide a DOF of feedback to each of 2 supported fingertips.

The drawbacks of the Rutgers Master are the limited finger flexion range because of the palmar placement and the required external air-compressor with connections that, similar to the transmissions of externally placed actuators, will interfere with the arm device and might limit the workspace of the arm.



Figure 1.10: Pneumatic hand master - Rutgers Master [29]

1.3.7 Commercial Devices

One of the few commercial hand masters is the CyberGrasp-CyberGlove combination in [24] (Fig. 1.11 (left)). It combines a glove with many sensors and a feedback device with a single DOF feedback per finger. This sensor-actuator asymmetry can be seen as an efficient trade-off between the use of actuators and sensors and will be addressed in Section 1.4.

While the CyberGrasp-CyberGlove finds popular use and has a pioneering role as commercial grasp master, it does show several limitations discussed before. Its externally placed actuators require cable transmissions that introduce me-

chanical losses, interferes with arm devices and limits arm workspace. Since this device only covers the hand and wrist, the arm is left free. Nevertheless, compatibility with arm masters is not optimal due to the difficulty of donning/doffing of the glove involving two palm fixtures and two interfaces per finger.

Two other commercial devices are the ForceDimension Omega7 and Sigma 7 in [30] (Fig. 1.11 (middle and right respectively)). It should be noted that such devices are not pure grasp masters, but in the first place hand masters that offer 3 translational and 3 rotational DOFs and one additional DOF for pinch grasping. The translational and rotational DOFs perform the role of an arm master in supporting the position and orientation of the hand, nevertheless this cannot replace an arm master in its function of supporting the whole posture of the arm. These table-top masters come with the usual fixed base limitations of not being portable and limiting the workspace of the arm, as addressed in Section. 1.3.3.



Figure 1.11: Commercial hand masters [24] (left) [30] (middle and right)

1.4 Problem Statement

From the state of the art in Section 1.3 it is clear that each device feature comes with advantages and drawbacks. It is thus crucial to make the right trade-offs in the design process of a new generic and efficient hand master design. Two influential factors are the placement of the device w.r.t. the user and its structural complexity.

1.4.1 Device Placement w.r.t. the User

As a wearable and mobile solution the complete device can be placed on the hand and arm (Section. 1.3.1). Possible issues are limited arm master compatibility due to arm coverage and low comfort and fatigue due to the mass and size. These drawbacks can be relieved by locating components such as actuators externally (Section. 1.3.2). This however, requires longer and more complicated transmissions which can introduce mechanical losses and backlash. In addition, the external connections might interfere with arm masters and might limit arm workspace and mobility. The long transmissions can be avoided by placing the whole device externally as a fixed base design. With this, mobility and workspace are further limited (Section. 1.3.3).

1.4.2 Structural Complexity

Structural complexity is defined in terms of the amount and nature of DOFs, actuators, transmissions and components. Common reasons to apply complex designs are to achieve robustness towards variable hand sizes over a large workspace and accurate control of feedback magnitude and orientation on one or multiple positions on the finger (Section. 1.3.4). The price to pay is increased mass, size, costs and possible consequences of this such as limited arm master compatibility, low comfort and fatigue. Compact designs on the other hand might avoid these drawbacks for the price of limited workspace and less accurate force direction control (Section. 1.3.6).

1.4.3 Device Efficiency

Each trade-off comes with gains and losses (e.g. by accepting the consequences of increased complexity, device features such as accurate control of feedback direction can be gained). In other words: *resources* can be spent to obtain *device- and user performance*.

Resources are expended in terms of mass, volume, DOFs, actuators, transmissions, components, sensors, drives, costs, etc.

Device performance is gained in terms of arm master compatibility, structural transparency, stiffness, mechanical bandwidth, backdrivability, resolution, decreased backlash, decreased friction, etc.

User performance is achieved in terms of robustness towards variable hand sizes, ease-of-use, intuitive operation, comfortable donning/doffing, etc.

It is important to realize that performance achieved with 'resource expensive' solutions does not guarantee successful results in practice. As an example: a resource expensive device with accurate control over feedback in multiple positions on the fingers in principle allows natural feedback to the full finger. In practice however, imperfections in the complicated mechanisms are susceptible to mechanical losses and misalignments may lead to unnatural constraint forces and consequently uncomfortable wear and operation. In addition, each interaction point requires fixation to the body and might involve troublesome donning/doffing. The achieved device- and user performance thus is low compared to the resources expended. In this sense the device is overly complex for the achieved results; we define such a device design as not efficient.

An *efficient* design comes with the right balance of resources expended and performance achieved. The overview of the state of the art in Section 1.3 and the analysis of existing grasp masters in Annex. C.V shows that existing devices in general are expensive in terms of resources and/or show limited device- and user performance. Because of this, *the ratio of performance achieved versus resources expended (the design efficiency)* can be seen as generally too low.

1.5 Goal

It is the goal of this thesis to develop an efficient grasp master device that can be used by various operators in space robotics teleoperation without requiring device adjustments. This involves the following sub-goals:

- Achieve a structurally simple device design by minimising the amount of DOFs.
- Separate control and feedback functions to allow the reduction of DOFs and to achieve comfortable device operation.
- Achieve a generic device design that is usable in different bilateral control architectures and in combination with various slaves.
- Achieve sufficient feedback DOFs to gain information about the tasks during bilateral control.

It is hypothesized that by following a human-centric design approach and by separation of control and feedback functions a high device efficiency can be established.

1.6 Approach

The human-centric design approach entails: a) Review of human factors and grasp methods to generalize the problem of grasping and to select the minimum number of sensor and feedback features to support hand functions during a majority of natural grasps. b) Conceive a mechanical and electrical device concept to support such minimum required functions. c) Perform a detailed device design with appropriate device parameters. This design is then verified by simulation and analysis. Next, a prototype is developed to enable validation.

The thesis approach can be divided into the following steps:

- 1 **Analysis of relevant background to enable human-centric design.**
This includes identification of relevant tasks in remote operations, the grasps types required for these, and possibilities to exploit psychophysical effects (Chapter. 3.II). In addition, device performance- and human factors requirements are identified (Chapter. 3.III). The basis for this was formed by the literature survey included in Annex. C.
- 2 **Formulation of the device concept** and its features by exploiting the knowledge on tasks, grasps, and psychophysical effects in the reduction of DOFs towards an efficient design (Chapter. 3.IV).
- 3 **Setup of a simulation framework** for ergonomic device design by means of a kinematic model of the human hand that can be easily adapted to different hand sizes. This model was used as a tool in the design and verification of device geometry, workspace and robustness against hand size variation. It is included in Chapter. 2 in the form of the paper: *A Functional Anatomy Based Kinematic Human Hand Model with Simple Size Adaptation (published in IEEE/ICRA 2012)*.
- 4 **Detailed design** of an ergonomic device prototype that contains all features as formulated in the device concept (Chapter. 3.V). Additional technical details are contained in Annex. A.
- 5 **Verification** of the detailed prototype design by simulation and by analysis to verify achieving the key human factors- and performance requirements (Chapter. 3.IV). This includes application of the hand model simulation framework to verify device workspace for robustness against hand size variation.
- 6 **Prototype implementation** to demonstrate the practical feasibility of the design and to enable verification by testing. The CAD drawings for

manufacturing have been included in Annex. B.

7 **Validation** of the implemented prototype in real scenarios where various users operate various slave devices.

This thesis is targeted to reach step 5). Up to that point, the proposed concept, based on analysed operation context, has been elaborated into a detailed design that has been verified by simulation and by analysis including the use of a human hand model developed for this purpose. The results will indicate the promising continuation of implementing a prototype for device verification by testing and validation in actual user operation.

Chapter 2

A Functional Anatomy Based Kinematic Human Hand Model with Simple Size Adaptation

Frank P. J. van der Hulst, Simon Schätzle, Carsten Preusche and André Schiele
*in Proc. of IEEE/ICRA International Conference on Robotics and
Automation, Saint Paul, Minnesota, USA, May. 2012, pp. 5123–5129*

This paper reports on the construction and verification of a kinematic hand model based on human functional anatomy and with simple adaptation to real hand sizes by a single parameter input. This forms step 3) of the approach introduced in Chapter. 1.6. In Chapter. 3 this model is used as a tool in the design and verification process of the device geometry, workspace and robustness with respect to hand size variation. Therefore, creating and adapting such a model was crucial for the thesis.

A Functional Anatomy Based Kinematic Human Hand Model with Simple Size Adaptation

Frank P. J. van der Hulst, Simon Schätzle, Carsten Preusche and André Schiele

Abstract—For the purpose of ergonomic human-machine interaction and geometrical design of hand held haptic devices, a kinematic model that represents the functional anatomy of different human hands is desired.

It is the goal of this paper to present a kinematic hand model that is based on human physiology and that is easily adaptable to represent various real human hand sizes. This is achieved by exploiting body proportions to derive finger segment lengths from the hand length.

A partial hand model validation, involving index- and middle finger validation using a group of subjects, indicates that the use of body proportions offers a good estimate of finger length from a given hand length. Model estimated fingertip positions over a motion trajectory remain within reasonable limits when compared with experimental data for this subject group.

The model is promising for usage in practical situations since only hand length, which is easy to measure or to obtain from literature, is required as an input. Phalange lengths, which are sparsely available from literature and difficult to measure, are generated by the model.

I. INTRODUCTION

MANY robotic devices are designed for interaction with humans and in particular for interaction with human hands. A typical example is the field of haptics for teleoperation and rehabilitation purposes, where interfaces and exoskeletons interact with, or connect to, the hand and fingers. Such devices are required to provide ergonomic human-machine interaction, not constraining natural movement and workspace during motion.

The complicated nature of the human hand raises the desire for a truly kinematic model of the hand, based on the physiology of its joints. Such a model could find its use in ergonomic human-machine interaction design for optimization of kinematic structures and geometrical design of hand held objects. Also, the hand model could be used to evaluate realistic hand functionality in the design of devices such as prosthetics and humanoid end-effectors. Another application of a hand model lies in estimating the state of a physical human hand. Forward kinematics can be applied to express the posture as function of the joint angles. The other way

F. P. J. van der Hulst and A. Schiele are with the Telerobotics and Haptics Laboratory, European Space Research and Technology Centre, European Space Agency, 2201 AZ Noordwijk, The Netherlands, and with the Delft Biomechanical Engineering Department, Mechanical Engineering Faculty, Delft University of Technology, 2628 CD Delft, The Netherlands. Frank.van.der.Hulst@esa.int, Andre.Schiele@esa.int

S. Schätzle and C. Preusche are with the Institute of Robotics and Mechatronics, German Aerospace Center (DLR). simon.schaetzle@dlr.de

around, inverse kinematics can be used to derive joint angles from a given posture.

For the hand to be able to grasp and to hold objects, the ability of the thumb to oppose each single finger is essential. This functionality is termed thumb-finger opposition and is the result of multiple factors that will be discussed in Section II. Multiple published hand models will be summarized, yet none of these combines all factors required to achieve natural thumb-finger opposition.

In addition to the observed limitations on natural thumb-finger oppositions, there is another factor limiting the practical use of hand models. While in an experimental environment a calibrated model might be usable, in a practical application it is often required to vary its dimensions. One can think of many applications, such as for instance: optimizing human-machine interaction for different operators, evaluating ergonomic object interaction for different users or calculating forward or inverse kinematics for different subjects.

It is the goal of this paper to present a kinematic hand model that is based on the real functional anatomy of the human hand and that is easily adaptable to represent different physical hand sizes. The applied approach is to make use of body proportions for segment length estimation. A partial validation of the model will be performed for a scenario where the finger end-point position is estimated from a given set of joint angle measurements for various subjects.

This paper is organized as follows. Section II describes the functional anatomy of the human hand. Section III covers the construction and the parameterization of the kinematic model. Section IV describes validation of finger length estimation and optimization of model parameterization. Section V reports on model validation by finger end-point estimation. Section VI presents the conclusion and future work.

II. ANATOMY OF THE HUMAN HAND

For clarifying the terminology, Fig. 1 shows the anatomical position of the hand and the movement conventions.

A. Bony Structure

The human hand is composed of 27 bones, arranged in 5 serial kinematic chains forming the fingers. The fingers are numbered as follows. 1: thumb, 2: index finger, 3: middle finger, 4: ring finger and 5: little finger. Each finger (2-5) consists of a metacarpal bone located in the hand and 3 phalanges named the proximal-, medial, and distal phalange (in the order from finger base to fingertip). The thumb only consists of a metacarpal and 2 phalanges; it does not have a

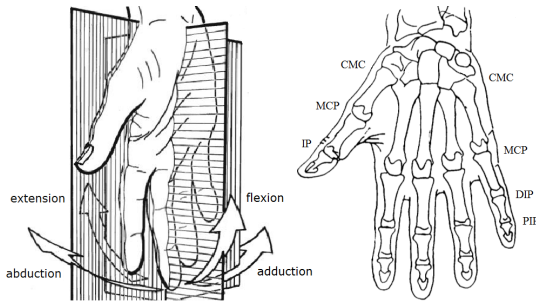


Fig. 1. Anatomical position of the hand. Left: pure flexion-extension takes place in the horizontally hatched sagittal plane. Pure adduction-abduction takes place in the vertically hatched frontal plane. Adapted from [31]. Right: bone structure of the hand with joint names indicated. Adapted from [32].

medial phalange. The remaining 8 hand bones are the carpals, located in the wrist.

The names of the joints depend on the bones they link. In the right half of Fig. 1 the bone structure and the following joints can be seen: carpometacarpal joint (CMC), metacarpophalangeal joint (MCP) and interphalangeal joints (IP). In the fingers the two IP joints are distinguished by the prefixes, proximal (PIP) and distal (DIP).

B. Hand Models - State of the Art

In the human hand, the thumb is able to oppose each finger. This functionality is termed thumb-finger opposition and is essential to grasp and to hold objects. It is achieved by: the placement of the thumb anterior to (in front of) the palm and the fingers, automatic opposition resulting from oblique flexion of the fingers by inclined axes of rotation, and the hollowing of the palm [31]. The two latter effects will be described in Section II-C3.

In the 24 DoF model in [33] and the 23 DoF model in [32] effects of palm hollowing have been implemented as CMC flexion-extension. While this allows arcing of the palm, the displacement is purely with respect to the frontal plane. No palm arcing effects have been included in the 26 DoF model in [34] where only CMC ad-/abduction within the frontal plane was implemented, and in [35] where a 16 DoF model with a rigid palm is presented.

The natural opposition effects in the thumb were described in [31]. This was modeled using 5 DoF in [32]. In all the other named hand models and the thumb model in [36], the thumb functionality is approximated by 4 DoFs.

While multiple of the mentioned models offer pure CMC flexion-extension or ad-/abduction, none combines these motions for a more natural hollowing of the palm. In all models, finger flexion-extension takes place purely in the sagittal plane, and thus no oblique flexion is supported. Judging from this information, none of the models combines the factors that are essential to achieve natural thumb-finger opposition.

C. Functional Anatomy

As a result of the specific anatomy of the joints in the hand, objects can be grasped stably. Most of the information in this section has been adopted from [37], where hand and finger anatomy effects from [31] have been summarized.

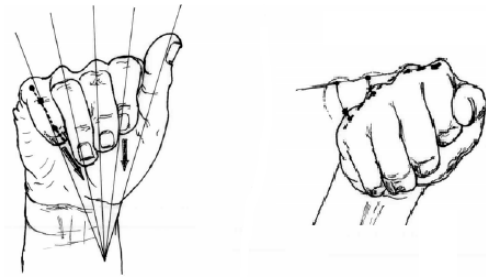


Fig. 2. Thumb-finger opposition effects. Left: automatic opposition by oblique finger flexion caused by inclined flexion-extension axes in the MCP, PIP and DIP joints. Right: hollowing of the palm by movement of the metacarpal heads in the CMC joints, with respect to the frontal plane (anteriorly) and slightly to the side (laterally).

1) *Thumb Joints Anatomy:* The thumb CMC is a saddle joint that offers 2 DoF: flexion-extension and ante-position-retro-position (moving the thumb in front of the hand and moving it back). The axes of rotation are perpendicular and cross each other, yet do not intersect. Therefore no axial rotation is possible. The MCP is a condyloid (ellipsoidal-socket) joint that offers 2 DoF: flexion-extension and ad-/abduction. A 3rd DoF is available by means of a slight pronation-supination (axial rotation). The IP is a 1 DoF hinge joint offering flexion-extension with a slight pronation caused by the inclination of the axis.

2) *Finger Joints Anatomy:* The finger MCP joints are condyloid joints with 2 DoF: flexion-extension with respect to the frontal plane and ad-/abduction with respect to the sagittal plane. The available axial rotation is only passive. The IP joints are the PIP and DIP, both offering 1 DoF flexion-extension. Depending on the finger, the flexion-extension axes are inclined, introducing motions directed sideways (lateral) and axial rotation [38].

3) *Thumb-finger Opposition:* The anatomical effects in the joints combine into the following two mechanisms that contribute to thumb-finger opposition.

Automatic opposition: During flexion, the fingers are directed towards the same point (the radial pulse) as shown in the left half of Fig. 2. This effect presents the pulp of the fingers to that of the thumb and to the object to grasp. The result is an increased contact surface contributing to the strengthening of the grip.

Automatic opposition results from inward finger flexion caused by the MCP flexion axis inclination and oblique finger segment flexion caused by the PIP and DIP flexion axes inclination. The PIP and DIP flexion axes are perpendicular to the long axis of the bone in full extension and become progressively more oblique during flexion [38]. This is an effect of asymmetry of the bone surfaces moving with respect to each other in the joints (the articular surfaces) and of the different tensions in the ligaments. Oblique flexion causes the finger segments not to flex in the sagittal plane, yet in an increasingly oblique plane.

The effects of inward finger flexion and oblique finger segment flexion increase from the index finger to the little finger, as also shown in the left half of Fig. 2.

The hollowing of the palm: The heads of the metacarpal

bones located in the CMC joints move with respect to the frontal plane (anteriorly) and slightly to the side (laterally). As illustrated in the right half of Fig. 2, this effect increases from the index finger (where it is negligible) to the little finger, causing hollowing of the palm.

III. HUMAN HAND MODEL

Using the functional anatomy of the hand, described in the previous section, a kinematic model description is defined.

A. Kinematic Structure

The kinematic structure of the hand model is defined by base transformations relating the finger bases to the hand base and by Denavit-Hartenberg (DH) parameters describing the kinematic chain of each finger. This model includes the following human hand joints.

Index- and middle finger: Both consist of 4 DoF. 2 DoF MCP: flexion-extension (θ_1) and ad-abduction (θ_2), 1 DoF PIP: flexion-extension (θ_3), and 1 DoF DIP: flexion-extension (θ_4).

Ring- and little finger: Both consist of 5 DoF. 1 DoF CMC: lateral (sideways) flexion-extension (θ_1), 2 DoF MCP: flexion-extension (θ_2) and ad-abduction (θ_3), 1 DoF PIP: flexion-extension (θ_4), and 1 DoF DIP: flexion-extension (θ_5).

Thumb: The thumb model consists of 6 DoF, enabling realistic thumb-finger opposition. 2 DoF CMC: flexion-extension (θ_1) and ad-abduction (θ_2) (ante-position-retro-position). These axes cross but do not coincide, forming a saddle joint. 3 DoF MCP: flexion-extension parallel to the previous flexion axis (θ_3), abduction-adduction parallel to the previous abduction axis (θ_4), and axial rotation collinear with the proximal finger segment (θ_5). 1 DoF IP: flexion-extension (θ_6).

The kinematic structure is shown in Fig. 3. The finger base frames CMC_1 , $MCP_{2,3}$, and $CMC_{4,5}$ (with the indices 1-5 indicating the fingers) are expressed with respect to the hand base frame O_b via the transformations T_{CMC1}^b , $T_{MCP_{2,3}}^b$, and $T_{CMC_{4,5}}^b$ respectively. Each transformation is composed of a translation and a rotation. The rotation matrices are given in (1) for the thumb, in (2) for the index- and middle finger, and in (3) for the ring- and little finger. The notation convention and rotation matrices: R_x , R_y , and R_z , are according to [39].

$$R_{CMC1}^b = R_x(\beta_t)R_z(-\alpha_f)R_y(-\alpha_e) \quad (1)$$

$$R_{MCP_{2,3}}^b = R_y(\phi_{mcp}) \quad (2)$$

$$R_{CMC_{4,5}}^b = R_y(\phi_{mcp})R_x(\beta_h) \quad (3)$$

The transformations from the fingertip to the finger base include the variable joint angles θ_i and are described using the DH-parameters given in Table I for each finger.

The thumb CMC saddle joint axes are placed at a distance r_{cmc} at either side of the joint center. This accounts for the joint head diameter.

The anterior placement of the thumb is defined by thumb base frame rotation of β_t , inclination of the thumb in its frontal

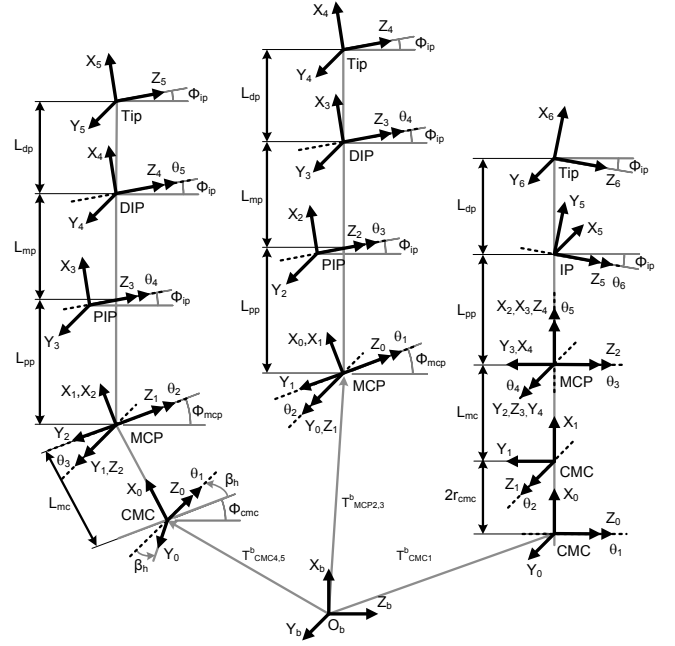


Fig. 3. Hand model kinematic structure frontal view. For visual clarity, thumb base rotations (1), and finger chain parameter indices are not shown.

plane α_f and inclination of the thumb in its sagittal plane α_s .

TABLE I
DENAVIT-HARTENBERG PARAMETERS

Thumb				
Joint	a_i [m]	d_i [m]	α_i [°]	θ_i [°]
T_1^0	$2r_{cmc}$	0	-90	θ_1
T_2^1	$L_{mc}-r_{cmc}$	0	90	θ_2
T_3^2	0	0	-90	θ_3
T_4^3	0	0	90	θ_4+90
T_5^4	0	L_{pp}	$90-\phi_{ip}$	θ_5-90
T_6^5	$L_{dp}C_{ip}$	$L_{dp}S_{ip}$	0	θ_6+90

Index and Middle Finger				
Joint	a_i [m]	d_i [m]	α_i [°]	θ_i [°]
T_1^0	0	0	-90	θ_1
T_2^1	$L_{pp}C_{ip}$	0	90	$\theta_2+\phi_{ip}-\phi_{mcp}$
T_3^2	$L_{mp}C_{ip}$	$(L_{pp}+L_{mp})S_{ip}$	0	θ_3
T_4^3	$L_{dp}C_{ip}$	$L_{dp}S_{ip}$	0	θ_4

Ring and Little Finger				
Joint	a_i [m]	d_i [m]	α_i [°]	θ_i [°]
T_1^0	L_{mc}	0	$-\beta_h$	θ_1
T_2^1	0	0	-90	θ_2
T_3^2	$L_{pp}C_{ip}$	0	90	$\theta_3+\phi_{ip}-\phi_{mcp}$
T_4^3	$L_{mp}C_{ip}$	$(L_{pp}+L_{mp})S_{ip}$	0	θ_4
T_5^4	$L_{dp}C_{ip}$	$L_{dp}S_{ip}$	0	θ_5

Joint angles: $\theta_1, \theta_2, \theta_3, \theta_4, \theta_5, \theta_6$; Phalange lengths: $L_{mc}, L_{pp}, L_{mp}, L_{dp}$; Axis inclination angles: ϕ_{ip}, ϕ_{mcp} ; Thumb CMC radius: r_{cmc} ; Ring- and little finger base rotation offset: β_h ; Shorthand notations: $S_{ip} = \sin(\phi_{ip})$, $C_{ip} = \cos(\phi_{ip})$. DH-convention according to [39].

These rotations are described in (1), where α_e is the thumb elevation, given by:

$$\alpha_e = \tan^{-1}(\tan(\alpha_s)\cos(\alpha_f)).$$

Palm hollowing is implemented for the ring- and little finger via a finger base rotation offset β_h and via the flexion-extension axes inclination angles ϕ_{cmc} in the CMC joints. Since the CMC joint motion is negligible for the index- and middle finger, their CMC joints are not modeled.

Automatic finger-thumb opposition by inward finger flexion and oblique finger segment flexion are implemented via the flexion-extension axes inclination angles ϕ_{mcp} and ϕ_{ip} respectively.

B. Model Parameters

In this section, the parameter values are defined. Distinction is made between parameters that are derived from body proportions, that are assumed a value, and that are unknown. Although the latter two categories contain rough estimates and unknown parameter values, the model is implemented such that it is ready to accept new parameter values whenever these come available.

1) *Parameters Derived from Body Proportions:* Simple adaptation of the model to represent different hand sizes is achieved by generating the link lengths L_{pp} , L_{mp} , and L_{dp} from a given hand length. A similar approach was used in [32], where dimensional measurements, expressed as percentage of hand length, breadth and thickness, were used to scale a hand model for different hand sizes. This approach is based on the assumption that normal hands maintain anatomical structure and dimensional proportions, regardless of their physical size [38].

The advantage is that the hand length, which is easy to measure or to obtain from literature, is used to generate link lengths that are difficult to measure and sparsely reported.

Table II presents all finger phalange lengths as percentages of the hand length. This conversion table was reported in [40] and is based on 32 subjects (15 male, 17 female). In Section IV this table will be optimized using experimental data.

2) *Assumed Parameters:* Since no detailed quantitative information has been found, the axis inclination angles (ϕ_{cmc} , ϕ_{mcp} , ϕ_{ip}), the thumb parameters (β_t , α_f , α_s , r_{cmc}), and the palm hollowing base orientation β_h are assumed based on qualitative knowledge of the anatomy of the hand described in [31]. The values used in the hand model are as proposed in [37].

TABLE II
HAND LENGTH TO PHALANGE LENGTH CONVERSION TABLE [40]

	Proximal (L_{pp})	Medial (L_{mp})	Distal (L_{dp})
Thumb	17.1	–	12.1
Index finger	21.8	14.1	8.6
Middle finger	24.5	15.8	9.8
Ring finger	22.2	15.3	9.7
Little finger	17.7	10.8	8.6

Each entry represents phalange length as percentage of hand length.

The IP axis inclination angle ϕ_{ip} is approximately 5-10° for the thumb [31], therefore a value of 7.5° is assumed in the model. The same source reports that the automatic opposition by inward and oblique flexion increases from the index finger, where it is negligible, to the little finger. Therefore the finger IP inclination angles are assumed increasing from the index- to the little finger: 0°, 2°, 4°, 8°. Thus ranging up to approximately the value for the thumb.

The MCP axes inclination angles ϕ_{mcp} are assumed such that all fingers are directed towards the radial pulse when flexed (left half of Fig. 2). The MCP axis inclination angles are assumed: -6.8°, 3.6°, 13.8°, 23.9° for the index- to the little finger, as proposed in [37]. The CMC axes inclination angles ϕ_{cmc} of the ring- and little finger are assumed equal to their ϕ_{mcp} angles.

The thumb base rotation offset β_t is assumed -90° and the projection angles α_f and α_s are assumed 30° and 40° respectively in the neutral thumb position [31]. The CMC saddle joint head radius r_{cmc} is estimated to be 5 mm.

The finger base rotation offset for palm hollowing β_h is set to 45°.

3) *Unknown Parameters:* No reliable quantitative information defining all finger base positions with respect to the hand base has been found. Therefore no finger base origin translations are proposed at this moment.

Also the metacarpal segment length L_{mc} is not assigned a value currently, it could be derived from body proportions in the future, analogue to the phalangeal segment lengths in Section III-B1.

IV. EXPERIMENTAL OPTIMIZATION OF THE HAND MODEL

As described in Section III-B1, Table II can be used to calculate all phalange lengths from a given hand length. This table, which was obtained from literature, was validated and optimized using experimental data. As a result, an updated conversion table for the index- and middle finger is presented, which will be applied in Section V during a partial model validation.

A. Method

For both the index- and middle finger, the terms in the original conversion table were multiplied by a correction factor, ensuring that the length relation between the phalanges holds, while the sum of phalange lengths now matches the finger length estimated from experimental data.

This method required the finger length to be estimated from experimental data, using a motion tracking experiment to identify the fingertip and base positions.

1) *Experimental Setup:* An optical motion capture system with passive markers was used for the tracking of the subjects' finger movements. Seven Vicon® MX3+ cameras were installed such that the reflective markers on the back of the hand and on the fingers, placed as shown in Fig. 4, were tracked for the full range of finger motion.

In order to minimize the effect of skin movement, markers were placed onto the finger segments rather than on the joints.

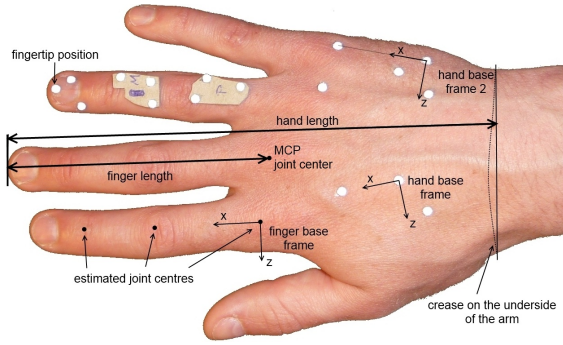


Fig. 4. Attachment of markers on one finger and the hand.

These 3 mm passive markers had no observable effect on the natural finger motion. Application of two frames on the back of the hand allowed to track the hollowing of the hand.

2) *Experimental Data:* Cartesian marker positions were registered during index- and middle finger motion. From this data, joint center positions were estimated. Subsequently, the finger length was calculated as the norm of the vector from the estimated MCP joint center to the measured fingertip marker position on the fully stretched finger.

Datasets of two female and five male subjects aged from 26 to 30 years were collected. Table III lists the subject hand parameters, including the hand length, measured as shown in Fig. 4.

After markers had been attached to the hand, a predefined trajectory composed of three phases was executed by the subjects with each finger subsequently. After the initial posture in which the fingers were fully stretched, the motion trajectory started with a flexion-extension, followed by an ad-/abduction with the finger stretched, and ended with a circumduction of the stretched finger, performing both flexion-extension and ad-/abduction of the MCP joint. This trajectory involved all relevant finger degrees of freedom. During this routine, marker positions were tracked and stored.

B. Data Processing

In the first part of the data processing, joint center positions were estimated. Based on this result, joint angles sets for each finger configuration will be calculated in Section V.

1) *Estimation of Joint Centers:* Joint center positions were derived from measured data by analyzing the movement of the adjoining finger segments. Markers were rotated from their initial position, around a specific inclination axis, until coinciding with the markers on the flexed segment.

The axes inclinations defined in the hand model were used for this estimation of joint center positions. In order to assure that the joint angles extracted from the measured

TABLE III
SUBJECT HAND DIMENSIONS

Subject	1	2	3	4	5	6	7
Hand length [mm]	170	177	189	200	192	200	198
Hand breadth [mm]	69	75	85	82	85	89	82

data are comparable with the modeled data, the definition of joint axes inclinations should match between modeled and measured data. If this is not the case, a single fingertip position is described by different joint angle sets in measured and modeled data. For that reason, axes inclinations from the model were used for the following processing.

Joint center positions have been estimated by solving the following nested optimization problem: The cost function of the outer algorithm, namely the joint center position optimization, is defined as follows:

$$\min_{\vec{x} \in \mathbb{R}^3} f(\vec{x}) \quad \text{with } f(\vec{x}) = \sqrt{\text{sum}_{posError}/N}$$

where \vec{x} is the position vector of the estimated joint center, N is the number of different measured finger flexions and $\text{sum}_{posError}$ is the result of the inner optimization algorithm. This inner optimization algorithm calculates a joint angle for each measured finger flexion with a given joint center from the outer optimization algorithm, so that the error between estimated and measured marker position is minimized as follows:

$$\min_{q \in \mathbb{R}} f(q) \quad \text{with } f(q) = \underbrace{\sum_{m=1}^M \|P_{m,meas} - P_{m,mod}\|^2 / M}_{\text{sum}_{posError}}$$

with M the number of markers on the flexed finger segment, P the Cartesian position vector from joint center to measured and estimated marker positions and q the joint angle.

Within a loop, a joint angle is optimized for each finger flexion angle, and the squared errors are summed, resulting in $\text{sum}_{posError}$. This sum is the root mean square distance error between measured and estimated marker positions resulting from a rotation around an axis with a specific position and inclination.

2) *Conversion Table Update:* The finger length estimated from measurement, as described in Section IV-A2 is termed reference finger length. The ratio between this length and the finger lengths from the conversion table (sum of phalange lengths), was taken as a correction factor for each subject and each finger. The table entries for each finger were multiplied by the corresponding correction factors so that an updated table resulted where the sum of phalange lengths is equal to the reference finger length.

In order to obtain one table that is applicable to the whole subject group, the conversion factors were averaged over all subjects for each finger. The updated conversion table is shown for the index- and middle finger in Table IV.

TABLE IV
UPDATED HAND LENGTH TO PHALANGE LENGTH CONVERSION TABLE

	Proximal (L_{pp})	Medial (L_{mp})	Distal (L_{dp})
Index finger	23.5	15.2	9.3
Middle finger	26.0	16.8	10.4

Each entry represents phalange length as percentage of hand length.

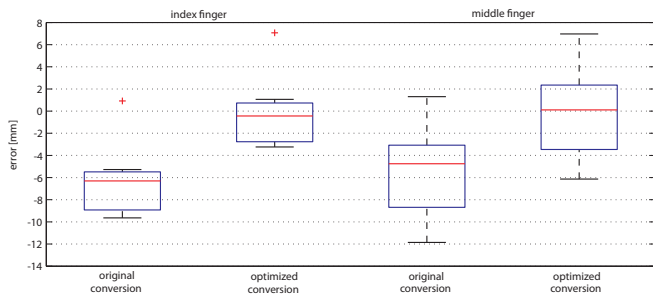


Fig. 5. Error of the finger lengths given by the sum of phalange lengths from the conversion tables, with respect to the reference finger length from measurements. Results are shown for both the original and updated conversion tables. All subjects ($N = 7$).

C. Discussion and Results

Fig. 5 shows the errors in finger lengths calculated using the two conversion tables, with respect to the reference finger lengths from measurement.

Using the original conversion table, the finger length error is $93.3\% \pm 3.8\%$ and $94.6\% \pm 4.1\%$ (mean \pm standard deviation (s.d.)) for the index- and middle finger respectively.

The mean error shows that the generated finger lengths consistently have an offset from the reference finger length. This suggests that the original conversion table is not optimal for this subject group. The optimized conversion table corrects the mean offset, while the spread is kept equal. The low s.d. indicates that a constant conversion table is suitable to estimate finger lengths for different subjects. This shows that the approach of using body proportions can be exploited to estimate finger length from a given hand length.

The optimized conversion table is based on few subjects only. If tests show that this table does not hold for new subjects, it should be optimized for a larger subject group.

In the following section, prediction of finger end-point position will be tested, using the optimized conversion table as a new model baseline for phalange length parametrization.

V. EXPERIMENTAL VALIDATION OF THE HAND MODEL

An experimental partial validation of the hand model, consisting of the index- and middle finger, was conducted in order to validate its performance of finger end-point position estimation. Furthermore, this validation should indicate the feasibility of using body proportions to parameterize the phalange lengths using only the hand length as an input.

A. Method

The hand model takes joint angles and the hand length of each subject as an input and returns the modeled Cartesian end-point position as an output. In order to verify this predicted position, it was compared to the measured fingertip marker position. This was done for each subject over the motion trajectory described in Section IV-A2.

For each point in time the end-point positions were measured. The corresponding sets of four joint angles for reaching

this position were extracted from the measured marker positions by optimization and were then used as an input into the hand model for calculation of the corresponding model fingertip positions over time.

The same hardware setup and measurement data as described in Section IV has been used for this validation test.

B. Data Processing

Along with the joint centers from Section IV-B1, joint angle sets based on the model defined axes inclinations have been calculated for each measured finger configuration.

In contrast to the estimation of joint center positions which uses only the markers of the adjoining finger segment, the optimization algorithm for calculating joint angle sets takes into account all finger markers, namely the full kinematic chain of one finger. The applied optimization algorithms are based on the methods described in [41] and [42].

For the comparison of measured and modeled data, a common base frame was required in order to represent marker positions. Each finger was assigned a finger base frame defined according to the hand model conventions and with an identical orientation for all fingers. Fingertip coordinates were then transformed and represented in the corresponding finger base frames. As shown in Fig. 4 the x-axis was directed distal along the finger, the y-axis was dorsal, and the z-axis was in the frontal plane such that it completed a right-handed coordinate frame.

C. Discussion and Results

Fig. 6 shows the plots of x, y and z components of the modeled and measured end-point positions during index finger motion (see Fig. 4 for axes definition). The corresponding error is shown in Fig. 7. This data is a typical result for one subject from the same subject group as used in Section IV.

The largest error occurs in the first third of the trajectory, which consists of a finger movement with intensive flexion. Due to the serial kinematics of the finger, small differences in finger segment lengths produce larger Cartesian end-point errors when the finger is flexed than when it is stretched. Furthermore it can be seen that the major error component is in the z-direction. This indicates a possible mismatch between joint axes inclination assumptions of the model and real axis inclinations of the human hands.

Fig. 8 shows the results for all subjects combined. The mean absolute error of the Cartesian end-point estimation using the optimized conversion is 7.0 ± 2.6 mm and 9.8 ± 2.5 mm for the index- and middle finger respectively. These results are valid for this subject group only, yet it can be seen that also the use of the original conversion from literature results in reasonable small errors, indicating that the approach of using body proportions is successful.

For the middle finger, the error is larger than for the index finger. This could suggest a larger mismatch in axis inclination angles in the middle finger.

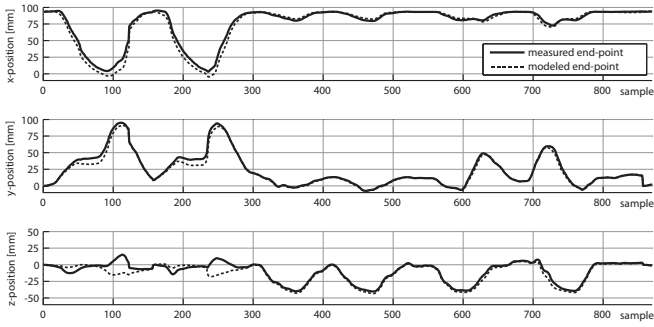


Fig. 6. Comparison of modeled and measured Cartesian fingertip position. Dataset from a single subject.

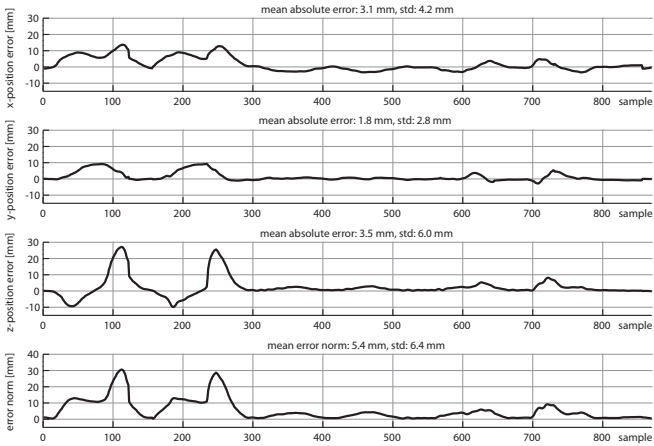


Fig. 7. Error of Cartesian fingertip position obtained from the model, with respect to that from measurement. Dataset from a single subject.

VI. CONCLUSION AND FUTURE WORK

A kinematic hand model based on the functional anatomy of the human hand was introduced. By the use of body proportions, the model is simple to adapt to different hand sizes, requiring only hand length as an input. The hand model returns an estimate of finger length and end-point position as was shown for the index- and middle finger.

Results suggest that body proportions can be exploited to derive phalange lengths from hand lengths. This approach was optimized for a subject group, showing improved results in finger length and end-point position estimation. The conversion table should be optimized for a larger subject group if the presented optimized conversion table does not hold for new subjects.

The error on end-point position estimation was found to be 7.0 ± 2.6 mm and 9.8 ± 2.5 mm for the index- and middle finger respectively. Validation results show that the mismatch between real and modeled axes inclinations forms the major contribution to this error. Further investigating the joint axes inclinations offers potential for improvement.

Since the applied conversion was optimized for the same subject group as in the validation, follow-up experiments must show if similar model predictions can be achieved for new subjects. In future work, the whole hand model and its parameterisation via body proportions should be validated.

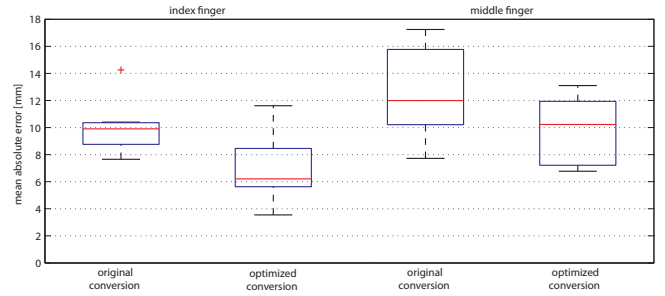


Fig. 8. Mean absolute error of Cartesian fingertip positions obtained from the model, with respect to those from measurements. All subjects ($N = 7$).

Including adaptation in hand width and palm hollowing.

The obtained results underline the practical use of the model by simple and quick adaptation to real human hand sizes, only requiring hand length as an input.

VII. ACKNOWLEDGMENTS

The authors thank G. Stillfried from DLR for his support in the data processing and G. Gil-Gómez for his illustrations (Fig. 2), summary of functional hand anatomy and the kinematic description derived from this.

REFERENCES

The references can be found in the overall bibliography at the end of this thesis.

Chapter 3

From Concept to Detailed Design and Verification:

An Efficient Grasp Master for Space Robotics Teleoperation

This paper reports on steps 1), 2), 4), and 5) of the approach (Chapter. 1.6) in the development of the efficient grasp master. It reaches from analysis of operation context via concept formulation and design of the prototype up to verification by simulation and analysis.

A user-centric approach is followed by taking into account the background analysed in Annex. C. The hand model reported in Chapter. 2 is used as a tool in the design and verification process of the device geometry, workspace and hand size robustness.

This paper was written with the intention to report on the complete process of operation context analysis, device concept formulation, prototype development, and verification by simulation and analysis. Therefore it shows a partial overlap with the introduction in Chapter. 1 and a condensed overview of the analysed context in Annex. C.

Along with Chapter. 2 this is the main body of the thesis.

An Efficient Grasp Master for Space Robotics Teleoperation

Frank P. J. van der Hulst and André Schiele

Abstract—It is the goal of this paper to present the development of an efficient grasp master device that can be used by various operators in space robotics teleoperation without requiring device adjustments.

Currently existing grasp masters share common issues that limit their use in the desired application. In general, those grasp masters appear to have a low ratio of device- and user performance versus expended resources (the device efficiency).

By following a human-centric design approach considering relevant remote tasks, required grasp types, and psychophysical effects, a reduction of the required number of degrees of freedom (DOFs) of a possible master was achieved. In combination with the separation of control and feedback channels this can constitute an efficient device concept and was elaborated into a detailed prototype design in this work.

Verification by analysis and simulation showed that key human factors- and performance requirements can be met. Lever interaction force of 5–10N (depending on the point of interaction) is reached at nominal motor torque. Controlled motor overloading allows worst-case scenarios where 10N interaction force and acceleration of 150m/s^2 can be reached at the fingertip simultaneously for periods of 7–13s.

Verification included simulation using the adaptable human hand model from [43] for workspace analysis that showed robustness against hand size variation from the 5th female- till 95th male percentile.

For the verification of device efficiency w.r.t. different existing grasp masters the use of device efficiency indicators was proposed and demonstrated. This indicates that the detailed prototype design is relatively efficient w.r.t. other compared devices, including the commercial CyberGrasp-CyberGlove, based on slave controllability, slave observability, and the quality of the force reflection.

After manufacturing of the proposed prototype, further verification by testing will be performed to define device performance. Also performance in real user interaction will be validated. The knowledge to be obtained will allow extending the framework of device efficiency indicators to form a more complete representation of overall device efficiency.

I. INTRODUCTION

WITH the recent arrival of NASA's Robonaut 2 [2] on board of the International Space Station (ISS), the first humanoid robot in space is a fact, emphasising that the field of space robotics is more alive than ever. The availability of advanced robotic systems in space comes with the need for appropriate means of control. For this purpose, the haptic

F. P. J. van der Hulst and A. Schiele are with the Telerobotics and Haptics Laboratory, European Space Research and Technology Centre, European Space Agency, 2201 AZ Noordwijk, The Netherlands, and with the Delft Biomechanical Engineering Department, Mechanical Engineering Faculty, Delft University of Technology, 2628 CD Delft, The Netherlands. Frank.van.der.Hulst@esa.int, Andre.Schiele@esa.int

human arm exoskeleton X-Arm-2 [1] has been developed for teleoperation of space robotic manipulators. This thesis reports on the development of an efficient grasp master that shall complement the X-Arm-2 to form a full haptic arm & hand master system, enabling bilateral teleoperation of robotic manipulators and their end-effectors.

A. Bilateral Teleoperation

Robots can be teleoperated when human flexibility is required to perform tasks on remote or dangerous locations. Classic examples are tasks in a nuclear-, (deep) sea-, or space environments.

The grasp master device developed within the context of this work is intended to link the operator to a large variety of robotic end-effectors. This can be either simple two-jaw grippers, multi fingered graspers or dexterous five-finger hands. The diversity of already existing slave devices underlines the importance of a generic solution for the master that allows interaction with various slaves.

The bilateral teleoperation system, in its most general form, is conceptually shown in Fig. 1. The operator input is sensed by the master device and used to control the slave device executing a task accordingly. Interactions sensed by the slave are displayed as feedback via the master device to the operator.

B. Space Robotics Teleoperation

Space robotics teleoperation is promising for its many future applications such as operation of robotic systems for planetary investigation, satellite servicing and support of extravehicular activity (EVA). The latter is maintenance and experimentation performed in an unpressurised space environment such as on the outside of the ISS [4]. In addition to being cost and time intensive, working conditions are highly limiting and impose risks and hazards to astronauts. Therefore assistance of, or substitution by, robotic systems is desirable.

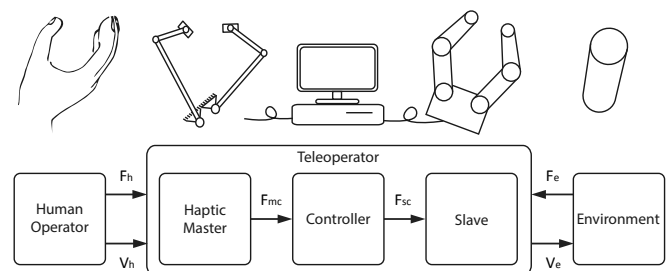


Fig. 1. General bilateral teleoperation system

Two versatile robotic platforms designed for this purpose are ESA's Eurobot [5] and NASA's Robonaut 2 [2]. Both are capable of performing similar tasks as an astronaut. The Eurobot is a non-anthropomorphic robot that uses both a limited set of specific purpose end-effectors and a general purpose robotic hand, while Robonaut 2 has a human form and two dexterous hands that allow holding and operating tools designed for humans. Robonaut 2 has been sent to the ISS in 2011 as part of the STS-133 Space Shuttle mission.

The X-Arm-2 enables bilateral teleoperation of such space robots with force-feedback. While this device does support the palm with sensing and actuated degrees of freedom (DOFs), the fingers are not supported yet. The grasp master development described in this paper will complement the X-Arm-2 in its function and philosophy and thus should allow easy integration with the X-Arm-2. It should provide the fingers with sensing and feedback functions, enabling bilateral teleoperation of various types of robotic end-effectors to perform a wide range of tasks. Just as the X-Arm-2, the hand master should be easy to use by various operators without requiring adjustments.

C. State of the Art

Some tens of grasp master devices have been reported in literature for the purposes of rehabilitation, assistance, virtual reality and teleoperation. Most masters are experimental prototypes, while few have been commercialised and are available for purchase, albeit for high costs.

The analysis of a rather complete set of devices existing at the time of writing reveals a range of issues originating from design choices that come with both advantages and drawbacks. Two influential factors in this trade-off are the placement of the device itself w.r.t. the operator and its structural complexity.

More detail on the comparison of existing master devices can be found in Annex C. V.

1) *Device Placement*: To be wearable and mobile, a complete device can be placed on the fingers and hand directly. The devices shown in [8], [9], and [11] do not only cover the hand, but the wrist as well. In [6], [7], [12], [13], [14], [15], [16], [17], [18], and [20] the arm is covered in addition. Possible issues from that are limited compatibility with the arm master due to arm coverage, low comfort, fatigue, mass and size. These drawbacks can be relieved by locating components such as actuators externally. This was done in [21], [19], [10], [23], and the commercial CyberGrasp-CyberGlove combination [24]. Here cable transmissions have been used to locate the actuators away from the hand and arm. While this can increase power density at the actuated joints as shown in [22], such designs are prone to suffer from mechanical losses, reduced backdrivability and backlash. Furthermore, external connections interfere with the arm master or might constrain the arm workspace and mobility. Those transmissions can be avoided by placing the whole device externally as a fixed base design such as in [25] and [26]. These devices can be large and heavy while avoiding aforementioned problems of arm coverage, reduced comfort and complicated transmissions, however, their drawbacks are limitation of mobility and natural human workspace.

2) *Structural Complexity*: Structural complexity is defined in terms of the amount and nature of DOFs, actuators, transmissions and components. Common reasons to apply complex designs are to support large workspace and accurate control of feedback magnitude and orientation on one or multiple positions on the fingers. To achieve this, mechanisms for joints with remote centres of rotation have been used in [9], [8], [23], [16] and [28] to allow bending around a flexing finger. Drawbacks of devices with such extensive mechanisms are their size, mass, and costs. Possible consequences of this, besides low comfort and fatigue during operation, are limited compatibility with arm master devices because collisions can occur at the wrist. Since the mechanisms are complicated and contain many joints they are susceptible to mechanical losses from friction and backlash.

Compact designs might avoid these drawbacks for the price of limited workspace and less control over force feedback direction. The Rutgers Master, as presented in [29], stands out for its small size, low mass and yet support of 4 fingers. It is especially striking to realize that this device provides a single DOF to each of 4 fingertips, while the devices in [17], [27], [26] and [9], require much more bulky and complex designs to provide a single DOF of feedback to each of 2 supported fingertips.

This poses the question whether really such complex designs are required to support such little hand functionality. This is addressed in more detail in the following section. On the other hand, the Rutgers master shows different limitations such as limited finger flexion range and an external air-compressor with connections that, similarly to the transmission of externally placed actuators, will interfere with the arm device or might limit the workspace of the arm.

D. Problem Statement

Each design choice involves a trade-off that comes with gains and losses (e.g. by accepting the losses through increased complexity, device features such as accurate control of feedback direction can be gained). In other words: *resources* can be spent to obtain *device- and user performance*.

Resources are expended in terms of mass, volume, DOFs, actuators, transmissions, components, sensors, electronics, costs, etc.

Device performance is gained in terms of arm master compatibility, sensing DOFs for slave controllability, active DOFs for slave observability, structural transparency, stiffness, mechanical bandwidth, backdrivability, resolution, decreased backlash, decreased friction, etc.

User performance is achieved in terms of robustness against hand size variation, ease-of-use, intuitive operation, comfortable donning/doffing, etc.

It is important to realize that performance achieved with 'resource expensive' solutions does not guarantee successful results in practice. As an example: in principle a resource expensive device with accurate control over force feedback direction can allow natural feedback. In practice however, complicated mechanisms are susceptible to mechanical losses and misalignments that may lead to unnatural constraint forces

and consequently uncomfortable wear and operation. The achieved device- and user performance can be low compared to the resources expended. In this sense the device is overly complex for the achieved results; we define such a device design as not efficient.

An *efficient* design, in our definition, comes with the right balance of resources expended and performance achieved. The state of the art summarized in the previous section shows that existing devices in general are expensive in terms of resources and/or show limited device- and user performance. Because of this, *the ratio of performance achieved versus resources expended (the design efficiency)* can be seen as generally too low.

E. Goal

It is the goal of this paper to present the development of an efficient grasp master device, in the sense as defined above, that can be used by varying operators for space robotics teleoperation without requiring device adjustments for interaction with different operators.

The device must be generic in the sense that it is usable in different bilateral control architectures and in combination with a large variety of dissimilar slaves.

It is hypothesised that a human-centric design approach (accounting for psychophysical effects and human factors) including separation of control and feedback channels and the reduction of mechanical DOFs can increase the overall device efficiency, as defined above.

F. Approach

II. BACKGROUND - TOWARDS HUMAN-CENTRIC DESIGN

This section summarizes the relevant tasks in remote operations, the grasp types required to perform these, and psychophysical effects involved in grasping, that might be exploited by a master device for complexity reduction.

A. Space Operations Relevant Tasks and Grasps

Distinct grasps are used by a human operator depending on the task at hand (i.e. depending on the object handled and the operation performed). Analysis of space environment operations and tools provides insight in the relevant tasks and the grasps required to perform these.

1) *Grasps in EVA Tool Use*: In [44] a classification of grasps was composed based on an analysis of tool usage in manufacturing tasks. This taxonomy, known as the Cutkosky taxonomy, makes distinction between power and precision grasps and further classifies according to geometry and task.

In [45] 242 different EVA aids, tools and interfaces from [46] were classified according to the Cutkosky taxonomy. In the concept design in Section. IV-A1 it will be shown that this data was reworked and combined into an overview showing the relative importance of grasp types in EVA tool use. In addition, application of grasp modelling in terms of oppositions gives insight in the effective functionality of each grasp type.

2) *Grasp Modelling*: When manipulating an object, the forces applied by all involved fingers combine into a limited number of resultant forces that stabilize the object in a prehensile grasp. Since the number of forces can be lower than the number of involved fingers, the concept of virtual fingers was proposed by Arbib in [47]. Each virtual finger consists of one or more physical fingers and possibly the palm that work together to exert one resultant force.

It was suggested in [48] that *virtual fingers* correspond to independently controlled contact sides, while *oppositions* proposed in [49] correspond to internal grasp forces. Using these concepts, grasp modelling can be simplified, while keeping functional aspects of the grasp clearly defined.

Three opposition types have been proposed in [50] and [49] (Fig. 2). *Pad opposition*: between the pads of one or multiple fingers and the thumb pad. *Palm opposition*: between one or multiple fingers and the hand palm. *Side opposition*: between the thumb pad and the side of the index finger.

More detail on grasp modelling using oppositions and virtual fingers can be found in Annex C. II-C.

B. Psychophysical Effects: Enslaving

Enslaving of the fingers is a psychophysical effect leading to coupled finger force perception and activation. Since this forms a reason for grouping haptic finger support, this effect has been exploited in this thesis for the reduction of DOFs, as described in more detail in Section. IV-A2.

Force production with an instructed finger tends to result in force production in adjacent uninstructed fingers during voluntary contraction [51]. As summarized from multiple references in [52] these enslaving effects were more evident in ring and little finger activity, while the index finger was the least affected by enslaving effects.

Enslaving is likely to have effect on the perception of finger forces. In [53] it was reported how the perceived finger force increased when adjacent fingers were activated. In [52] and [54], experiments with force matching tasks showed evidence that the absolute magnitude of the forces exerted by all fingers, both instructed and uninstructed, is perceived.

An effect observed in [51], that might result from the differences in coupling, is that the the index finger force is the most accurately estimated, while the little finger force is the least. These are important findings that are used as guidelines to allow for reducing master device complexity, while keeping sufficient feedback information.

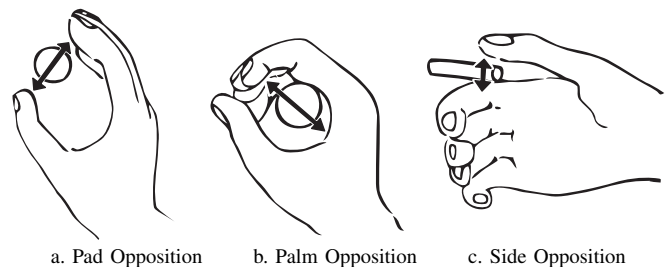


Fig. 2. Opposition types for grasp modelling. Adapted from [49]

III. SUMMARY OF KEY REQUIREMENTS

This section summarises the requirements from human factors and general teleoperation performance requirements.

A. Human Factors

Human factors provide important requirements for the prototype design in Section. V. It is important to realise that the presented data in many cases is based on varying experiments with small or unknown subject groups, these values should therefore be considered as rough indications only.

The human factors summarised in the following sections have been further elaborated in Annex A.1.

1) *Maximum Finger Force*: Several experiments have been performed in [55], [56], and [57] to obtain an indication of fingertip force. From this information the following maximum force levels result: 50–65 N for the index finger, 48–68 N for the middle finger, 37–44 N for the ring finger, and 31 N for the little finger. It is assumed that the reported values correspond to the maximum voluntary contraction (MVC),

Muscle fatigue, resulting in discomfort, pain and shifting of force perception can be avoided by remaining below 15% MVC for long durations and remaining below 25% MVC for short durations [58].

This results in the requirement that the grasp master should be able to display force levels of 15% MVC continuously. That is: 8–10 N for the index finger, 7–10 N for the middle finger, 6–7 N for the ring finger, and 5 N for the little finger. Short term force levels up to 25% MVC can be suggested. Higher levels should be avoided considering fatigue and discomfort.

2) *Finger Force Magnitude JND*: The resolution of force perception is expressed in terms of just noticeable difference (JND), which is defined as "the minimum noticeable variation between a base stimulus intensity and an increased or decreased stimulus intensity" [59]. By combining results from that source and [60], [61], [62], [63], an indication of force magnitude JND is obtained, being 5-13% at reference force levels ranging from 0.77–10 N. At lower reference force levels, the JND increases considerably [59].

Based on this, the grasp master is required to provide force feedback with a resolution of 0.04 N (5% of 0.77N) or better.

3) *Finger Force Direction JND*: In [64] it was found that force direction JND roughly ranged from 26–32°. According to [65], this JND is not dependent on absolute reference force direction.

This suggests that the force reflected by a grasp masters may have a direction mismatch up to 26° without the user being able to perceive this.

4) *Finger Joint Angle JND*: In [65] finger joint angle perception JND was found to be 2.5° for the PIP joint and 2.0–2.7° for the MCP joint. It was derived that this results in a JND at the fingertip of roughly 2.2 mm.

This suggests that a grasp masters may have a position mismatch up to the listed values without the operator being able to perceive this.

5) *Maximum Fingertip Velocity*: In [66] it was suggested during an expert survey to support human fingertip velocity of 1.1 m/s. In [8] a preliminary experiment gave a comparable result of 1.0 m/s. Also it was stated that 0.95 m/s was sufficient to track finger flexion.

Judging from this data, the device should support the finger up to a fingertip velocity of 1.0 m/s.

6) *Maximum Fingertip Acceleration*: In [66] it was suggested during an expert survey to support human fingertip acceleration of 12.2 m/s². In [8] a preliminary experiment gave a different result of 300 m/s². The device constructed in the same source reached a tip acceleration of 350 m/s² during flexion. It was stated that this was sufficient to track the human finger movement.

Judging from this scarce data, a maximum fingertip acceleration of roughly 300 m/s² could be suggested, but should not be considered a stringent requirement.

7) *Bandwidth*: In [66], it was described that the human is able to exert motion and force with bandwidths up to 5-10 Hz depending on the given task and to sense with bandwidths ranging up to 20 and 30 Hz for kinesthetic- and proprioceptive sensing respectively. Tactile sensing of vibrational information up to 10,000 Hz has been reported, yet the ability to discriminate vibrations declines above 320 Hz.

Judging from this, a grasp master should have a mechanical bandwidth of at least 30 Hz. If displaying vibrational information is desired, the output bandwidth should go up to 320 Hz. Preserving a realistic sensation, higher frequencies can be mapped down to this bandwidth.

B. Device Performance

In [66], [57], and [67] guidelines for performance required in haptic master devices have been summarized. These can be used during the design process to work towards achieving good performance at the device-body interfaces. Because of the diversity of this information, it is not summarised here further.

IV. CONCEPT DESIGN

With a reduction of DOFs the device gets less expensive in terms of resources such as mass, volume, parts, actuators, costs, power, control and electronics. At the same time, the simpler design holds less mechanical losses and can be compatible with an arm master. This leads to better device performance. Also, better user performance can be achieved in a simpler device by more light-weight, small size and usable designs.

This approach allows the reduction of resources expended and the increase of performance. Therefore, this works two-way in achieving increased device efficiency.

Separation of sensor and actuator paths is proposed to increase slave controllability with respect to observability. The consequent controllability-observability asymmetry is made suitable for interaction with varying slave types by applying the concepts of grasp mapping and grasp primitive switching.

A. Reduction of Mechanical DOFs

Reduction of DOFs is achieved by taking into account the most important grasping functions and exploiting psychophysical effects.

1) *Predominant Grasping Functions*: By reworking the presented information on the classification of grasp in EVA tool use [45] and by combining this with grasp modelling by oppositions [49], as presented in Section. II-A, Table. I was constructed. This indicates the percentage of all power- and precision grasps belonging to each of six grasp categories. The opposition types used in the different grasp categories are listed, except for the composite grasps which contain multiple oppositions simultaneously.

As shown in the table, 60% of all power grasps are cylindrical power grasps and 31% are composite grasps. Only 9% are circular power grasps. Of all precision grasps 90% are thumb - 1/2 finger pinch grasps. The thumb - 3/4 finger pinch and circular precision pinch are used least often with 2% and 8% respectively.

The subset of cylindrical power grasps, composite grasps, and thumb - 1/2 finger precision pinches thus is used most often in EVA tool use. It should be noted that the composite grasps all require side opposition of the thumb with the index finger. This generally is not supported by robotic slaves, which makes the relevance of composite grasps low in a hand master device.

TABLE I
EVA TOOLS OPERATION - GRASP USE AND OPPOSITIONS

Power Grasps		
Grasp Category		palm oppositions
Cylindrical Power Grasps	60%	2-4, 2-5 – palm
Composite Grasps	31%	note*
Circular Power Grasps	9%	2-3, 2-4, 2-5 – palm
Precision Grasps		
Grasp Category		pad oppositions
Thumb - 1/2 Finger Pinch	90%	2, 2-3 – thumb
Thumb - 3/4 Finger Pinch	2%	2-4, 2-5 – thumb
Circular Precision Grasps	8%	2-3, 2-4, 2-5 – thumb

Reworked representation of data adapted from [45] where grasping on 242 EVA aids, tools and interfaces was analysed and classified according to the Cutkosky Taxonomy [44]. This table indicates which percentage of all power- and all precision grasps belongs to the different grasp categories (e.g. 60% of all power grasps on EVA tools is of a cylindrical type).

Fingers are indicated with numbers: 1: thumb, 2: index-, 3: middle-, 4: ring-, 5: little finger.

Palm and pad oppositions indicate the finger or finger groups in oppositions with the palm and thumb respectively (e.g. 2-4 – palm: the grouped index-, middle-, and ring finger oppose the palm).

The categories are composed of the grasps from the Cutkosky taxonomy as follows: *Cylindrical power grasps*: small diameter, medium wrap, large diameter. *Composite grasps*: adducted thumb, light tool, lateral pinch. *Circular power grasps*: disk (power), sphere (power). *Thumb - 1/2 finger precision grasp*: thumb - 1 finger, thumb - 2 finger. *Thumb - 3/4 finger precision grasp*: thumb - 3 finger, thumb - 4 finger. *Circular precision grasps*: disk (precision), sphere (precision).

* Composite grasps contain multiple simultaneous opposition types in a single grasp. These are not listed here.

The only oppositions in cylindrical power grasps are 2-4 and 2-5 – palm opposition while the only oppositions in thumb - 1/2 finger precision grasps are 2 and 2-3 – thumb pad opposition. Thus, to perform 60% of all power grasps and 90% of all precision grasps only four oppositions are required. These predominant grasping functions are shown in Fig. 3.

2) *Grouped Finger Support*: The enslaving effects introduced in Section. II-B lead to coupled finger force perception and activation. This effect can be exploited in the reduction of DOFs by grouping the fingers that show strong enslaving effects. It is proposed to provide individual support to the index finger (least enslaving and best force accuracy) and to group the middle-, ring-, and little fingers.

This grouping does not mean that the fingers are constraint together, but rather that those fingers receive feedback as a group. When leaving the fingers unconnected from the device, the proposed finger grouping allows to perform all predominant grasping functions (Fig. 3). Unconnected fingers effectively are able to exclude from the group (e.g. when making the finger 2-3 – thumb pad opposition, the ring- and little finger do not flex and thus are not in contact with the device and do not receive feedback of constraint forces). It is important to note that finger contact must be detected when e.g. only feedback to one or some fingers is desired. Leaving the fingers unconnected results in comfortable operation where no constraint forces act on the fingers. Moreover, this configuration also allows to perform part of the less used grasps, such as the thumb - 3/4 finger pinches, or even holding a powered pistol grip tool such as a torque driver or flash light with the fingers 3-5 and using finger 2 to control or activate the tool.

3) *Pinch Grasping Support*: In order to reduce the mechanical complexity of the grasp master even further, the palm oppositions can be replaced by pad oppositions between the same fingers. In practice this means that palm oppositions in the slave are controlled using pad oppositions in the master and thus there is a mismatch between operator and slave postures. This results in the set of oppositions supported by the grasp master as shown in Fig. 4.

The reasoning behind this decision is the assumption that human operators do not require a perfect match between the posture/motion of the slave finger and their own finger for natural perception in teleoperation. This because the JND of joint angle perception at the fingers is rather low, being 2.5° at the PIP joint and $2.0-2.7^\circ$ at the MCP joint as summarized

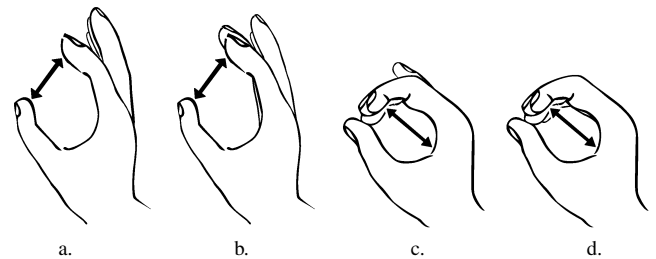


Fig. 3. Predominant grasping functions in EVA tool use: a. finger 2 - thumb pad opposition, b. fingers (2-3) - thumb pad opposition, c. fingers (2-4) - palm opposition, d. fingers (2-5) - palm opposition. Oppositions a. and b. allow 90% of all precision grasps. c. and d. allow 60% of all power grasps.

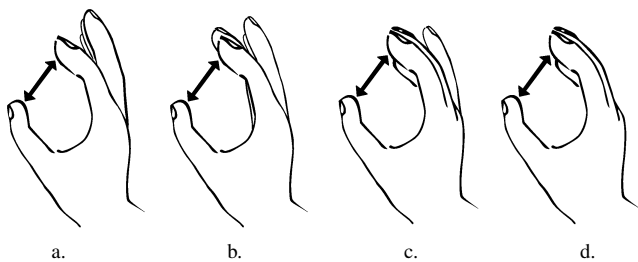


Fig. 4. Oppositions supported in the grasp master: a. finger 2 - thumb pad opposition, b. fingers (2-3) - thumb pad opposition, c. fingers (2-4) - thumb pad opposition, d. fingers (2-5) - thumb pad opposition

in Section. III-A. Also the JND of force direction is low, being roughly 26-32% as summarized in the same section. Furthermore, as stated in [67], resolution is the most critical feature of a haptic device, while precision matters less. Finally, it is important to realize that when operating slave devices that are dissimilar from the human hand, a mismatch between human and slave posture and motion is unavoidable.

B. Device Structure

The rough concept structure proposal is shown in Fig. 5. The main components are the device body where the actuators are placed, the hand support where the operator's hand slides through and three levers to support the fingers. All fingers are left unconnected from the levers and the fingers 3-5 are grouped, as proposed in Section IV-A2. The thumb lever is fixed to the device body, while the index finger lever and the grouped finger lever both have a single actuated rotary DOF at their base. This allows pinching between the fingers and the thumb.

While many devices suffer from unnatural reaction forces in the fingers or hand, termed the 'force ground', this concept exploits the force ground as useful and natural pinching feedback by placing it on the thumb.

C. Controllability Increase by Separation of Sensor and Actuator Paths

As in classical designs, sensors are placed in the actuated DOFs. This means that when few actuators are used to keep

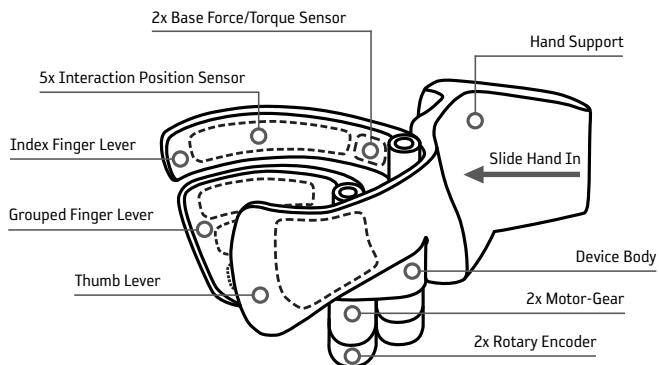


Fig. 5. Grasp master concept device structure

mass and size low, as a consequence few sensors are used. Separation of sensor- and actuator paths allows the use of sensors different in number, nature and position than the actuators. This enables flexibility in device construction to achieve an efficient design.

Especially effective for improving efficiency is exploiting sensor-actuator asymmetry by spending few expensive resources (e.g. actuators) while not limiting the use of inexpensive resources (e.g. position sensors).

1) *Interaction Point Sensing*: As outlined in Section. IV-A2 the fingers are left unconnected from the device. This requires sensing the positions of finger-device interaction such as by position sensors placed on the lever surface. So, while having 2 actuated and sensed DOFs at the lever base, the sensing dimensionality can be increased with a position sensing DOF for each fingertip position.

Additional force/torque sensors can be placed at the base of the levers for measuring the actual interaction force/torque. From the measured force/torque and the point of interaction, the interaction force can be estimated.

The placement of all sensors and actuators is indicated in the concept device structure in Fig. 5.

2) *Control Parameters*: In the proposed concept, multiple signals are available for sensing and/or reflection. The joint space parameters \hat{q} comprise the joint torque τ_i , joint angle θ_i , and joint angular velocity ω_i . The operational space parameters $\hat{\Psi}$ comprise the interaction force F_i , interaction point d_i , and interaction point velocity \dot{d}_i . All control parameters are indicated in Fig. 6.

Table. II lists all joint- and operational space parameters to indicate how these are sensed and whether these are controllable. Three signals are sensed directly: angular position of the rotating axis θ_i , force/torque at the lever base F/T_i , and the point of interaction on the lever surface p_i . From these signals, the parameters τ_i , F_i , and d_i (composed of d_{x_i} and d_{y_i}) are derived. The parameters ω_i and \dot{d}_i are derivatives of θ_i and d_i respectively.

Alternatively to deriving τ_i from the force torque and position sensor signals, it could be derived from the motor torque τ_{mi} , which is directly related by the torque constant to the applied motor current. Considering the dynamics and non-linearities of the transmission from the motor to the joint axis, the first option gives a more accurate estimate of the actual joint torque.

The availability of force, position and velocity sensor in-

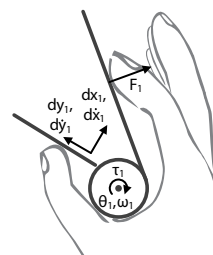


Fig. 6. Joint space parameters of the upper lever (one active dof) (τ_1 , θ_1 , ω_1) and operational space parameters of the index finger (F_1 , d_{x1} , d_{y1} , \dot{d}_{x1} , \dot{d}_{y1}).

TABLE II
JOINT- AND OPERATIONAL SPACE PARAMETERS SENSING AND CONTROL

Joint Space Parameters			
	τ_i	θ_i	ω_i
Sensing	$f(F/T_i, p_i)$ or $f(\tau_{mi})$	direct	$\frac{d}{dt}\theta_i$
Control	Torque Loop	Position Loop	Velocity Loop

Operational Space Parameters			
	F_i	d_i	\dot{d}_i
Sensing	$f(F/T_i, p_i)$	$f(p_i, \theta_i)$	$\frac{d}{dt}d_i$
Control	Force Loop	-	-

For each joint- and operation space parameter it is indicated whether it is directly sensed, or derived from other parameters. Also it is indicated which parameters can be controlled.

F/T_i is the force/torque sensor signal, p_i is the lever surface position sensor signal.

Note: the joint torque τ_i can be estimated via two different methods. That is: as function of p_i and the force/torque sensor signal F/T_i , or as function of the motor torque τ_{mi} (this signal is available as the sensed motor current multiplied by the torque constant).

formation allows implementation of various bilateral control architectures such as different 2-channel or the 4-channel architectures [68]. Detailed controller implementations depend on the full teleoperator system including the slave device and will not be considered further here.

D. Generic Slave Operation

Various slave devices come with differences in number of fingers, number of DOFs, workspace and control. Providing generic slave support by a grasp master thus requires controlling and observing dissimilar slave grasps.

This involves dealing with unequal sensing and/or actuation dimensionality between master and slave, termed controllability–observability asymmetry. When the number of sensed master DOFs matches the number of actuated slave DOFs, the master offers full controllability of the slave. When the number of actuated master DOFs matches the number of sensed slave DOFs, the master offers full observability of the slave.

Considering the low amount of actuators in the grasp master, observability will be limited in most cases. However, in [69] it was shown that a low number of actuated DOFs still can lead to good grasping performance. The extra sensing functions in the master offer increased controllability, but still this might be lower than the number of actuated slave DOFs. Means to deal with controllability–observability asymmetry for varying slaves are proposed in the following sections as ‘grasp mapping’ and ‘grasp primitive selection’.

1) *Grasp Mapping*: Fig. 7 conceptually shows how the master can be interfaced to slave devices of different nature and complexity. In the theoretical case that a slave is identical to the master, the slave is fully controllable and observable. Here ‘identical’ means being equal in structure and having the same inputs as the master has outputs and the same outputs as the master has inputs.

When the slave is less complex than the master, the available master outputs should be mapped to a lower number of slave inputs and the available slave outputs should be mapped to a higher number of master inputs. When a more complex slave is interfaced, the available master outputs should be mapped to a higher number of slave inputs and the available slave outputs should be mapped to a lower number of master inputs. Naturally, also variations could exist where the slave inputs have higher- and the slave outputs have lower dimensionality

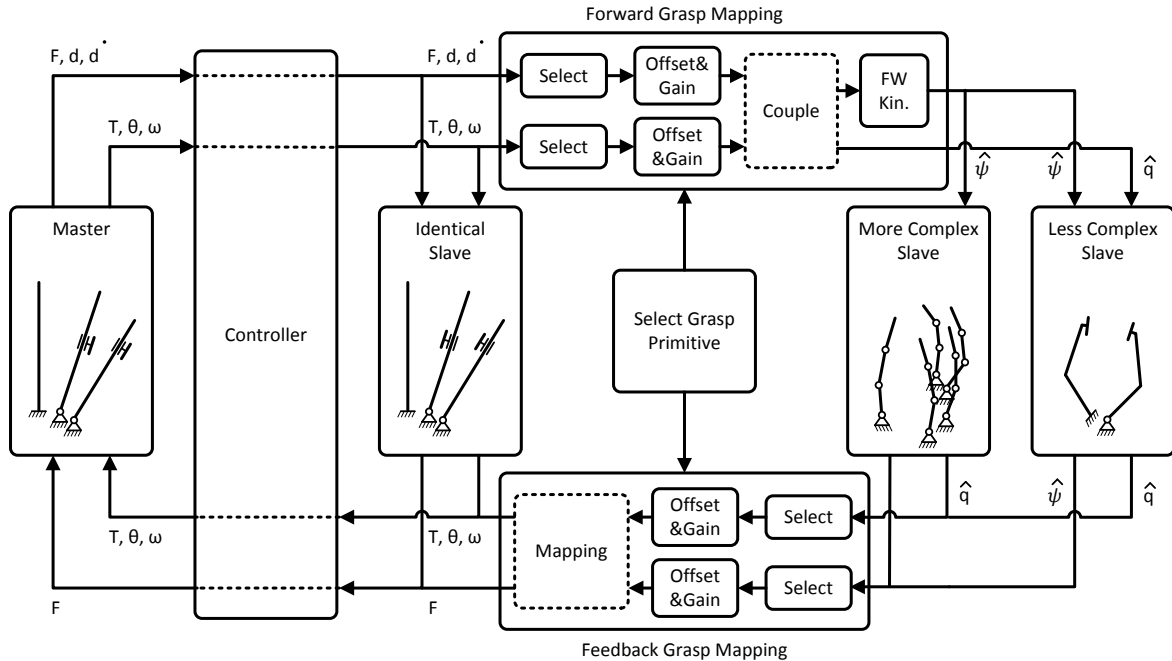


Fig. 7. Conceptual diagram of generic slave interaction, describing how the master can be interfaced to slaves of different nature and complexity.

than the master outputs and inputs respectively, or vice versa.

The forward grasp mapping defines which master outputs are used (selected), the offsets and gains on these signals, and possible couplings to either increase or reduce the number of parameters available as an input to the slave. Similarly, the feedback grasp mapping allows increasing or reducing the number of parameters available as an input to the master.

For the less complex slave shown in Fig. 7, both joint- and operational space parameters could be used (e.g. for controlling or sensing, either the joint torque (joint space) or pinching force (operational space) could be used). For a complex slave, the set of joint space parameters that should be controlled is much larger than the signals available from the masters. Here, the slave can be controlled in operational space, possibly involving inverse kinematics at the slave side. Similarly, observing the slave requires reducing the set of signals from the slave.

2) *Grasp Primitive Selection*: A pair of forward- and feedback grasp mappings, termed a 'grasp primitive' defines interaction with a slave device using a single grasp type. It is proposed to allow the operator to actively select from a predefined set of grasp primitives of the slave to enable choosing the grasp type most suitable to perform the actual task at hand. For example, when using a 5-fingered dexterous slave, the operator selects a thumb – 2-finger pinch grasp primitive or a 5 finger cylindrical power grasp primitive depending on the task to be performed. With this choice, the forward- and feedback mappings are updated to implement the behaviour of the selected grasp primitive.

V. DETAILED DESIGN

While taking into account performance- and human factors requirements given in Section. III, a detailed prototype design was established from the concept proposed in Section. IV.

Along the design process, the concept was verified by simulation and analysis. This includes using the adaptable hand model presented in [43] for analysis of device geometry, workspace and robustness against hand size variation.

In addition, controlled motor overloading, that should allow increasing power density for limited duration, was analysed.

As will be discussed in Section. VII, the detailed prototype design was found to fulfil the intended concept and is planned to be implemented for performing verification by testing of device functions and for validation in real user interaction.

A. Prototype Overview

An overview of the prototype design and its components is shown in Fig. 8. The device consists of a body where the motors and transmissions are located, a hand support, and three levers for the thumb, index finger and grouped middle-, ring-, and little finger.

The operator's hand slides through the hand support, placing the fingers on the corresponding levers. This support is only intended for positioning and holding the device in the hand. No significant reaction force is reflected to the hand since in the supported pinch grasping motions the force ground resides at the thumb to provide useful reaction force. The hand support

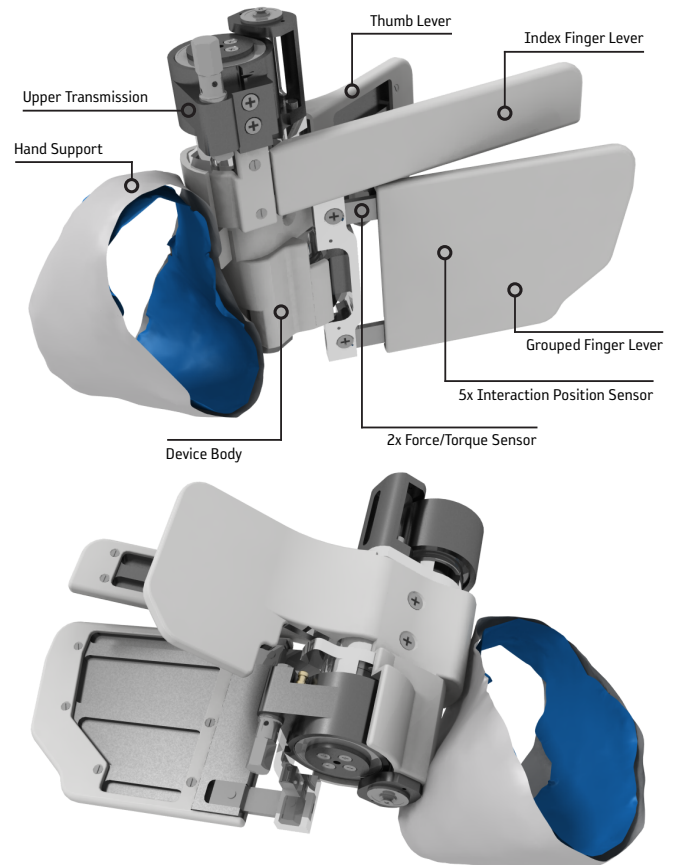


Fig. 8. Grasp master detailed prototype design CAD model. The upper view shows the side with the moving levers where the fingers interact. The lower view shows the side of the thumb lever that is rigidly connected to the device body. The operator's right hand slides in through the hand support such that the palm and dorsal side of the hand contact the blue surface and the fingers rest on the corresponding levers.

only contacts the steady part of the palm and the dorsal side of the hand, avoiding contact with joints and phalanges to ensure that the workspace is not limited. Although not shown in this figure, the hand support should allow comfortable donning/doffing and operation to different hand sizes by using a quick fixture such as a Velcro band on the dorsal side.

A schematic representation of the functional device structure is shown in Fig. 9. This describes how all components physically are interconnected. The thumb lever is rigidly connected to the device body and only contains a position sensor. The index finger lever and grouped finger lever both consists of a full drivetrain, including a motor-gearhead-encoder combination, Capstan transmission, force/torque sensor, a lever, and position sensors (one for each finger).

B. Mechanical Construction

The mechanical construction consists of an upper half that includes the full drivetrain of the upper lever and a lower half that includes the drivetrain of the lower lever. The upper half is shown in Fig. 10 along with views of the physical sensors and actuators.

Each lever is actuated by one Maxon EC13 brushless motor (13 mm diameter, 12 Watt, including Hall sensors) with a

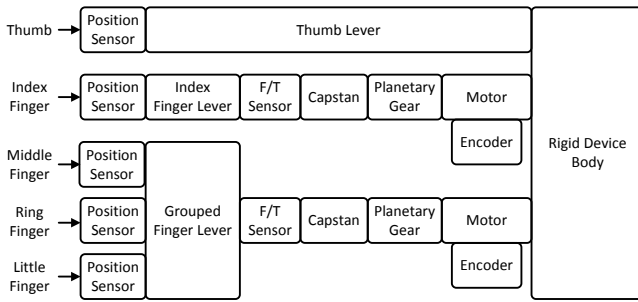


Fig. 9. Schematic representation of the functional device structure. The three levers are shown including the drivetrain for the index finger lever and the grouped finger lever.

GP13A planetary gearhead (26:1 reduction ratio) and encoder MR Type S (256 counts/turn). The motors are controlled by a Maxon EPOS2 24/2 drive.

This motor type was selected for its small size, low mass, low torque ripple, and high power density. In addition, its thermal characteristics are specifically suitable for short term overloading as will be analysed in Section. VI-C2. For the same purpose, the mechanical design ensures increased heat capacity and good conductive contact of plain aluminium components over the full length of the motor.

The levers are connected via force/torque sensors to the rotating base to allow sensing the finger interaction. These BCM Sensor Technologies' 159A bending beam sensors consist of a thin steel plate with 4 strain gauges mounted in a Wheatstone bridge configuration to sense bending deflection while rejecting components from torsion.

Tekscan Flexipot resistive membrane linear position sensors are placed on the lever surface. This is basically a touch-sensitive linear potentiometer. One position sensor is located on the thumb lever, one on the index finger lever, and three on the grouped finger lever (one for each finger).

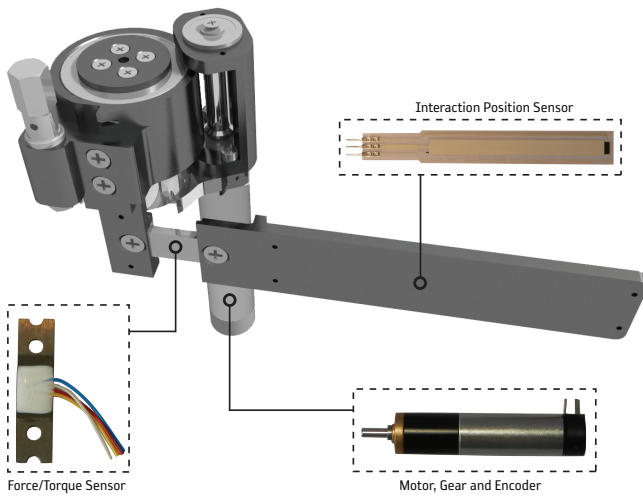


Fig. 10. Upper device half consisting of the full drivetrain for the index finger lever only. This consists of a motor-gear-encoder combination that drives the Capstan transmission. The lever is connected via a force/torque sensor to the outside of the rotating Capstan drum

It should be noted that standard sensors have been applied in the prototype, yet this technology allows for custom shapes to optimize finger contact position. Alternatively, capacitive position sensors - as used in touch-screen and touch panel devices such as smartphones - can be used, providing more flexibility in placement and configuration for the price of more complex electronics.

C. Drivetrain Design

The drivetrain of each lever is composed of the actuator with gearhead, Capstan transmission, and lever. The motor-gear combination drives the low-diameter Capstan spindle that on its turn drives the larger-diameter Capstan drum onto which the lever is connected via the force/torque sensor. This is shown in Fig. 10 for the index finger lever.

The selection of all components in the drivetrain was an iterative process that not only involved parameters inside the drivetrain (such as size, efficiency, reduction ration, and thermal behaviour), but also parameters from outside the drivetrain that influenced the required output torque and velocity, such as the inertia and points of interaction that depend on the geometric.

1) *Gear-Capstan Transmission:* Since miniature motors typically have low output torques, a considerable reduction ratio is required to achieve sufficient torque at the lever base. To avoid low efficiency and high backlash involved with multi-stage gearheads, a Capstan transmission, introducing negligible friction and backlash, was used in combination with a low reduction planetary gearhead. Like presented in [1], the resulting transmission has high efficiency and low backlash. The price to pay is the increased structure size from the Capstan gear, but as can be seen in Fig. 11, this is compensated for by locating the motors partially inside the free space in this structure.

A planetary gearhead with reduction ration 26:1 in combination with a Capstan reduction ration of 5.5:1 was found as a suitable solution with a sufficiently small design achieving the required lever force and velocity.

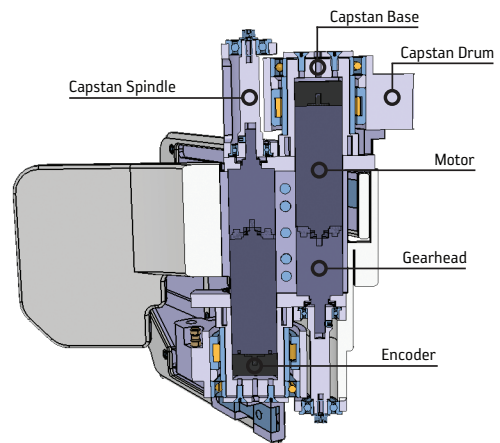


Fig. 11. Cross-section of the full device. This shows how the actuators are shifted inside the Capstan transmissions for size reduction. Furthermore, the mechanical construction of the drivetrain including the motor, gearhead, Capstan spindle and Capstan drum is can be seen.

2) *Capstan Construction*: In Fig. 11 the cross-section of the complete Capstan transmission can be seen. The gearhead output axis drives the Capstan spindle ($\varnothing 5.45$ mm) and the spindle drives the Capstan drum ($\varnothing 30$ mm) via a tensioned cable wound multiple times around the spindle and connected to the Capstan drum.

The spindle is suspended by two ball bearings to offload the motor shaft from high radial forces. The construction allows easy assembly/disassembly and axial pre-tensioning of the bearings. The Capstan drum rotates around a fixed base with a ball bearing that constrains axial displacement and takes axial force components and a needle roller bearing to take the higher radial force components.

3) *Capstan Cable Tensioning*: The cable that connects the Capstan spindle to the drum is coated Dyneema SK75 ($\varnothing 1$ mm). It was selected for its high specified tensile strength of 130 kg and low stretch of $< 1\%$.

The system was designed such that high cable tension can be achieved via a repeatable procedure. The cable is connected around a pin at one end (Fig. 12 left) and is constraint with a steel pin, spliced through the cable, behind a small hook at the other end (Fig. 12 right). For tensioning, the cable is wound around a 'cable tensioner' that can be rotated using a standard torque driver. After this, the cable tensioner can be removed for size and mass reduction.

D. Torque Propagation Modelling

The propagation of the motor torque T_m through the full drivetrain up to the actual output torque T_o provided to the operator, is modelled as shown in Fig. 13. Annex. A.3 gives more detail on the model.

The reduction ratios of the gearhead N_g and Capstan transmission N_c increase the torque towards the output, while losses from motor friction $T_{m,w}$, gearhead friction $T_{g,w}$, and Capstan friction $T_{c,w}$ reduce the actual outputs torque. Here the gearhead- and Capstan friction are accounted for by the efficiency terms $\eta_g = 83\%$ and $\eta_c \approx 100\%$ (assumption) respectively. The motor friction torque is given by the product of the torque constant $k_m = 6.42 \frac{mNm}{A}$ and the no-load current $I_0 = 79.2mA$, that is: $T_{m,w} = 0.51mNm$.

Since torque is required to accelerate all inertial elements in the drivetrain, the actual output torque is a function of the

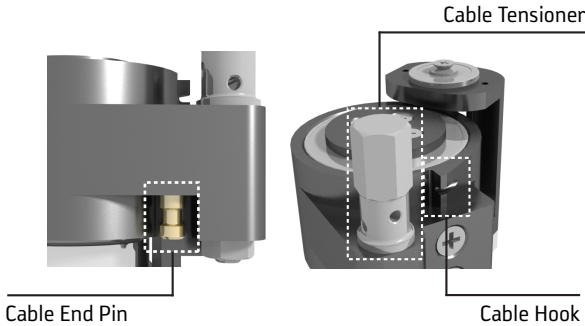


Fig. 12. Detailed view of Capstan cable tensioning mechanism. The cable is tightened by rotating the tensioner tool and is locked behind the hook. After this, the tensioner tool can be removed.

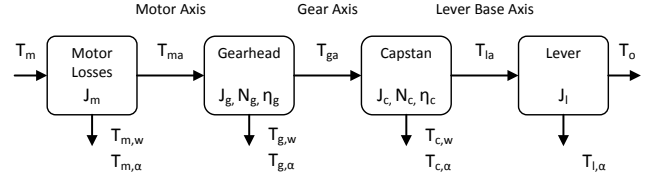


Fig. 13. Drivetrain torque propagation model including reduction ratios, friction losses (by gear efficiency), and torque components for acceleration.

acceleration. The torque required for acceleration is given by the products of the motor, gearhead, Capstan, and load inertias (J_m , J_g , J_c , and J_l respectively) with the accelerations at the corresponding points in the system. That is: α_{ma} , α_{ga} , and α_{la} are the accelerations at the motor axis, gear axis (between gearhead and Capstan) and load axis (the lever base) respectively. The accelerations are related by the reduction ratios as: $\alpha_{ga} = N_c \alpha_{la}$ and $\alpha_{ma} = N_g \alpha_{ga}$.

Combining these relations results in (1) expressing the actual output torque to the operator. This equation will be used in Section. VI-C1 for the verification of available torque for force reflection to the operator.

$$T_o = ((T_{ma} - T_{g,\alpha}) N_g \eta_g - T_{c,\alpha}) N_c \eta_c - T_{l,\alpha} \quad (1)$$

with the torque at the motor output axis:

$$T_{ma} = T_m - T_{m,\alpha} - T_{m,w}$$

and with the acceleration torques as function of the acceleration at the lever base α_{la} :

$$T_{m,\alpha} = J_m \alpha_{ma} = J_m N_g N_c \alpha_{la}$$

$$T_{g,\alpha} = J_g \alpha_{ga} = J_g N_g N_c \alpha_{la}$$

$$T_{c,\alpha} = J_c \alpha_{ga} = J_c N_c \alpha_{la}$$

$$T_{l,\alpha} = J_l \alpha_{la}$$

1) *Inertial Components*: The motor (rotor) inertia and gear inertia are specified in the data sheets as $J_m = 0.325gcm^2$ and $J_g = 0.015gcm^2$ respectively. The Capstan inertia at the input axis (that is the gear axis in Fig. 13) is given by:

$$J_c = J_{cSpindle} + \frac{J_{cDrum}}{N_c^2 \eta_c} \quad (2)$$

J_{cDrum} is the inertia of the Capstan drum, $J_{cSpindle}$ is the inertia of the Capstan spindle, and J_l contains all inertia of the lever and the connected components. These components were obtained from the CAD model as: $J_{cSpindle} = 0.171gcm^2$, Capstan drum inertia $J_{cDrum} = 64.5gcm^2$, upper lever inertia $J_{lUpper} = 934.1gcm^2$, and lower lever inertia $J_{lLower} = 1957gcm^2$.

Filling in (2) gives an input inertia of the Capstan transmission of $J_c = 2.30gcm^2$ when $N_c = 5.5$ en $\eta_c = 100\%$.

VI. RESULTS

This section covers the verification of the resulting detailed prototype design that was developed to implement the efficient grasp master concept proposed in Section. IV. This includes verification of the achieved device efficiency w.r.t. other existing grasp masters and the verification of the performance- and human factors requirements summarized in Section. III.

This prototype will be manufactured to allow further verification by testing and validation in real user operation. The complete set of CAD drawings can be found in Annex. B.

A. Efficiency Comparison

The development process was aimed at achieving an efficient design. That is, a design where the ratio of device- and user performance achieved versus the resources expended is high. This was outlined in Section. I-D where the design efficiency was defined as (3) and where a list with examples of *resources*, *device performance* and *user performance* was given.

$$\text{Efficiency} = \frac{\text{Device Performance} + \text{User Performance}}{\text{Resources}} \quad (3)$$

The verification of overall device efficiency requires a framework that quantifies resources, device performance, user performance, and the relations between those concepts. This is a complex problem considering the large design space and the fact that not all factors involved are (easily) measurable or quantifiable. This is underlined by [67] where it was stated that comparison between haptic devices remains difficult since no consensus has been reached in the specification and evaluation of haptic devices.

The summarised issues prevent the exact quantification of the overall device efficiency by the use of detailed performance metrics. Nonetheless, an indication of device efficiency can be obtained by comparing the bits of information that actually have been reported. Therefore we introduce the concept of *device efficiency indicators (DEI)* that define the relations between well-specified measures of performance in relation to well-specified measures of expended resources.

The following analysis considers a limited number of device efficiency indicators. It is proposed to use overall mass as a first straight-forward measure of expended resources. This way, a DEI effectively indicates mass performance density. Similarly, using volume as measure of expended resources effectively indicates volume performance density. Since volume has been scarcely reported for existing devices, mass is used in the following analysis.

As performance measures for the slave observability and controllability that a grasp master provides, it is proposed to analyse the actuated and sensed DOFs at the points of interaction. This covers only an aspect of the overall device performance, but is of high relevance in the operation of slave devices. The performance metrics have been defined at the end-points where device-body interaction takes place. This does not necessarily include all device-body interfaces since a haptic device might connect to multiple phalanges of

the finger, however, the end-point interaction exists for each supported finger and is thus specified for each device, basically enabling comparison of all devices based on this metric. (Note: the end-point does not necessarily need to be the fingertip).

1) *Performance: Slave Observability*: For each finger supported by a haptic master device there is one end-point interaction of maximally 6 DOFs. This results in a maximum of 30 end-point DOFs when all fingers are supported. The total number of unique actuated end-point DOFs N_{DOFa} is a measure of the slave observability enabled by the master. By taking this as a performance measure, and the mass M as measure of resources expended, the efficiency indicator for slave observability DEI_{obs} is defined by:

$$DEI_{obs} = \frac{1}{M} \sum_{i=1}^{N_{DOFa}} \kappa_{a,i} \quad (4)$$

Here $\kappa_{a,i}$ accounts for the types of control available per actuated DOF. $\kappa_{a,i} = 1$ when either torque or position/velocity control is available. When both are available $\kappa_{a,i} = 2$.

2) *Performance: Slave Controllability*: Similarly to the efficiency for slave observability, the indicator for slave controllability can be defined with the number of uniquely sensed end-point DOFs N_{DOFs} by:

$$DEI_{ctr} = \frac{1}{M} \sum_{i=1}^{N_{DOFs}} \kappa_{s,i} \quad (5)$$

Here $\kappa_{s,i}$ accounts for the types of sensory information available per sensed DOF. $\kappa_{s,i}$ is equal to the amount of sensed signal types from the set of {torque-, position/velocity-, and acceleration} sensing.

3) *Performance: quality of Reflection*: While the device efficiency indicator for slave observability DEI_{obs} contains information on the quantity of observed DOFs, no information is contained about the quality of the reflected force, position, and/or velocity. This can be captured into the quality factors QF_F , QF_d , and QF_i respectively.

Here, the quality factor QF_F will be further elaborated. It represents the quality of the interaction force in terms of the range, resolution, and mechanical bandwidth, all measured at the device-body interface. The human factor requirements in Section. III-A define the minimum levels that should be achieved. That is: a force range of 15% MVC (10 N, 10 N, 7 N, and 5 N for the index-, middle-, ring-, and little finger respectively), a force resolution of 0.04 N and a mechanical bandwidth of 30 Hz. The quality factor, given by (6) is unity when all these requirements are met, if not, it is < 1 .

$$QF_F = \frac{1}{N_f} \sum_{i=1}^{N_f} \left(\frac{1}{3} (QF_{F,i} + QF_{resF,i} + QF_{bwF,i}) \right) \quad (6)$$

with N_f the number of supported fingers and:

$$QF_{F,i} = \min \left\{ \frac{\|F_i\|}{F_{15\%MVC,i}}, 1 \right\}$$

$$QF_{resF,i} = \min \left\{ \frac{0.04N}{resF_i}, 1 \right\}$$

$$QF_{bwF,i} = \min \left\{ \frac{bwF_i}{30Hz}, 1 \right\}$$

Here, the norm of the force vector (the absolute force) is used. If sufficient information is available, this can be separated into the three Cartesian components. Note that this quality factor could be extended with other terms such as minimum force level and precision.

Since the quality factors represent the performance of the interaction for each finger, dividing by the resources in terms of mass gives an indication of the efficiency with which this quality of reflection is obtained.

The device efficiency indicator for end-point interaction force DEI_F is given by (7). This represents the average quality of end-point force with respect to the device mass.

$$DEI_F = \frac{QF_F}{M} \quad (7)$$

4) *Performance: quality of Sensing:* Analogue to the DEI of interaction force to indicate the quality of the observable DOFs, a DEI for sensing can be defined to indicate the quality of controllable DOFs. Just as with the presented DEI_F this can include a quality factor QF as a function of range, resolution, bandwidth, etc.

5) *Efficiency Indicators of Proposed Concept:* The proposed concept has a mass of 452g including motor drives and encasing (393g without drives). It provides 5-10N continuously to the fingers, depending on the position of interaction with the levers. (Section. VI-C1). It provides 2 unique actuated DOFs (controllable in either a force, position or velocity loop) and 11 unique sensing DOFs (1 DOF position sensing at the thumb, 2 at each other finger, and 2 independent DOFs for force sensing). Both actuated and sensed DOFs have been specified at the fingertips, as required for the DEI's.

By filling in (4) and (5) the device efficiency indicators for maximum slave observability and controllability are $DEI_{obs} = 8.8kg^{-1}$ and $DEI_{ctr} = 24.3kg^{-1}$ respectively.

By filling in (6), the quality factor of the reflected force can be obtained. Since bandwidth and resolution have been

reported only scarcely for existing devices, the $QF_{resF,i}$ and $QF_{bwF,i}$ are disregarded and assumed unity here and in the comparison in the next section. Since the force actually depends on the point of interaction, the minimal continuous force of 5N is used and consequently $QF_{F,i} = 0.5$ for the index finger. This results in $QF_F = 0.83$.

By filling in (7) the efficiency indicator for end-point interaction force $DEI_F = 1.8kg^{-1}$.

6) *Device Comparison using Efficiency Indicators:* The following demonstrates the use of the proposed device efficiency indicators to place the prototype device design in perspective to existing grasp masters.

In Table. III, four distinct devices of which both end-point force and mass have been specified are compared to the novel proposed concept, based on the device efficiency indicators for slave observability DEI_{obs} , slave controllability DEI_{ctr} , and end-point interaction force DEI_F . Among the devices are the commercial CyberGrasp/CyberGlove [24] combination and the well accepted Rutgers Master.

Since the Rutgers Master has been adequately specified in [29], the full quality factor QF can be determined. The force resolution has been specified to be 12-bit. By assuming this gives a decent indication of actual force resolution at the fingertip, $resF_i = \frac{16N}{2^{12}} = 4.6mN$. The mechanical bandwidth at the fingertip bwF_i was reported to be 10 Hz. Filling in (6) gives $QF_{F,i} = 1$, $QF_{resF,i} = 1$, and $QF_{bwF,i} = 0.33$, resulting in $QF = 0.78$. Filling in (7) gives $DEI_F = 4.2kg^{-1}$.

As can be seen from Table III, the proposed concept outperforms the HEXOSYS [17] and HIRO III [25] grasp masters based on all efficiency indicators. Although the HIRO III offers great slave controllability and observability, the mass involved is so high that the actual efficiency remains moderate.

Since for both the Rutgers Master and the CyberGrasp the mass of the externally placed components has not been specified, the actual DEIs will be lower than shown. This means that the proposed concept will outperform the commercially available CyberGrasp/CyberGlove based on the efficiency of achieved force quality DEI_F and the efficiency of slave observability DEI_{obs} . Thanks to the high amount

TABLE III
DEVICE COMPARISON BY EFFICIENCY INDICATORS

Device	Max. End-point	Mass	DEI_F			DEI_{obs}		DEI_{ctr}
	Force [N]	[kg]	QF_F	[kg^{-1}]	$\sum_{i=1}^{N_{DOF^a}} \kappa_{a,i}$	[kg^{-1}]	$\sum_{i=1}^{N_{DOF^s}} \kappa_{s,i}$	[kg^{-1}]
Rutgers Master II [29]	16	0.185 ¹	1 (0.78)	5.4 (4.2) ^{1 2}	4	21.6 ¹	12	64.9 ¹
CyberGrasp/CyberGlove [24]	12	0.539 ¹	1	1.9 ¹	5	9.3 ¹	25	46.4 ¹
HEXOSYS [17]	45	1.000	1	1	4	4	8	8
HIRO III [25]	3.6	3.780	0.5	0.1	30	7.9	30	7.9
Proposed Concept	5-10	0.452	0.83	1.8	4	8.8	11	24.3

Device efficiency comparison by efficiency indicators of slave controllability DEI_{ctr} , slave observability DEI_{obs} , and end-point force quality DEI_F .

¹ The mass specified for the Rutgers Master excludes the control electronics, compressor and pneumatic switches. Because of this reason, the actual efficiency indicators are lower. The mass specified for the CyberGrasp includes the mass of the CyberGlove, but not that of the external motors, drives and control electronics. The actual DEIs of the CyberGrasp/CyberGlove combination fall below that of the proposed concept grasp master.

² For the Rutgers Master in [29] the resolution and bandwidth have been specified, this allows determining the real quality factor QF_F , as given between brackets. For all other values QF_F , the resolution and bandwidths have been disregarded and thus their actual DEI_F could be lower than indicated.

of sensors in the CyberGlove, the controllability of the CyberGrasp/CyberGlove combination is high. Yet, the efficiency of achieved slave controllability DEI_{ctr} also falls below that of the proposed concept because the actual total mass is larger than 1kg. Also the Rutgers master is less efficient than indicated in the table. Using its real overall mass would reduce its DEIs. Still, the Rutgers Master is remarkable for its high amount of sensed DOFs with respect to the small and light hand part of the device.

To improve the indication of overall device efficiency, the concept of DEIs could be extended with efficiency indicators for workspace, operator variability, comfort, compatibility with arm master devices, etc.

B. Workspace Verification

The upper and lower lever of the prototype design rotate from a closed position (where the finger levers are parallel to the thumb lever) over a range of $0^\circ - 55^\circ$ up to an open position.

This does not directly correspond to the workspace of the fingers since these are unconnected from the levers and thus can flex each segment independently. Therefore the model presented in [43] was used to simulate device interaction for workspace analysis by varying operator hand sizes ranging from 5th percentile female hands up to 95th percentile male hands. As model input, the corresponding hand lengths from [4] were used. The joint limits applied to the model are listed in Annex. A.2.

Hand models generated for the 5th female- and 95th male percentile were used as extreme cases to represent the whole 5th- till 95th percentile hand size range. Typical pinching motion of all fingers is shown in Fig. 14. Maximum MCP flexion in the 5th percentile female hand model is roughly: 58° , 64° , 50° , and 52° for the index-, middle-, ring-, and little fingers respectively. For the 95th male percentile this is: 55° , 55° , 53° , and 46° . No over-extension of the fingers is supported while remaining in lever contact. Considering the maximum MCP flexion range reported in [38], this is 60-70% for the index- and middle finger and 50-60% for the ring- and little finger flexion range. This workspace is reasonably when realising that hand sizes ranging from the 5th till 95th percentile are supported.

Since the fingers are not connected to the levers, the PIP and DIP joints can flex- and extend freely to slide the fingertip over the lever surface, as shown in Fig. 15. This also allows the fingers to exclude freely from lever contact to allow performing a range of grasp types as described in Section. IV-A2.

Using the hand model, good fingertip contact (not using the backside of the finger) was analysed for the 5th percentile hand in maximum flexion, and the 95th percentile hand in maximum extension. Results suggest that index finger contact only appears between 47–111mm measured from the base. For the middle-, ring-, and little finger this is 35–114mm, 34–109mm, and 33–81mm respectively. This information will be used in Section. VI-C1 to indicate the actually used contact area on the levers.

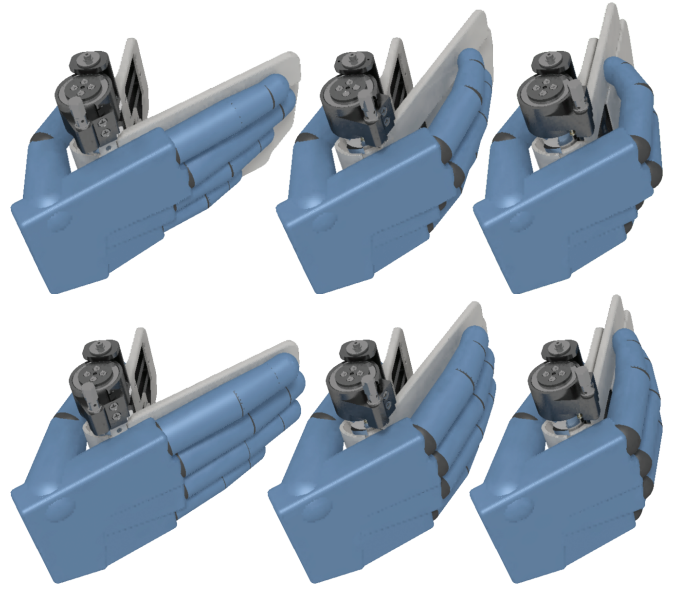


Fig. 14. Hand model workspace verification by simulation using the adaptable hand model from [43] to represent female 5th percentile- (upper) and male 95th percentile interaction (lower) in the extreme device positions when the levers are fully opened and closed.

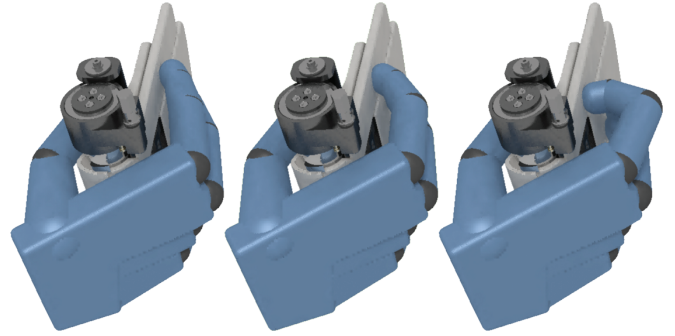


Fig. 15. 5th percentile female hand model sliding the index fingertip over the lever surface.

C. Interaction Force Verification

By analysis of the torque propagation through the system and the available motor torque, the requirements from human factors on the interaction force (Section. III-A) can be verified.

1) *Lever Torque Verification:* By using (1) in combination with the parameters presented in Section. V-D the maximum torque available for reflection to the user as function of the position on the lever surface was obtained. This is shown in Fig. 16 for the upper lever under the condition that acceleration of 150 m/s^2 is reached at the fingertip, which is half the maximum acceleration as suggested in Section. III-A.

Different curves have been generated for different motor torques defined by the overload factor (OF) times the nominal motor torque. As will be verified in Section. VI-C2 overload conditions can be maintained during limited term operation.

The results show that the maximum available force reflection to the operator depends on the point of interaction on the lever. In the worst-case continuous condition that 15% MVC is required under maximum acceleration, the motor

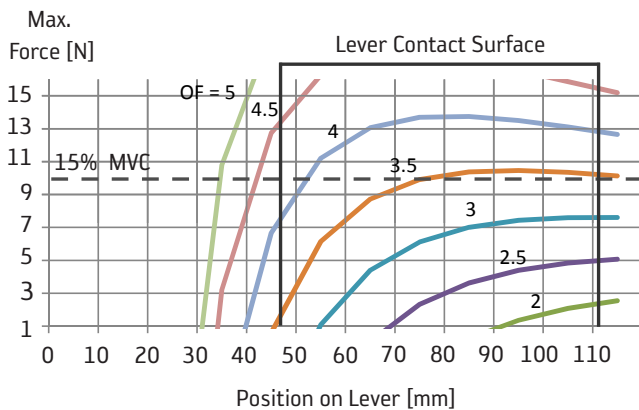


Fig. 16. Maximum interaction force available on the upper lever during fingertip acceleration of 150m/s^2 . The different graphs indicate overload conditions at overload factors OF representing multiples of the nominal motor torque.

should operate at 3.5-4.2 times the nominal torque to achieve the required force levels at the used lever area between 47 and 111 mm (Section. VI-B). In Section. VI-C2 it will be verified that this can be achieved for limited duration. The analysed situation in which both high accelerations and maximum interaction force are required, will only be reached intermittently in real operation.

Under the steady-state condition that the acceleration is zero, the most predominant in haptic interaction with stiff objects, the results in Fig. 17 were obtained for the upper lever. Here it is shown that at nominal motor torque, a theoretical interaction force of at least 5 - 10N can be achieved over the used lever surface. At light overload conditions of approximately 1.7 times the nominal current, the minimum interaction force is at the level of 15% MVC. This can be maintained for up to 140s.

Graphs with the force profile over the lower lever have been included in Annex A.4. Due to the higher inertia of the lower lever, achieving the worst-case scenario of 10N and 150m/s^2 simultaneously requires motor torques to be increased with 0.5 times the nominal torque. When only the middle finger interacts with the lever, 15% MVC is reached at mild overload conditions of 2 times the nominal current over the full lever surface. During continuous operation, 15% MVC cannot be reached simultaneously on the middle-, ring-, and little finger (23N in total). However, this can be reached during short term overload at 2-4 times the motor torque.

2) *Motor Overloading*: As mentioned in Section. V-B the selected actuators have thermal characteristics specifically suitable for overloading to achieve increased output torque for limited duration.

The following results have been obtained using a thermal model (Maxon e-learning [70]) based on the thermal resistances winding-housing R_{th1} , housing-ambient R_{th2} , and the thermal capacitances of the winding C_{thw} and the stator C_{ths} . These parameters have been specified in the Maxon datasheet for operation under standard conditions when mounted to a non-conducting flange in free air without forced convection. By mounting the motor in contact with good heat conductive

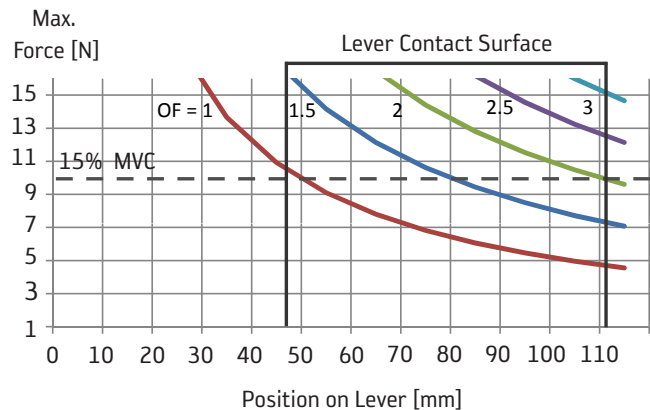


Fig. 17. Maximum interaction force available on the upper lever during steady-state conditions. The different graphs indicate overload conditions at overload factors OF representing multiples of the nominal motor torque.

materials, the thermal resistance housing-ambient could be halved, as suggested by Maxon. This will greatly improve the time to winding overheating and the maximum winding temperature reached. Thanks to this, higher torques may be maintained for longer durations. The actual thermal resistance, however, is to be verified by physical prototype testing. Both the applied thermal model and the simulation results at half the specified R_{th2} can be found in Annex A.5.

Fig. 18 shows the thermal behaviour of the motor under different applied current levels, defined as the nominal current times the overload factor OL . As shown in the graphs, the motor can run continuously without reaching the maximum winding temperature at nominal current and thus nominal torque. At twice the nominal torque, the maximal winding temperature is reached in 89s. This decreases down to 1.5s at $OL = 5$.

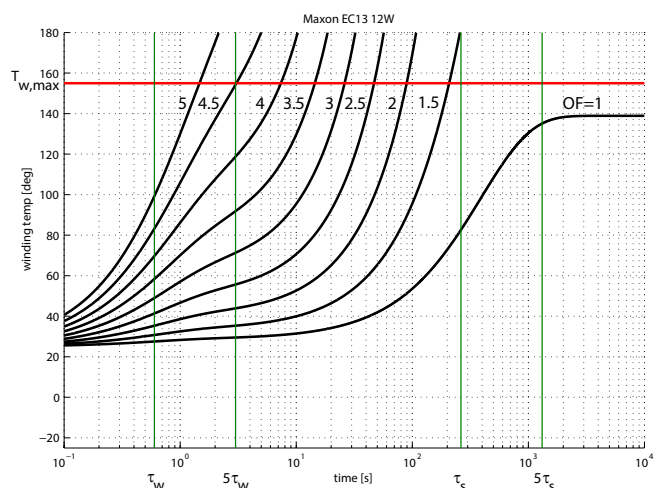


Fig. 18. Thermal behaviour of Maxon motor EC13 12W in overload conditions. The graphs show the heating of the motor winding over time under continuously applied current equal to the specified nominal current times the overload factor OF . (i.e. the graph indicated with '2' thus shows the thermal behaviour while operation at twice the nominal current). Reaching $T_{w,max}$ means overheating of the winding and results in irreversible damage to the winding.

With this it can be shown that the worst-case condition defined in Section. VI-C1, where 3.5-4.2 times the nominal torque is required to reach 15% MVC force reflection to the operator during maximum acceleration, can be maintained for a duration of 7–13s (when starting at ambient temperature of 25deg).

So far, all presented key requirements have been used throughout the document (for verification and device efficiency indicators), yet not all have been verified (such as resolution and bandwidth). These are measures that should be measured as actual values at the point of interaction. This is left for the verification by testing of the actual prototype device that will be implemented.

VII. DISCUSSION AND SUMMARY

With the proposed concept and the prototype design that was partially verified, the goals can be discussed.

It was found that a subset of grasp types is used most often in EVA tool operation, requiring only 4 predominant grasping functions. By realising that psychophysical enslaving effects lead to coupled finger activation and sensing, these predominant grasping functions can be supported while grouping feedback to the middle-, ring-, and little finger. This allows the reduction of active DOFs in the device design.

To exploit sensor-actuator asymmetry, more sensors of different nature and in different positions were implemented. This offers increased slave controllability while not increasing the master complexity significantly. Comparison by device efficiency indicators in Section. VI-A showed that the efficiency of controllability DEI_{ctr} is roughly three times that of observability DEI_{obs} .

The availability of distinct sensors allows implementation of various local and bilateral controllers. In combination with the proposed concepts of grasp mapping and grasp primitive switching, various slaves can be operated in multiple predefined useful grasps.

Since only 2 actuated DOFs are required in the proposed concept, a simple design with low weight, small size and short transmissions was achieved. In other words, a design inexpensive in terms of resources was achieved.

Device performance can be high since short transmissions are used, introducing little losses and backlash. This was further improved by balancing between the use of a classical gearhead and a Capstan transmission. User performance can be high since the relatively small and light device leaves the fingers unconnected, resulting in comfortable donning/doffing and operation. This also allows operation by various operators without requiring device adjustments. The combination of this resource inexpensive design with good device and user performance is promising to be an efficient design.

The validation by device efficiency indicators puts the developed concept in perspective to other existing grasp masters based on the efficiency of slave controllability and observability. This not only involves the quantity of DOFs, but also the quality of the force reflected. The results show that the prototype design is relatively efficient on these points. It should be realised that other device efficiency indicators,

such as those for arm workspace and arm master compatibility, yet have to be constructed from well-defined performance and resource definitions to allow a more complete indication of overall device efficiency.

The developed prototype was verified by simulation of force feedback, thermal motor behaviour, and by analysis of device geometry and workspace for hand size robustness. This indicated that the developed prototype design meets the key requirements. Further validation of detailed requirements have been planned by testing the actual device prototype. Also the device will be validated in actual user interaction.

VIII. CONCLUSION

1) A novel grasp master design was presented, based on sensor-actuator asymmetry with 2 actuators and 9 sensors for various signals, providing 11 unique sensed DOFs at the fingertips (9 DOF position, 2 DOF force) and 2 unique active DOFs (for force, position or velocity control).

2) The variety of sensor positions and types allows operating slave devices with varying complexity in terms of kinematic structure (nr. of fingers, nr. of joints) and control architectures. The active DOFs can provide the operator with fundamental feedback from the slave.

3) The master device supports the operator in performing 90% of all natural precision grasps in EVA tool use. 60% of all power grasps can be performed when pad oppositions are used instead of palm oppositions.

4) The device is compatible with an arm master since the wrist and arm are not covered and no external transmissions are required.

5) Since the fingers are unconnected from the device, comfortable donning/doffing and operation by hands ranging from the 5th female- till 95th male percentile, is supported without requiring device adjustments.

6) At nominal motor torque, a theoretical interaction force of 5-10 N, depending on the point of interaction on the lever surface, can be achieved. Reaching 10 N interaction force over the whole lever surface requires mild overload conditions of that can be maintained up to 140s.

7) Controlled overloading of the motors is proposed to increase power-density of the mechatronic system for intermittently reaching high torques. To reach an interaction force of 10N and an acceleration of $150m/s^2$ simultaneously at the fingertip, the motor should be operated at approximately 3.5–4.2 times its nominal current. This can be maintained for 7–13s when starting from ambient temperature.

8) The use of device efficiency indicators (DEI) was proposed to verify device efficiency with respect to other existing devices. Results from this comparison suggest that the proposed design is relatively efficient in terms of controllability and observability over slave devices.

REFERENCES

The references can be found in the overall bibliography at the end of this thesis.

Chapter 4

Conclusions

1) A novel grasp master device was proposed for space robotics bilateral teleoperation. Since the design does not cover the wrist and arm and does not have external transmissions, it allows operation in combination with the haptic human arm exoskeleton X-Arm-2.

2) By following a human centric design approach including analysing background on space relevant tasks, operator grasps, and psychophysical effects in human hands, guidelines were obtained for reducing the number of actuators to the minimum required for supporting fundamental grasp functions to perform the majority of intended tasks.

3) An adaptable hand model that was constructed proved to be valuable tool in the design process of device geometry and workspace. In an early stage of the design this model provided guidelines for dimensioning the system and in the final stage it was used in workspace verification to show that the device can be used by various operators with hand sizes ranging from the 5th- till 95th percentile.

4) A framework for the comparison of grasp masters based on the design efficiency (the ratio of user- and device performance achieved w.r.t. the resources expended) was proposed in the form of device efficiency indicators. These are the ratios between well-specified measures of performance and well-specified measures of resources. This concept was demonstrated using indicators for the efficiency of available controllability over slave devices, observability over slave devices, and interaction force quality. Comparison with 4 other slave devices, including the commercially available CyberGrasp-CyberGlove combination and the well-accepted Rutgers Master, suggests that the proposed concept is relatively efficient in terms of observability and controllability over slave devices.

It was hypothesised that a human-centric design approach (for psychophysical effects and human factors) including separation of control and feedback functions, can increase the device efficiency. In this chapter it was concluded that following a human centric design approach gave guidelines for the reduction of the number of actuators while maintaining fundamental grasping functions. By the separation of control and feedback paths, the use of sensors was not limited. Moreover, this enabled the use of sensors dissimilar in type and placement. With light weight, low size membrane position sensors and strain-gauge force/torque sensors, the controllability of the device was increased without influencing the mass significantly. As verified with the use of device efficiency indicators, the

device is efficient w.r.t. slave controllability. Judging from this, the hypothesis is plausible, yet, considering the overall device efficiency, more information is required. That is: more metrics in the framework for device efficiency comparison should be developed and verified.

This requires that device designs are well specified in terms of performance and resource metrics. The prototype device that is going to be manufactured and implemented will be verified by testing actual device performance. This information could be used in demonstrating and extending the framework of device efficiency indicators.

Bibliography

- [1] A. Schiele and G. Hirzinger, “A new generation of ergonomic exoskeletons - the high-performance x-arm-2 for space robotics telepresence,” in *IEEE/RSJ Int. Conf. Intelligent Robots and Systems*, San Francisco, California, Sept 2011, pp. 25–30, (to appear).
- [2] M. Diftler, J. Mehling, M. Abdallah, N. Radford, L. Bridgwater, A. Sanders, R. Askew, D. Linn, J. Yamokoski, F. Permenter, B. Hargrave, R. Piatt, R. Savely, and R. Ambrose, “Robonaut 2 - the first humanoid robot in space,” in *IEEE/ICRA International Conference on Robotics and Automation*, May 2011, pp. 2178–2183.
- [3] F. Bosquillon de Frescheville, S. Martin, N. Policella, D. Patterson, M. Aiple, and P. Steele, “Set-up and validation of meteron end-to-end network for robotic experiments,” in *11th Symposium on Advanced Space Technologies in Robotics and Automation, ASTRA*, 2011.
- [4] *Man-Systems Integration Standards, Volume I*, NASA-STD-3000, Rev. Rev. B, Jul. 1995.
- [5] F. Didot, P. Schoonejans, E. Pensavalle, G. Battistoni, S. Ferraris, S. Estable, T. Huesling, and EADS-Astrium, “Eurobot underwater model: System overview, test results & outlook,” in *i-SAIRAS 02*, 2008.
- [6] Y. Hasegawa, Y. Mikami, K. Watanabe, and Y. Sankai, “Five-fingered assistive hand with mechanical compliance of human finger,” in *IEEE Int. Conf. Robotics and Automation ICRA*, 2008, pp. 718–724.
- [7] A. Chiri, F. Giovacchini, N. Vitiello, E. Cattin, S. Roccella, F. Vecchi, and M. C. Carrozza, “Handexos: Towards an exoskeleton device for the rehabilitation of the hand,” in *Proc. IEEE/RSJ Int. Conf. Intelligent Robots and Systems IROS*, 2009, pp. 1106–1111.
- [8] S. Nakagawara, H. Kajimoto, N. Kawakami, S. Tachi, and I. Kawabuchi, “An encounter-type multi-fingered master hand using circuitous joints,” in *IEEE Int. Conf. Robotics and Automation ICRA*, Apr 2005, pp. 2667–2672.
- [9] M. Fontana, A. Dettori, F. Salsedo, and M. Bergamasco, “Mechanical design of a novel hand exoskeleton for accurate force displaying,” in *Proc. IEEE Int. Conf. Robotics and Automation ICRA*. Piscataway, NJ, USA: IEEE Press, 2009, pp. 2599–2604.
- [10] C. Tzafestas and P. Coiffet, “Computing optimal forces for generalised kinesthetic feedback on the human hand during virtual grasping and manipulation,” in *Proc. IEEE Int. Conf. Robotics and Automation*, vol. 1, 1997, pp. 118–123.
- [11] B. Choi and H. Choi, “Skk hand master-hand exoskeleton driven by ul-

- trasonic motors,” in *IEEE/RSJ Int. Conf. Intelligent Robots and Systems IROS*, vol. 2, 2000, pp. 1131–1136 vol.2.
- [12] M. DiCicco, L. Lucas, and Y. Matsuoka, “Comparison of control strategies for an emg controlled orthotic exoskeleton for the hand,” in *Proc. IEEE Int. Conf. Robotics and Automation ICRA*, vol. 2, 2004, pp. 1622–1627.
- [13] M. F. Rotella, K. E. Reuther, C. L. Hofmann, E. B. Hage, and B. F. BuSha, “An orthotic hand-assistive exoskeleton for actuated pinch and grasp,” in *IEEE 35th Annual Northeast Bioengineering Conference*, 2009, pp. 1–2.
- [14] B. Eberman and B. An, “Exos research on force reflecting controllers,” *SPIE Telemanipulator Technology*, vol. 1833, pp. 9–19, 1992.
- [15] S. Ito, H. Kawasaki, Y. Ishigure, M. Natsume, T. Mouri, and Y. Nishimoto, “A design of fine motion assist equipment for disabled hand in robotic rehabilitation system,” *Journal of the Franklin Institute*, vol. 348, no. 1, pp. 79–89, 2011, mechatronics and its Applications.
- [16] Y. Fu, P. Wang, S. Wang, H. Liu, and F. Zhang, “Design and development of a portable exoskeleton based cpm machine for rehabilitation of hand injuries,” in *Proc. IEEE Int. Conf. Robotics and Biomimetics ROBIO*, 2007, pp. 1476–1481.
- [17] J. Iqbal, N. Tsagarakis, A. Fiorilla, and D. Caldwell, “A portable rehabilitation device for the hand,” in *IEEE Int. Conf. Engineering in Medicine and Biology Society EMBC*, Sept 2010, pp. 3694–3697.
- [18] T. T. Worsnopp, M. A. Peshkin, J. E. Colgate, and D. G. Kamper, “An actuated finger exoskeleton for hand rehabilitation following stroke,” in *Proc. IEEE 10th Int. Conf. Rehabilitation Robotics ICORR*, 2007, pp. 896–901.
- [19] M. Lelieveld, T. Maeno, and T. Tomiyama, “Design and development of two concepts for a 4 dof portable haptic interface with active and passive multi-point force feedback for the index finger,” in *ASME International Design Engineering Technical Conference & Computers and Information in Engineering Conference*, 2006.
- [20] B. L. Shields, J. A. Main, S. W. Peterson, and A. M. Strauss, “An anthropomorphic hand exoskeleton to prevent astronaut hand fatigue during extravehicular activities,” *IEEE Transactions on Systems, Man and Cybernetics, Part A: Systems and Humans*, vol. 27, no. 5, pp. 668–673, 1997.
- [21] A. Wege and A. Zimmermann, “Electromyography sensor based control for a hand exoskeleton,” in *Proc. IEEE Int. Conf. Robotics and Biomimetics ROBIO*, 2007, pp. 1470–1475.
- [22] A. Schiele, “Performance difference of bowden cable relocated and non-relocated master actuators in virtual environment applications,” in *IEEE/RSJ IROS International Conference on Intelligent Robots and Systems*, Sep 2008, pp. 3507–3512.
- [23] J. Wang, J. Li, Y. Zhang, and S. Wang, “Design of an exoskeleton for index finger rehabilitation,” in *Proc. IEEE Annual Int. Conf. Engineering in Medicine and Biology Society EMBC*, 2009, pp. 5957–5960.
- [24] Cybergrasp[®]. CyberGlove Systems. (checked 26-06-2012). [Online]. Available: <http://www.cyberglovesystems.com/products/cybergrasp>
- [25] T. Endo, H. Kawasaki, T. Mouri, Y. Doi, T. Yoshida, Y. Ishigure, H. Shimomura, M. Matsumura, and K. Koketsu, “Five-fingered haptic interface robot: Hiro iii,” in *Proc. and Symp. EuroHaptics conf. Haptic Interfaces for Virtual Environment and Teleoperator Systems. World Haptics 2009*.

- Third Joint*, 2009, pp. 458–463.
- [26] M. Monroy, M. Oyarzabal, M. Ferre, A. Campos, and J. Barrio, “Masterfinger: Multi-finger haptic interface for collaborative environments,” in *Proc. 6th Int. Conf. Haptics: Perception, Devices and Scenarios EuroHaptics '08*. Berlin, Heidelberg: Springer-Verlag, 2008, pp. 411–419.
- [27] P. Stergiopoulos, P. Fuchs, and C. Laugeau, “Design of a 2-finger hand exoskeleton for vr grasping simulation,” in *EuroHaptics, Trinity College, Dublin and Media Lab Europe*, 2003.
- [28] H. Fang, Z. Xie, and H. Liu, “An exoskeleton master hand for controlling dlr/hit hand,” in *IEEE/RSJ Int. Conf. Intelligent Robots and Systems IROS*, 2009, pp. 3703–3708.
- [29] M. Bouzit, G. Burdea, G. Popescu, and R. Boian, “The rutgers master ii - new design force-feedback glove,” *IEEE/ASME Transactions on Mechatronics*, vol. 7, no. 2, pp. 256–263, 2002.
- [30] Forcedimension. (checked on 26-05-2012). [Online]. Available: <http://www.forcedimension.com/>
- [31] I. Kapandji, *The Physiology of the Joints. Volume I: Upper Limb*. Churchill Livingstone, 1982.
- [32] N. Davidoff and A. Freivalds, “A graphic model of the human hand using catia,” in *International Journal of Industrial Ergonomics*, vol. vol. 12, no. no. 4, 1993, pp. pp. 255–264.
- [33] S. Cobos, M. Ferre, M. A. Sanchez Uran, J. Ortego, and C. Pena, “Efficient human hand kinematics for manipulation tasks,” in *Proc. IEEE/RSJ International Conference on Intelligent Robots and Systems*, 2008.
- [34] H. Du and E. Charbon, “3d hand model fitting for virtual keyboard system,” in *Proc. IEEE Workshop Applications of Computer Vision WACV*, 2007.
- [35] H. Hashimoto, H. Murakoshi, A. Sasaki, Y. Ohyama, K. Makino, and S. Yokota, “Dynamical analysis of grasping with hand model for high quality product design,” in *Proc. SICE Annual Conf.*, 2010.
- [36] K. Kim, Y. Youm, and W. K. Chung, “Human kinematic factor for haptic manipulation: the wrist to thumb,” in *Proc. of 10th Symp. Haptic Interfaces for Virtual Environment and Teleoperator Systems HAPTICS*, 2002.
- [37] G. Gil Gómez and A. Schiele, “Compendium of human factors for designing an ergonomic haptic exoskeleton for the human hand,” ESA internal documentation, 2006.
- [38] E. Y. S. Chao, K.-N. An, W. P. Cooney III, and R. L. Linscheid, *Biomechanics of the Hand. A Basic Research Study*. World Scientific, 1989.
- [39] B. Siciliano, L. Sciavicco, L. Villani, and G. Oriolo, *Robotics Modelling, Planning and Control*. Springer-Verlag London Limited, 2009.
- [40] A. Freivalds, *Biomechanics of the Upper Limbs: Mechanics, Modeling and Musculoskeletal Injuries*. CRC Press, 2004.
- [41] G. Stillfried, U. Hillenbrand, M. Settles, and P. van der Smagt, “MRI-based Skeletal Hand Movement Model”, *The Human Hand - A Source of Inspiration for Robotic Hands*. Springer Tracts on Advanced Robotics, (to be published).
- [42] G. Stillfried and P. van der Smagt, “Movement model of a human hand based on magnetic resonance imaging (mri),” in *1st International Conference on Applied Bionics and Biomechanics (ICABB)*, 2010.
- [43] F. P. J. van der Hulst, S. Schätzle, C. Preusche, and A. Schiele, “A func-

- tional anatomy based kinematic human hand model with simple size adaptation,” in *in Proc. of IEEE/ICRA International Conference on Robotics and Automation*, May. 2012, pp. pp. 5123–5129.
- [44] M. Cutkosky, “On grasp choice, grasp models, and the design of hands for manufacturing tasks,” *IEEE Transactions on Robotics and Automation*, vol. 5, no. 3, pp. 269–279, 1989.
- [45] D. Akin, C. Carignan, and A. Foster, “Development of a four-fingered dexterous robot end effector for space operations,” in *IEEE Int. Conf. Robotics and Automation ICRA*, vol. 3, 2002, pp. 2302–2308.
- [46] *EVA Tools and Equipment Reference Book*, NASA-TM-109350, Rev. B, Nov 1993.
- [47] M. Arbib, T. Iberall, and D. Lyons, “Coordinated control program for movements of the hand,” *Experimental Brain Research*, 1985.
- [48] M. R. Cutkosky and R. D. Howe, *Human grasp choice and robotic grasp analysis*. New York, NY, USA: Springer-Verlag New York, Inc., 1990, pp. 5–31.
- [49] T. Iberall, “The nature of human prehension: Three dextrous hands in one,” in *IEEE Int. Conf. Robotics and Automation.*, vol. 4, 1987, pp. 396–401.
- [50] T. Iberall, G. Bingham, and M. A. Arbib, “Opposition space as a structuring concept for the analysis of skilled hand movements,” *Experimental Brain Research Series*, vol. 15, pp. 158–173, 1986.
- [51] S. Li, “Perception of individual finger forces during multi-finger force production tasks,” *Neuroscience Letters*, vol. 409, no. 3, pp. 239 – 243, 2006.
- [52] S. Li and C. Leonard, “The effect of enslaving on perception of finger forces,” *Experimental Brain Research*, vol. 172, pp. 301–309, 2006.
- [53] S. L. Kilbreath and S. C. Gandevia, “Independent digit control: Failure to partition perceived heaviness of weights lifted by digits of the human hand,” *The Journal of Physiology*, vol. 442, no. 1, pp. 585–599, 1991.
- [54] W.-H. Park, C. Leonard, and S. Li, “Finger force perception during ipsilateral and contralateral force matching tasks,” *Experimental Brain Research*, vol. 189, pp. 301–310, 2008.
- [55] K. N. An, L. J. Askew, and E. Y. Chao, “Biomechanics and functional assessment of upper extremities,” *Trends in Ergonomics/Human Factors III, Elsevier Science Publishers, B.V.*, 1986.
- [56] P. Sutter, J. Iatridis, and N. Thakor, “Response to reflected-force feedback to fingers in teleoperations,” in *Proc. NASA Conf. Space Telerobotics*, 1989.
- [57] H. Tan, M. Srinivasan, B. Eberman, and B. Cheng, “Human factors for the design of force-reflecting haptic interfaces,” in *Proc. Haptic Interfaces for Virtual Environment and Teleoperator Systems, ASME/IMECE, DSC:55-1, Design of Haptic Icons 363*, 1994.
- [58] G. Burdea, *Force and Touch Feedback for Virtual Reality*. New York, NY, USA: John Wiley & Sons, Inc., 1996.
- [59] M. H. Zadeh, “Factors affecting human force perception and performance in haptic-enabled virtual environments,” Ph.D. dissertation, Waterloo, Ontario, Canada, 2009.
- [60] L. A. Jones, “Matching forces: Constant errors and differential thresholds,” *Perception*, vol. 18(5), pp. 681–687, 1989.
- [61] X. Pang, H. Tan, and N. Durlach, “Manual discrimination of force using

- active finger motion,” *Attention, Perception, and Psychophysics*, vol. 49, pp. 531–540, 1991.
- [62] D. V. Raj, K. Ingty, and M. S. Devanandan, “Weight appreciation in the hand in normal subjects and in patients with leprosy neuropathy,” *Brain*, vol. 108 (1), pp. 95–102, 1985.
- [63] S. Allin, Y. Matsuoka, and R. Klatzky, “Measuring just noticeable differences for haptic force feedback: implications for rehabilitation,” in *Proc. 10th Symp. Haptic Interfaces for Virtual Environment and Teleoperator Systems HAPTICS 2002*, pp. 299–302.
- [64] F. Barbagli, K. Salisbury, C. Ho, C. Spence, and H. Z. Tan, “Haptic discrimination of force direction and the influence of visual information,” *ACM Trans. Applied Perception*, vol. vol. 3, Apr. 2006.
- [65] H. Z. Tan, M. A. Srinivasan, C. M. Reed, and N. I. Durlach, “Discrimination and identification of finger joint-angle position using active motion,” *ACM Transactions on Applied Perception (TAP)*, vol. Vol. 4, no. no. 2, Jul. 2007.
- [66] T. Brooks, “Telerobotic response requirements,” in *IEEE Int. Conf. Systems, Man and Cybernetics*, Nov 1990, pp. 113–120.
- [67] V. Hayward and O. Astley, “Performance measures for haptic interfaces,” in *7th Int. Symp. Robotics Research*. Springer Verlag, 1996, pp. 195–207.
- [68] K. Hashtrudi-Zaad and S. E. Salcudean, “Analysis of control architectures for teleoperation systems with impedance/admittance master and slave manipulators,” *The International Journal of Robotics Research*, vol. vol. 20, no. no. 6, pp. 419–445, Jun. 2001.
- [69] N. Lii, Z. Chen, B. Pleintinger, C. Borst, G. Hirzinger, and A. Schiele, “Exploratory investigations of the effects of visual and low performance force feedback on robotic hand grasping performance for space teleoperations,” *IEEE/RSJ Int. Conf. Intelligent Robots and Systems.*, 2010.
- [70] Thermal behaviour e-learning. Maxon Motor. (checked on 21-06-2012). [Online]. Available: <http://www.maxonmotor.com/maxon/view/content/service-academy-thermal-behavior>
- [71] G. A. Gescheider, *Psychophysics: The Fundamentals*. Lawrence Erlbaum Associates, 1997.

Annex A

Design Details: Human Factors, Modelling, and Simulation

This annex includes details that complement the grasp master development presented in Chapter. 3. This includes details on human factors, applied hand model joint limits, torque propagation modelling, lower lever interaction force simulation, and motor thermal behaviour simulation.

A.1 Human Factors Details

The following gives more detail on the human factors that have been used to derive key requirements for grasp master devices in Chapter. 3.III.

It should be noted that reported data is sparsely available, obtained via specific experiments, and often based on few subjects. For this reason, the presented data should be considered a rough estimate.

A.1.1 Finger Force Range

The data reported in various sources can be combined into an indication of the maximum exertable finger force. A fingertip force up to 65 N during pinch grasping by male subjects was reported in [55]. Maximum exertable index fingertip force, measured for 10 subjects, was reported to be 50 N in [56]. Controllable fingertip force for male subjects was reported to be 51 N in [57]. Index finger distal phalange force during cylindrical power grasping was reported to be 62 N for male subjects in [55]. Important to note is that these values were obtained via dissimilar experiments and for small or unknown subject groups.

For the middle-, ring- and little fingers less data is available. In [56] the maximum exertable tip force was reported to be 48 N for the middle finger and 37 N for the ring finger. In [55] the distal phalange force during power grasping was found to be 68 N, 44 N and 31 N for the middle-, ring-, and index finger respectively.

It is assumed that the reported values give an indication of the maximum voluntary contraction (MVC). The summarised values suggest 50-65 N MVC for the index finger, 48-68 N MVC for the middle finger, 37-44 N MVC for the ring finger, and 31 N MVC for the little finger.

As summarised in [58], exerting force for a longer duration can lead to muscle fatigue, resulting in discomfort, pain and shifting of force perception. At 15% MVC, moderate levels of discomfort were reported after 103 minutes. At higher force levels, perception shifted over time and significant levels of discomfort were reached quickly (10 minutes at 25% MVC).

The minimal level of force perception can be defined as the absolute perception threshold, which is the smallest stimulus that can be perceived. In practice, this threshold can not be sharply defined and adapts over time. In [71] the threshold is defined as "the stimulus intensity that would be detected 50% of the time". In [59], subjects were still able to detect a force below 0.12 N.

A.1.2 Finger Force JND

The resolution of force perception is expressed in terms of just noticeable difference (JND), which is defined as "the minimum noticeable variation between a base stimulus intensity and an increased or decreased stimulus intensity" [59]. As summarised in that work, the following studies report on force JND. 5–9% force JND for the human elbow over a range of base reference forces (15-85% MVC) was reported in [60]. 5–10% force JND for finger thumb pinching over a range of base reference forces (2.5–10 N) was reported in [61]. 12–13% force JND for middle finger lifting at base forces (0.8–2 N) was reported in [62]. 10% force JND for the index finger was reported in [63] for a base reference force of 2.25 N. Force JND of 10–11% was found for a base force of 0.77 N in [59].

Although the summarised values were obtained using dissimilar experiments, they give an indication of force JND, being 5-13% for reference forces ranging from 0.77–10 N.

As found in experiments (16 subjects) presented in [59], the force JND increases considerably at low base reference forces. Force JND increased to 12–15% at a base force of 0.42 N, to 29–32% at a base force of 0.27 N and up to 43–64% at a base force of 0.12 N. It was stated that this observed effect answers to the *Weber trend* [71], which holds that the JND is constant for relatively large base stimuli, but increases significantly for low base stimulus intensity.

Another effect described in [59] is that the force JND increases with velocity. At a low base force of 0.27 N this was 18.6% force JND at 0.03–0.05 m/s, which increased up to 35.6% JND at 0.22–0.88 m/s. In the same source it was observed that subjects lose sensitivity to force changes by adaptation over time in motion tasks. This change was not affected by the base force.

Considering the human force exertion resolution, values of 0.22 N and 0.28 N were found for the PIP and MCP joint respectively (3 subjects) [57].

A.1.3 Finger Joint Range

Table. A.1 and A.2 list the natural joint movement range of the thumb and fingers respectively, as summarised in [37]. Forced movements caused by an external force can exceed the reported limits.

This data was used for parametrisation of the hand model joint limits (Section. A.2).

Table A.1: Thumb Joints Range of Motion

Joint	Motion	Thumb Range of Movement [°]
CMC	anteponition	25 - 35
	retroponition	15 - 25
	flexion	20 - 35
	extension	30 - 45
MCP	flexion	60 - 70
	extension	0
	ab-adduction	5 (medial displacement) 20 (lateral displacement)
	supination	5 - 7
	pronation	20 - 24
IP	flexion	75 - 80
	extension	5 - 10

Overview of thumb joint limits constructed using data from [31].

CMC: carpometacarpal joint, MCP: metacarpophalangeal joint, IP: interphalangeal joint.

Table A.2: Finger Joints Range of Motion

Joint	Motion	Fingers Range of Movement [°]				Source	
		Index	Middle	Ring	Little		
CMC	flexion	~0	~0				
	extension	~0	~0	10	20	[40]	
MCP	flexion	83	90	88	90	[38]	
		70			95	[40]	
	extension			20 - 30		[40]	
				30 - 40		[31]	
				22 - 23	34	[38]	
ab-adduction	60	45	45	50	[40]		
PIP	flexion	increasing from index finger >90					
		up to little finger 135				[31]	
		100 - 105				[38]	
	100 - 110				[40]		
	extension	0				[31]	
DIP	flexion	<90				up to 90	[31]
		73 - 80				[38]	
		60 - 70				[40]	
	extension	0 - 5				[31]	

Reworked table with data adapted from [37].

CMC: carpometacarpal joint, MCP: metacarpophalangeal joint, PIP: proximal interphalangeal joint, DIP: distal interphalangeal joint, IP: interphalangeal joint.

A.2 Hand Model Joint Limits

Table. A.3 and A.4 list the joint limits for the thumb and fingers respectively, as applied to the kinematic hand model from [43]. These values are based on the joint motion ranges listed in Table. A.1 and A.2.

Table A.3: Hand Model: Thumb Joint Limits

Joint	Motion	Thumb Joint Limits[$^{\circ}$]
CMC	ante-position	35
	retro-position	25
	flexion	35
	extension	45
MCP	flexion	70
	extension	0
	ab-/adduction	5 (medial displacement) 20 (lateral displacement)
	supination	7
	pronation	24
IP	flexion	80
	extension	10

Overview of thumb joint limits applied to the hand model from [43]. This table was constructed using data from [31].

CMC: carpometacarpal joint, MCP: metacarpophalangeal joint, IP: interphalangeal joint.

Table A.4: Hand Model: Finger Joint Limits

Joint	Motion	Finger Joint Limits [°]			
		Index	Middle	Ring	Little
CMC	flexion	~0	~0	10	20
	extension ¹	~0	~0	15	30
MCP	flexion	83	90	88	95
	extension	40	40	40	40
	abduction ²	30	13	20	40
	adduction	30	13	5	10
PIP	flexion ³	110	115	125	135
	extension	0	0	0	0
DIP	flexion	90	90	90	90
	extension	5	5	5	5

Overview of finger joint limits applied to the hand model from [43]. This table was constructed using data from [31], [40], and [38]

CMC: carpometacarpal joint, MCP: metacarpophalangeal joint, PIP: proximal interphalangeal joint, DIP: distal interphalangeal joint, IP: interphalangeal joint.

¹ In the hand model, the CMC extension is set to 0 since this motion cannot be actively performed.

² It has not been specified which parts of the full MCP ab-/adduction range correspond to actual abduction and adduction. For parametrising the hand model joint limits, it was assumed that the range is equal in both directions for the index- and middle finger. Since the ring- and little finger mostly allow abduction rather than adduction, 80% of the range was assigned to abduction.

³ The PIP flexion was reported to be increasing from more than 90 deg for the index finger up to 135 deg for the little finger in [31]. Steps of 10 deg between the different finger ranges were assumed for parametrising the hand model joint limits.

A.3 Torque Propagation Modelling

The propagation of torque produced by the motor T_m through the system up to the output torque at the lever T_o can be modelled as shown in Fig. A.1.

For each subsystem, torque components from acceleration, friction and external load may contribute. The total torque produced by the motor can be expressed in these components. In order to do so, the torque on each axis is expressed as function of the torque components.

This model was used in Chapter. 3.V.D to model the output torque as function of the motor torque and the acceleration.

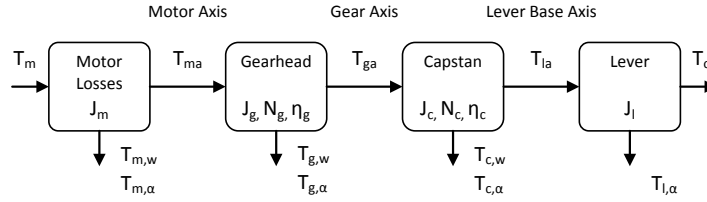


Figure A.1: Propagation of produced motor torque T_m through the system up to the output torque at the lever for operator interaction T_o .

Lever Axis

The lever axis connects the Capstan transmission to the load. Since the Capstan output is physically connected to the lever, this is a virtual axis used for calculation only. $T_{l,\alpha}$ is the torque required for the acceleration of the lever. J_l is the mass inertia as seen at the input axis of the lever. $T_{l,w}$ is the friction of the lever. The latter is assumed negligible.

$$T_{la} = T_{l,\alpha} + T_{l,w} + T_o \quad (\text{A.1})$$

$$T_{l,\alpha} = J_l \alpha_{la} \quad (\text{A.2})$$

$$T_{l,w} = 0 \quad (\text{A.3})$$

Gear Axis

The gear axis connects the gearhead output to the Capstan input. $T_{c,\alpha}$ is the torque required for the acceleration of the Capstan transmission. J_c is the mass inertia as seen at the input of the Capstan transmission. $T_{c,w}$ is the friction introduced in the Capstan, which is set to zero, since the friction is accounted for by the efficiency η_c .

$$T_{ga} = \frac{T_{la}}{N_c \eta_c} + T_{c,\alpha} + T_{c,w} \quad (\text{A.4})$$

$$T_{c,\alpha} = J_c \alpha_{ga} \quad (\text{A.5})$$

$$T_{c,w} = 0 \quad (\text{accounted for by } \eta_c) \quad (\text{A.6})$$

Motor Axis

The motor axis connects the motor output to the gearhead input. $T_{g,\alpha}$ is the torque required for the acceleration of the gearhead. J_g is the mass inertia as seen at the input of the gearhead. $T_{g,w}$ is the friction in the gearhead, which is set to zero, since the friction is accounted for by the efficiency η_g .

$$T_{ma} = \frac{T_{ga}}{N_g \eta_g} + T_{g,\alpha} + T_{g,w} \quad (\text{A.7})$$

$$T_{g,\alpha} = J_g \alpha_{ma} \quad (\text{A.8})$$

$$T_{g,w} = 0 \quad (\text{accounted for by } \eta_g) \quad (\text{A.9})$$

Motor Torque

T_m is the torque actually produced by the motor. Since this torque is subject to losses, it is unequal to the torque torque at the output motor axis. $T_{m,\alpha}$ is the torque required for the acceleration of the rotor. J_m is the rotor inertia. α_{ma} is the acceleration at the motor axis. $T_{m,w}$ is the motor friction torque in the bearings and the commutation system, which is given by the product of the torque k_m and no-load current I_0 .

$$T_m = T_{ma} + T_{m,\alpha} + T_{m,w} \quad (\text{A.10})$$

$$T_{m,\alpha} = J_m \alpha_{ma} \quad (\text{A.11})$$

$$T_{m,w} = k_m I_0 \quad (\text{A.12})$$

Axes Acceleration Relations

The accelerations of the axes is related by the reduction ratios.

$$\alpha_{ga} = N_c \alpha_{la} \quad (\text{A.13})$$

$$\alpha_{ma} = N_g \alpha_{ga} \quad (\text{A.14})$$

A.4 Lower Lever Interaction Force Simulation

In Chapter. 3.VI.C the maximum available interaction force was presented as function of the point of interaction on the upper lever. In this annex, the results for the lower lever are contained.

Fig. A.2 shows the maximum force available over the lever surface in the worst-case operation scenario that an acceleration of 150m/s^2 is reached at the point of interaction. The multiple graphs indicate different levels of motor torque overload. The applied motor torque is the nominal motor torque multiplied by the overload factor QF . Fig. A.3 indicates the maximum force available over the level surface in steady-steady operations when acceleration is zero.

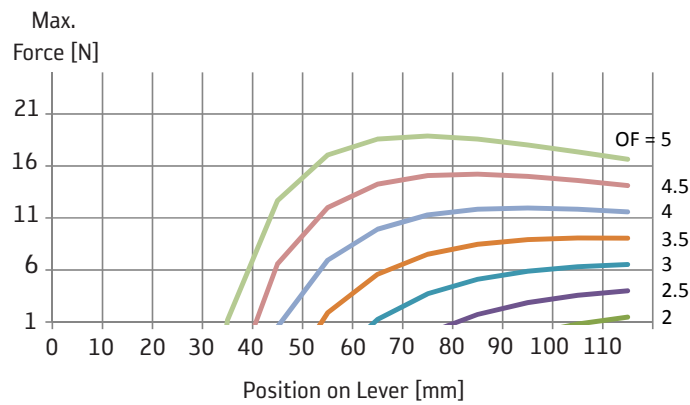


Figure A.2: Maximum interaction force available on the lower lever during fingertip acceleration of 150m/s^2 . The different graphs indicate overload conditions at overload factors OF representing multiples of the nominal motor torque.

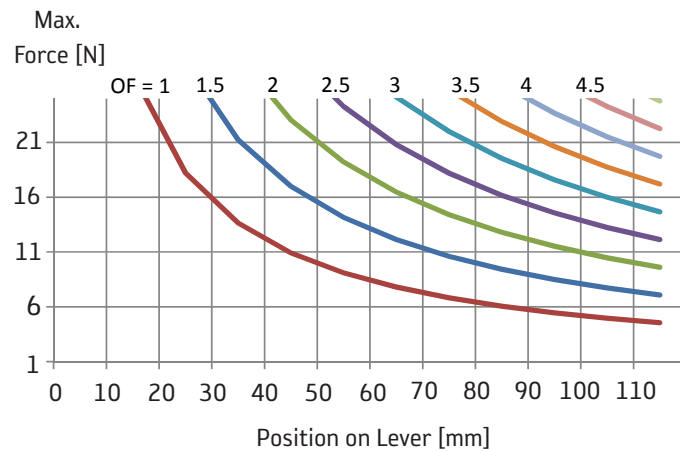


Figure A.3: Maximum interaction force available on the lower lever during steady-state conditions. The different graphs indicate overload conditions at overload factors OF representing multiples of the nominal motor torque.

A.5 Motor Thermal Behaviour Simulation

For the simulation of motor thermal behaviour under overload conditions, used in Chapter. 3.VI.C, the model (Maxon e-learning [70]) shown in Fig. A.4 was implemented in MATLAB/Simulink.

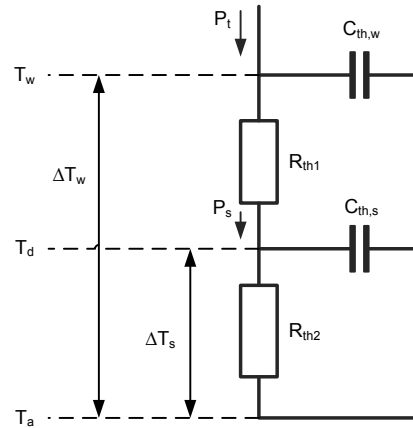


Figure A.4: Motor thermal model including the heat capacitance of the motor winding $C_{th,w}$ and stator $C_{th,s}$, and the thermal resistance from winding to housing R_{th1} and from housing to environment R_{th2} .

The Simulink diagram is shown in Fig. A.5. The system input is the motor current I_m and the outputs are the winding and stator temperature T_w and T_s respectively. The winding resistance R_w determines the power dissipated as heat and is a function of the winding temperature itself, resulting in a feedback loop.

The heating of the winding and stator are functions of the thermal resistance from winding to housing R_{th1} and from housing to environment R_{th2} , and of the heat capacitance of the winding $C_{th,w}$ and stator $C_{th,s}$. This has been implemented via the transfer functions (A.15) and (A.16).

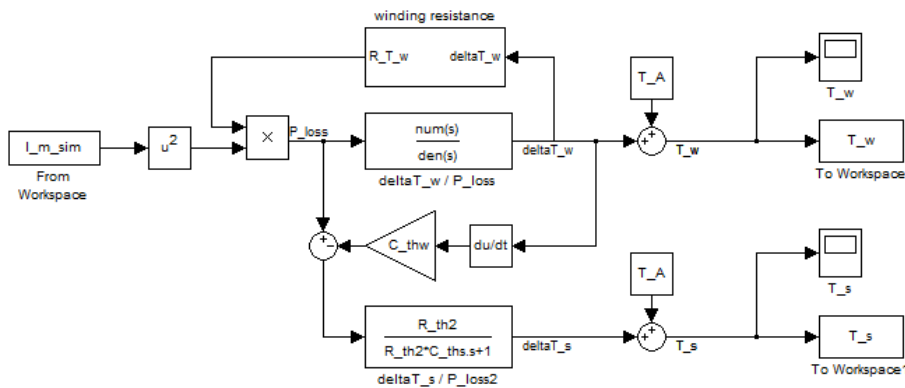


Figure A.5: MATLAB/Simulink implementation of the motor thermal model

$$H_s(s) = \frac{\Delta T_s}{P_s} = \frac{R_{th2}}{R_{th2}C_{ths}s + 1} \quad (\text{A.15})$$

$$H_w(s) = \frac{\Delta T_w}{P_t} \quad (\text{A.16})$$

$$= \frac{R_{th1}R_{th2}C_{ths}s + R_{th1} + R_{th2}}{R_{th1}R_{th2}C_{thw}C_{ths}s^2 + (R_{th1}C_{thw} + R_{th2}C_{thw} + R_{th2}C_{ths})s + 1}$$

Here $P_t = R_w I_m^2$ is the total heat dissipation in the windings and P_s is the heat flow into the stator.

In Chapter. 3.VI.C, results for Maxon motor EC13 12W under various overload conditions have been shown. These results are based on the specified motor data, which is valid under standard conditions where the motor is mounted to a non-conducting flange in free air (no forced convection). By mounting the motor in contact with a good heat conducting material, it was suggested by Maxon that the thermal resistance housing–ambient R_{th2} can be halved. This was simulated and is shown in Fig. A.6. It can be seen that the duration until overheating of the winding improved, especially under low levels over overload. At the nominal current, the maximum winding temperature was greatly reduced from 140°C in standard mounting conditions to roughly 75°C in good conductive mounting conditions.

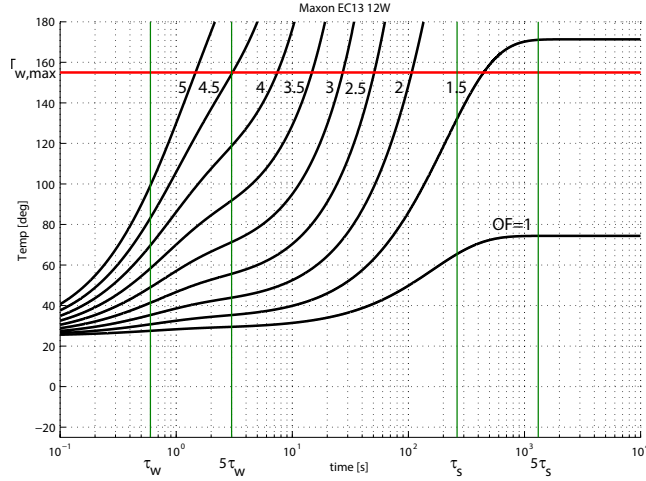


Figure A.6: Thermal behaviour of Maxon EC13 12W in overload conditions. The thermal resistance housing–ambient R_{th2} is assumed half the specified value under standard conditions. The graphs show the heating of the motor winding over time under continuously applied current equal to the specified nominal current times the overload factor OF (i.e. the graph indicated with '2' shows the thermal behaviour for operation at twice the nominal current). Reaching $T_{w,max}$ means overheating of the winding, resulting in irreversible damage.

Annex B

Prototype CAD Drawings

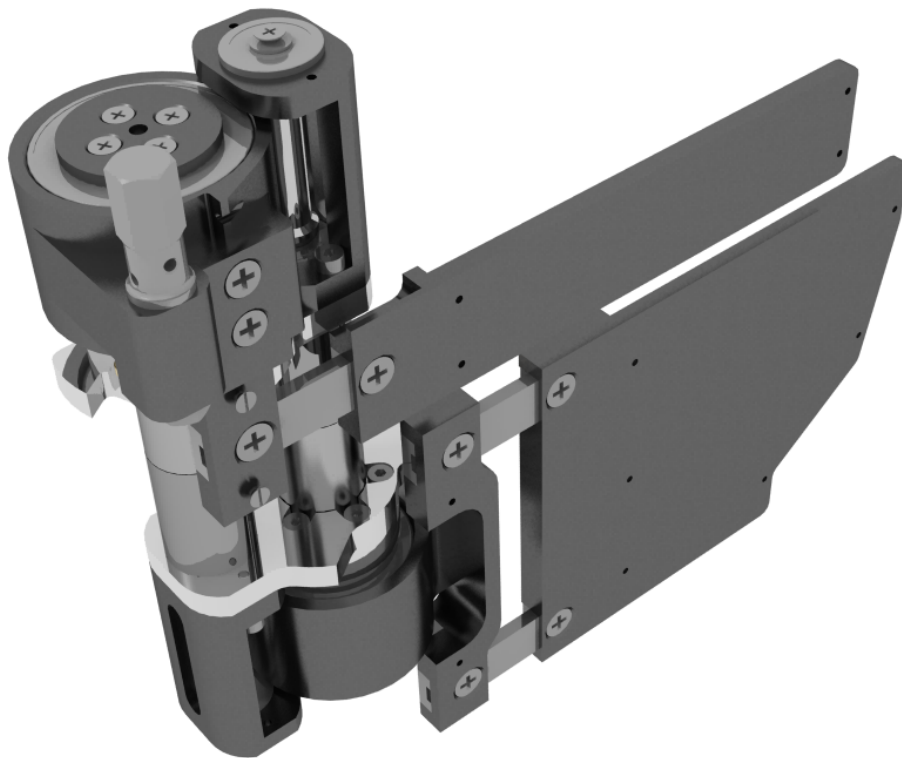
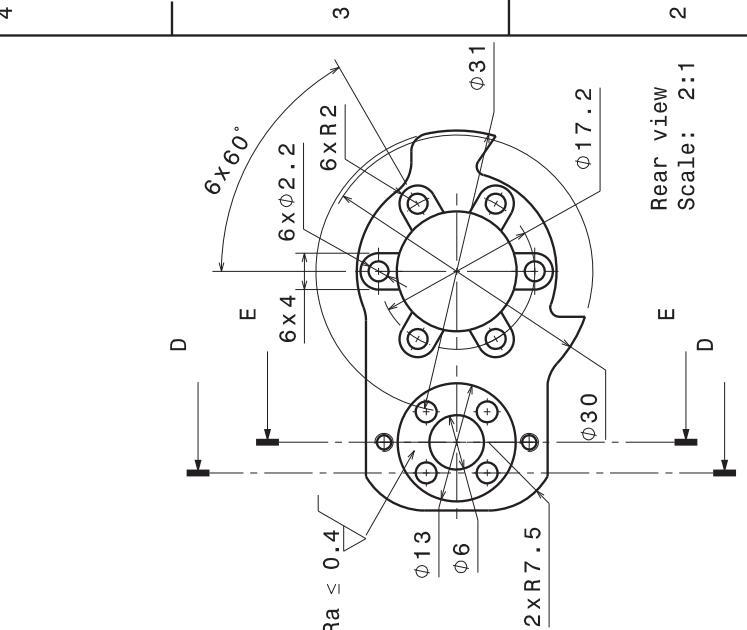
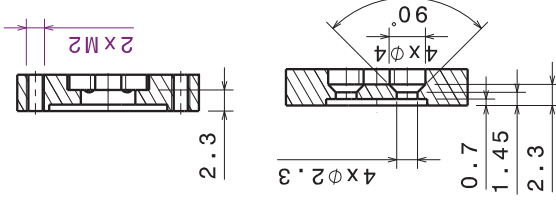


Figure B.1: Grasp master concept mechanical device structure

This annex includes the CATIA CAD drawings of all custom mechanical components that are part of the prototype design. As a reference, a view of the device without covers is given in Fig. B.1.

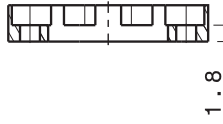
REV	DATE	DESCRIPTION	INIT
A	dd-mm-yyyy

Section view E-E
Scale: 2:1

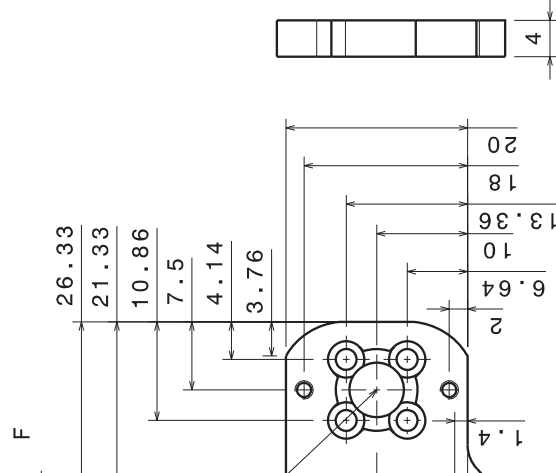


Section view D-D
Scale: 2:1

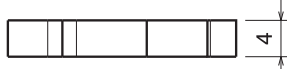
Rear view
Scale: 2:1



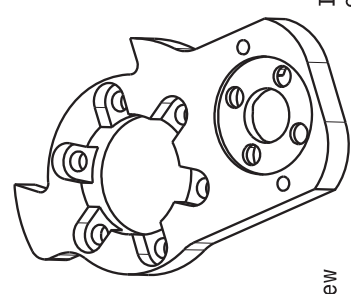
Section view F-F
Scale: 2:1



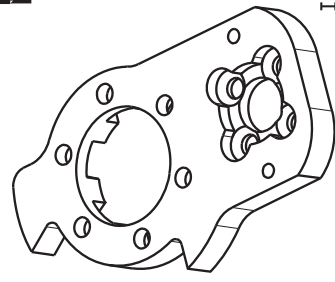
Front view
Scale: 2:1



Left view
Scale: 2:1



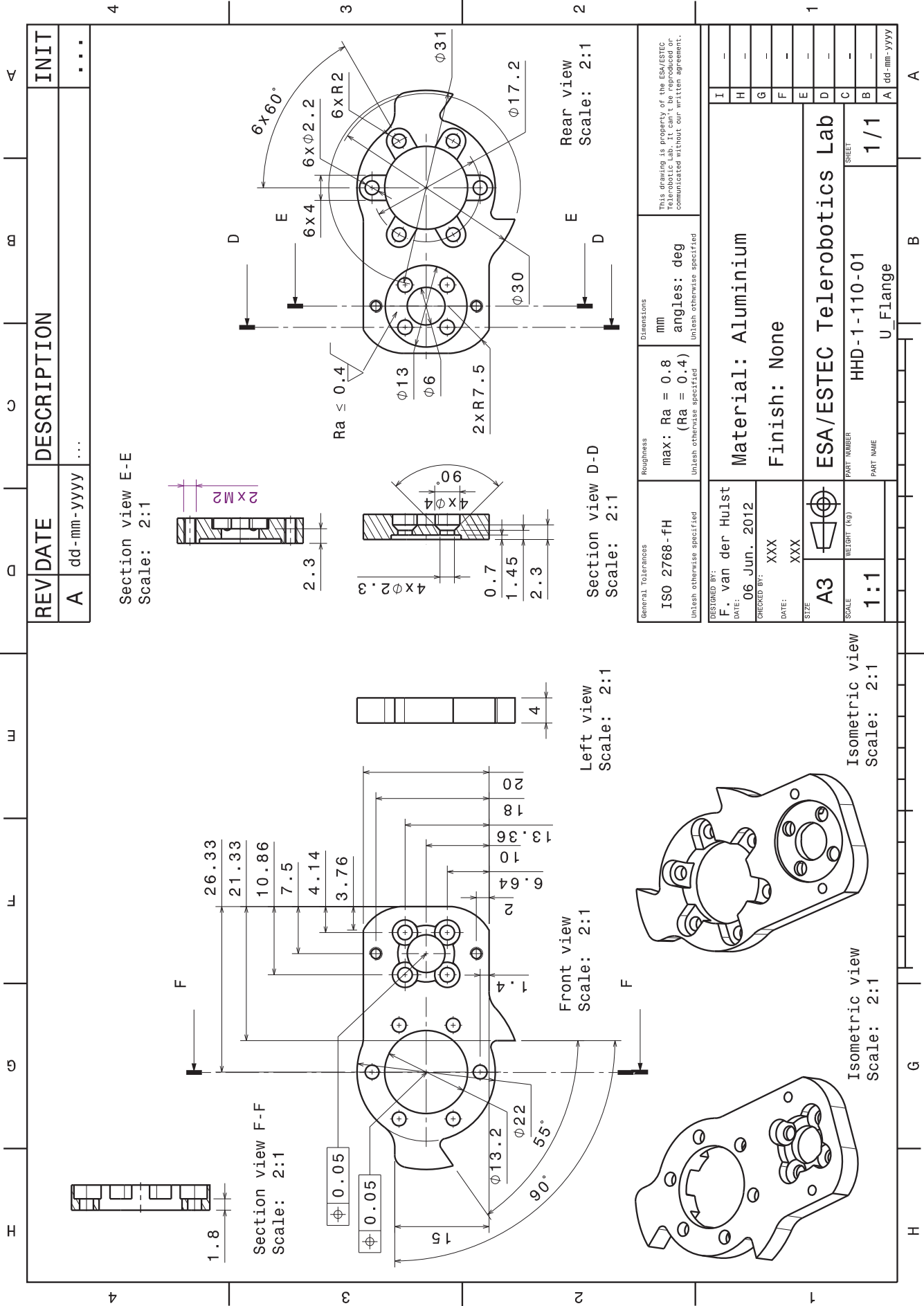
Isometric view
Scale: 2:1



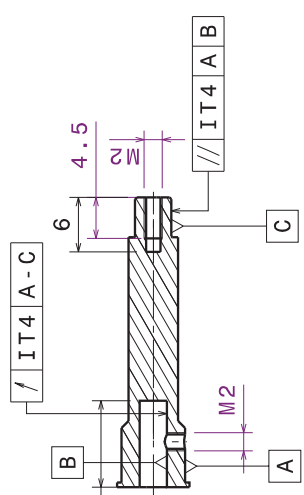
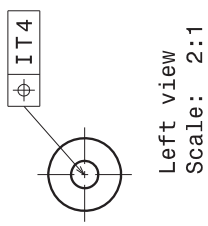
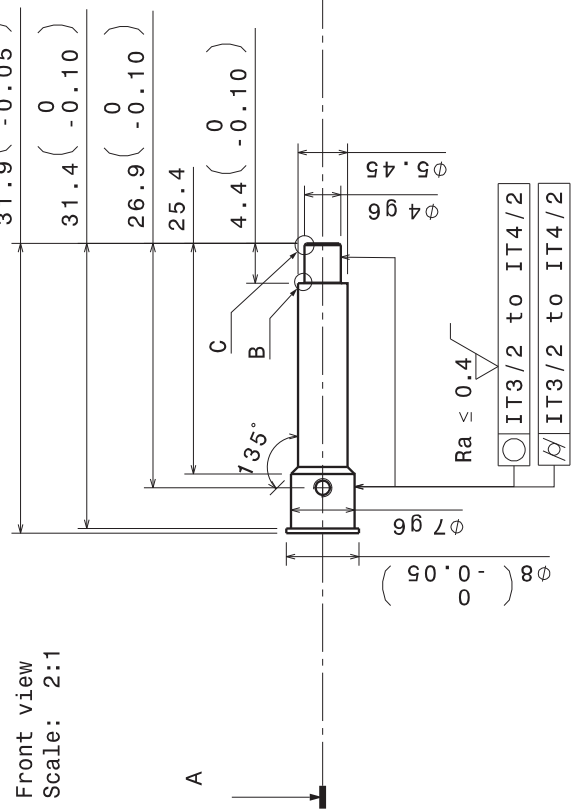
Isometric view
Scale: 2:1

General Tolerances	Roughness	Dimensions	Material	Finish	Part Number	Part Name	Sheet
ISO 2768-fH Unless otherwise specified	max: Ra = 0.8 angles: deg (Ra = 0.4) Unless otherwise specified	mm Unless otherwise specified	Aluminium	None	HHD-1-110-01	U Flange	1/1
DESIGNED BY: F. van der Hulst							
DATE: 06 Jun. 2012							
CHECKED BY: XXX							
DATE: XXX							
SIZE: A3							
SCALE: 1:1							
WEIGHT (kg)							

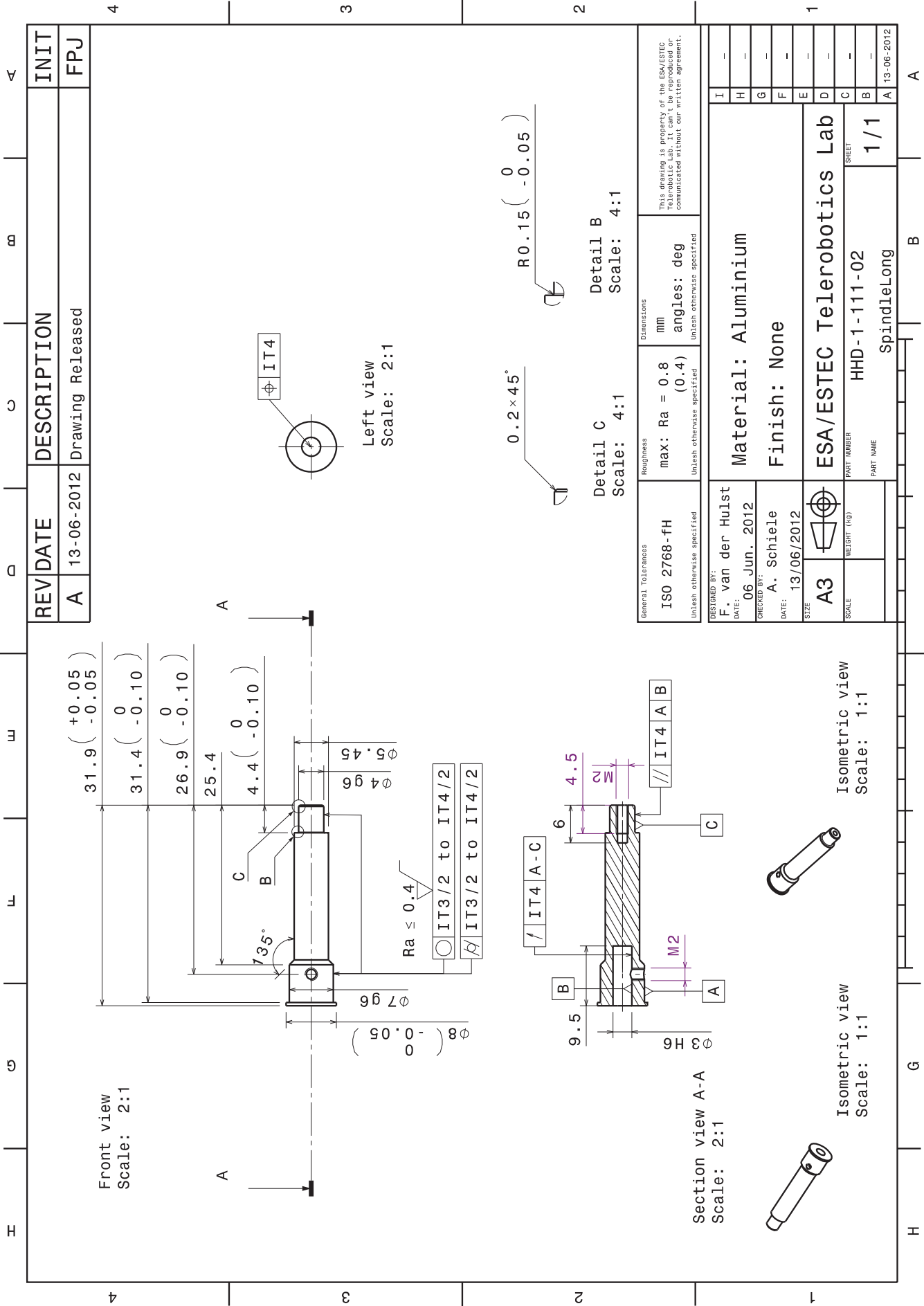
This drawing is property of the ESA/ESTEC
The use of this drawing for other
purposes is prohibited without our written agreement.



REV	DATE	DESCRIPTION	INIT
A	13-06-2012	Drawing Released	FPJ

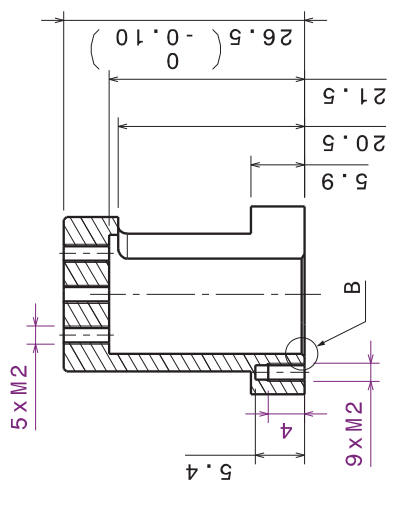


General Tolerances	Roughness	Dimensions	angles: deg
ISO 2768-fH Unless otherwise specified	max: Ra = 0.8 (0.4) Unless otherwise specified	mm Unless otherwise specified	Unless otherwise specified
DESIGNED BY: F. van der Hulst	Material: Aluminium		
DATE: 06 Jun. 2012	Finish: None		
CHECKED BY: A. Schiele	ESA/ESTEC Telerobotics Lab		
DATE: 13/06/2012	HHD-1-111-02		
SIZE: A3	SpindleLong		
SCALE	PART NUMBER	SHEET	
		1/1	
	WEIGHT (kg)	A 13-06-2012	
	PART NAME	A	

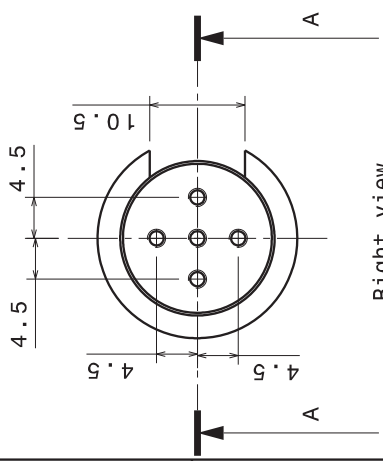
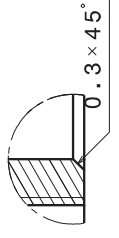


REV	DATE	DESCRIPTION	INIT
A	08-06-2012	Released Drawing	FPJ

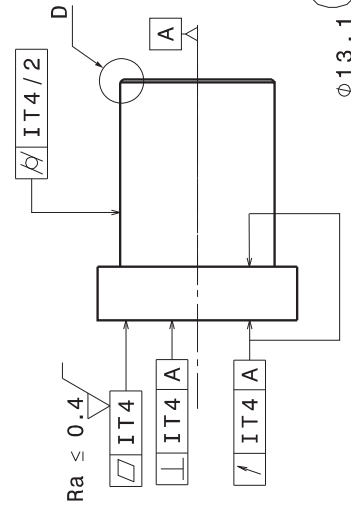
Section view A-A
Scale: 2:1



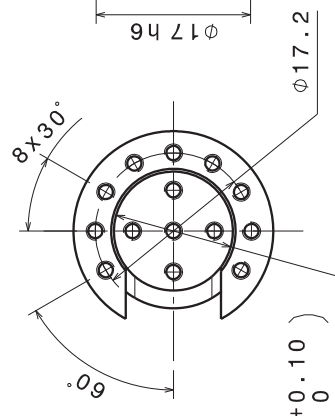
Detail B
Scale: 8:1



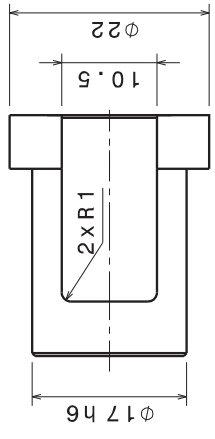
Right view
Scale: 2:1



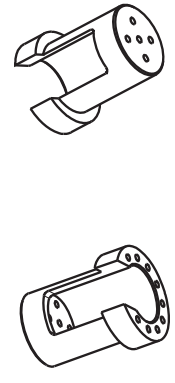
Front view
Scale: 2:1



Left view
Scale: 2:1



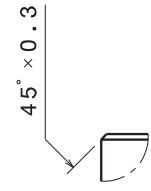
Rear view
Scale: 2:1



Isometric view
Scale: 1:1

Isometric view
Scale: 1:1

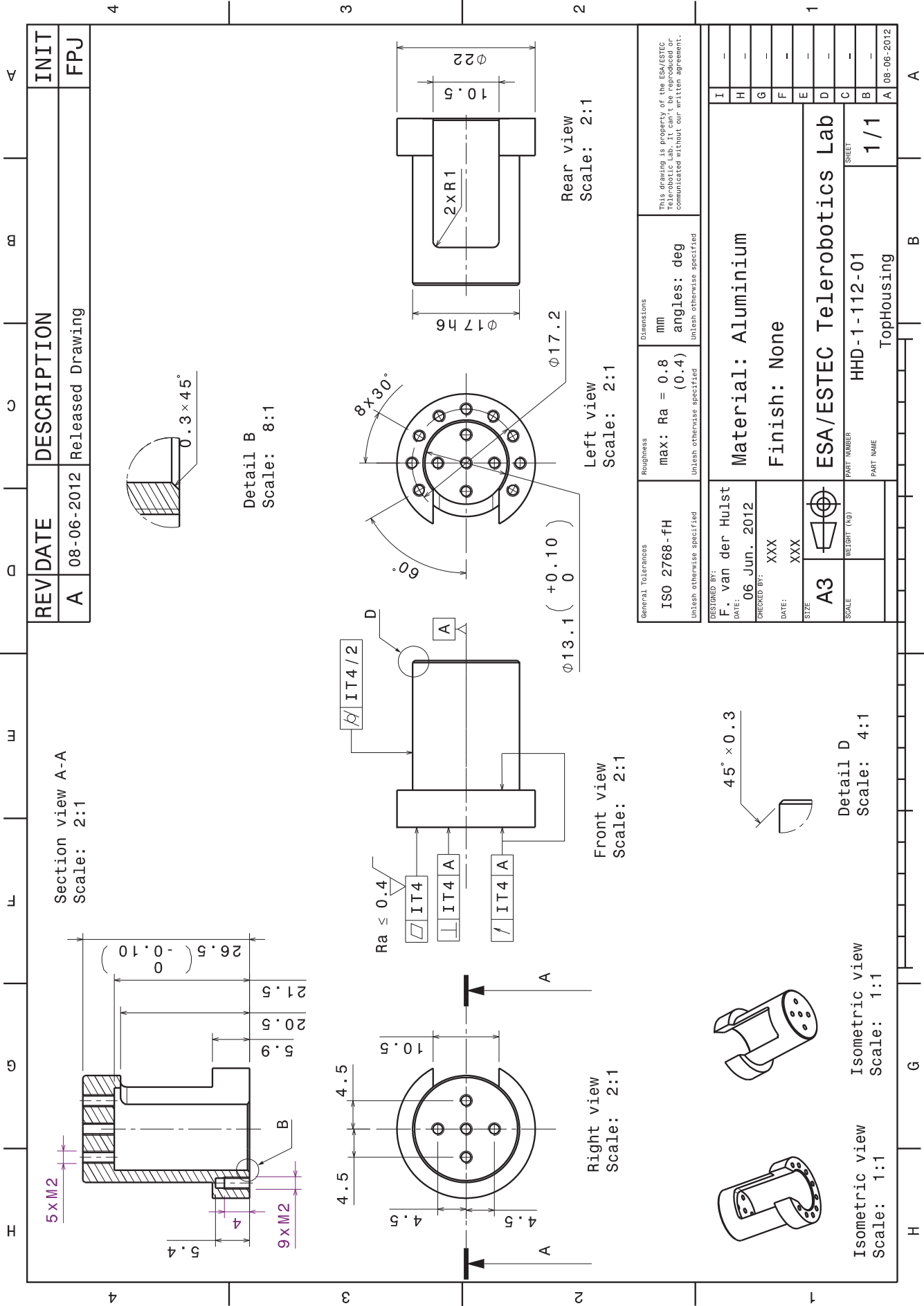
Detail D
Scale: 4:1



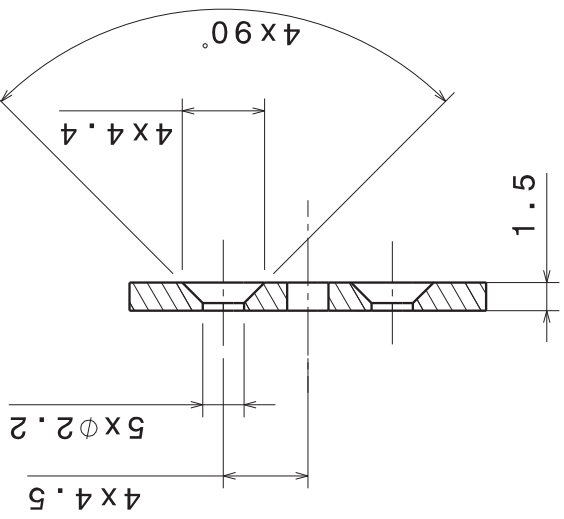
General Tolerances	Roughness	Dimensions	mm
ISO 2768-fH Unless otherwise specified	max: Ra = 0.8 (0.4) Unless otherwise specified	angles: deg Unless otherwise specified	

DESIGNED BY: F. van der Hulst	Material: Aluminium
DATE: 06 Jun. 2012	
CHECKED BY: XXX	Finish: None
DATE: XXX	
SIZE: A3	ESA/ESTEC Telerobotics Lab
SCALE: WEIGHT (kg)	
	PART NUMBER HHD-1-112-01
	PART NAME TopHousing
	SHEET 1/1

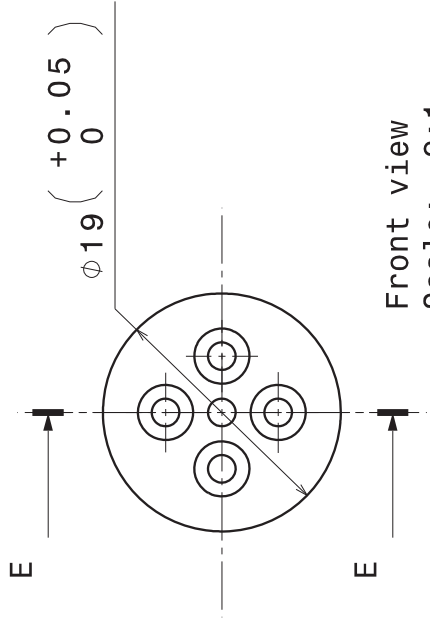
This drawing is property of the ESA/ESTEC TopHousing. It is not to be reproduced or communicated without our written agreement.



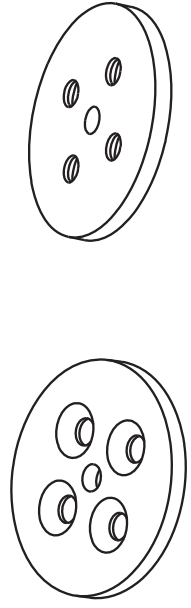
REV	DATE	DESCRIPTION	INIT
A	13-06-2012	Drawing Released	FPJ



Section view E-E
Scale: 3:1



Front view
Scale: 2:1



Isometric view
Scale: 2:1

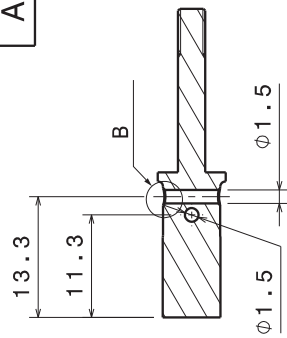
Isometric view
Scale: 2:1

General Tolerances ISO 2768-fH Unless otherwise specified	Roughness max: Ra = 0.8 Unless otherwise specified	Dimensions mm angles: deg Unless otherwise specified	This drawing is property of the ESA/ESTEC. The content shall not be reproduced or communicated without our written agreement.
DESIGNED BY: F. van der Hulst DATE: 06 Jun. 2012	Material: Aluminium		
CHECKED BY: A. Schiele DATE: 13.06.2012	Finish: Dark Grey Anodized		
SIZE A4	ESA/ESTEC Telerobotics Lab		
SCALE	PART NUMBER HHD-1-112-02	SHEET 1/1	
	PART NAME TopHousingBearingClamp		
	WEIGHT (kg)		
			A 13-06-2012

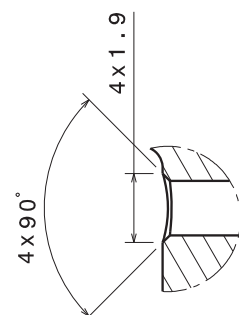
A

D

REV	DATE	DESCRIPTION	INIT
A	dd-mm-yyyy

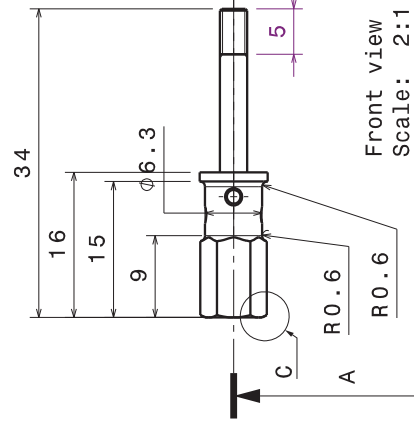
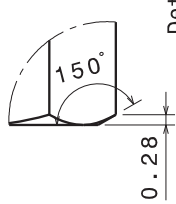


Section view A-A
Scale: 2:1

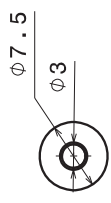


Detail B
Scale: 8:1

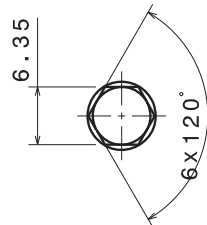
Detail C
Scale: 8:1



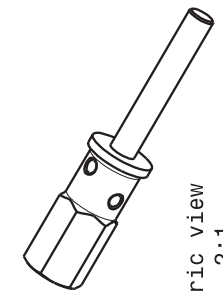
Front view
Scale: 2:1



Right view
Scale: 2:1



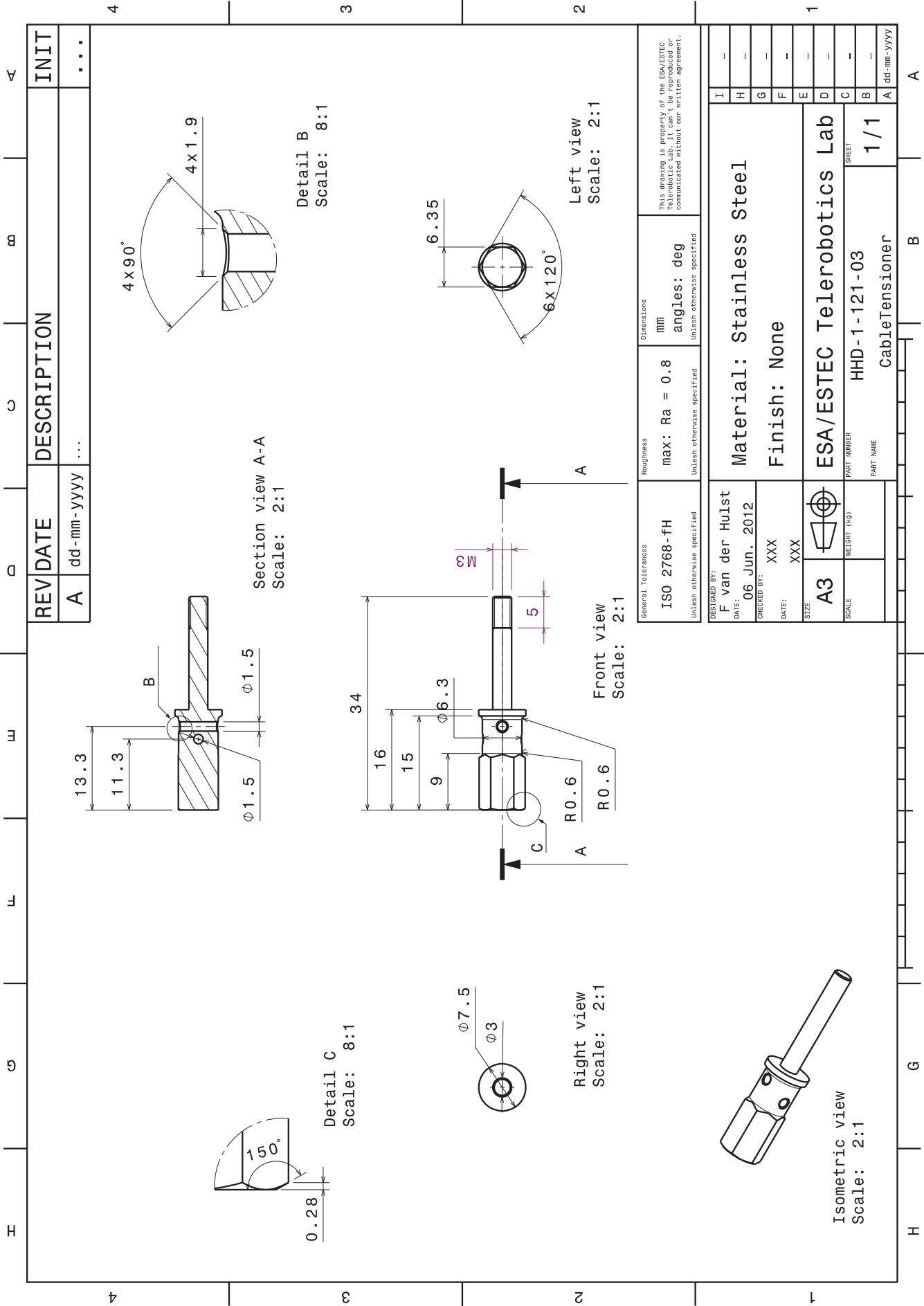
Left view
Scale: 2:1



Isometric view
Scale: 2:1

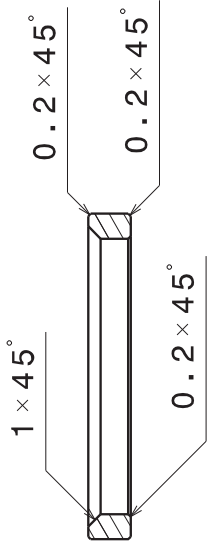
General Tolerances	Roughness	Dimensions
ISO 2768-fH Unless otherwise specified	max: Ra = 0.8 Unless otherwise specified	mm angles: deg Unless otherwise specified

DESIGNED BY: F van der Hulst	Material: Stainless Steel Finish: None
DATE: 06 Jun. 2012	
CHECKED BY: XXX DATE: XXX	
SIZE: A3	ESA/ESTEC Telerobotics Lab
SCALE: (WEIGHT (kg))	
PART NUMBER: HHD-1-121-03	SHEET 1 / 1
PART NAME: CableTensioner	

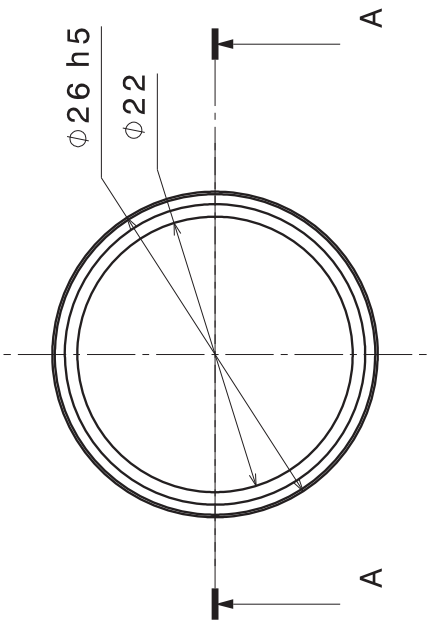


This drawing is property of the ESA/ESTEC Telerobotics Lab. It is not to be reproduced or communicated without our written agreement.

REV	DATE	DESCRIPTION	INIT
A	dd-mm-yyyy



Section view A-A
Scale: 2:1



Front view
Scale: 2:1

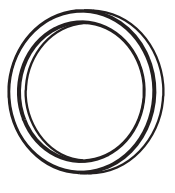


Left view
Scale: 2:1

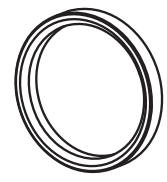
General Tolerances	Roughness	Dimensions	This drawing is property of the ESA/ESTEC. It is not to be reproduced or communicated without our written agreement.
ISO 2768-fH Unless otherwise specified	max: Ra = 0.8 Unless otherwise specified	mm angles: deg Unless otherwise specified	

DESIGNED BY: F. van der Hulst	Material: Aluminium Finish: None
DATE: 06 Jun. 2012	
CHECKED BY: XXX	Material: Aluminium Finish: None
DATE: XXX	

SIZE A4	Material: Aluminium Finish: None
SCALE	
WEIGHT (kg)	Material: Aluminium Finish: None
PART NUMBER HHD-1-121-04	Material: Aluminium Finish: None
PART NAME BearingSpacer	
SHEET 1/1	Material: Aluminium Finish: None



Isometric view
Scale: 1:1

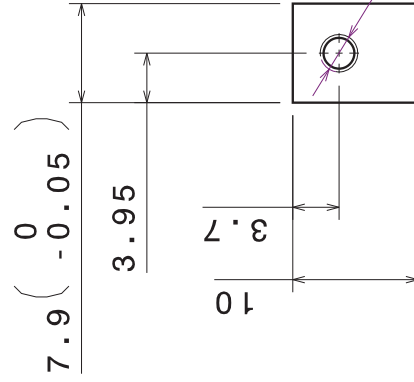


Isometric view
Scale: 1:1

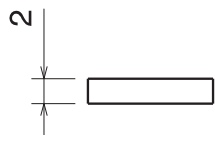
A

D

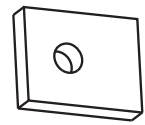
REV	DATE	DESCRIPTION	INIT
A	dd-mm-yyyy



Front view
Scale: 2:1



Left view
Scale: 2:1



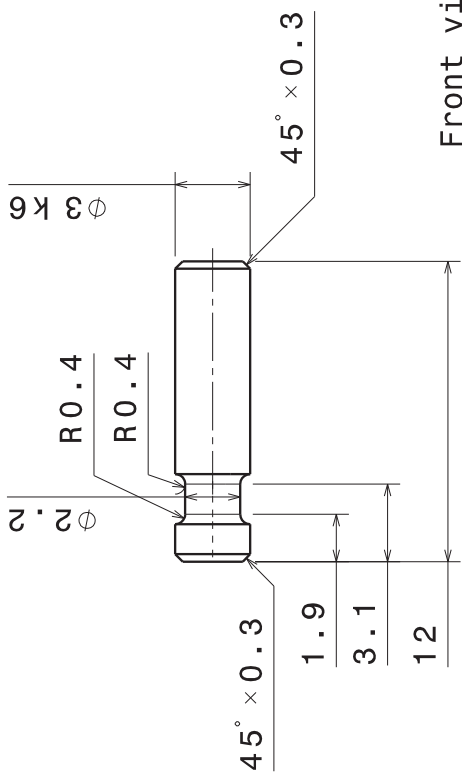
Isometric view
Scale: 2:1

General Tolerances		Roughness	Dimensions	This drawing is property of the ESA/ESTEC. It is not to be reproduced or communicated without our written agreement.
ISO 2768-fH Unless otherwise specified		max: Ra = 0.8 Unless otherwise specified	mm angles: deg Unless otherwise specified	
DESIGNED BY: F. van der Hulst DATE: 06 Jun. 2012		Material: Stainless Steel		
CHECKED BY: XXX DATE: XXX		Finish: None		
SIZE A4	ESA/ESTEC Telerobotics Lab		I	
SCALE 1:1	WEIGHT (kg)	PART NUMBER HHD-1-121-05	H	
		PART NAME SensorClampPlate_2mm	G	
			F	
			E	
			D	
			C	
			B	
			A	

A

D

REV	DATE	DESCRIPTION	INIT
A	dd-mm-yyyy



Front view
Scale: 4:1



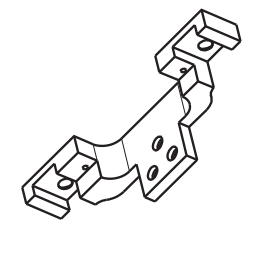
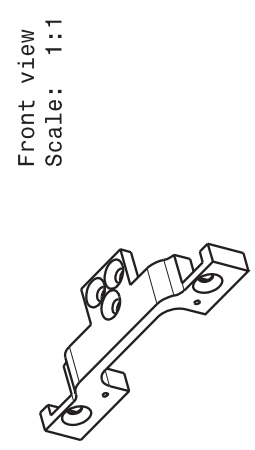
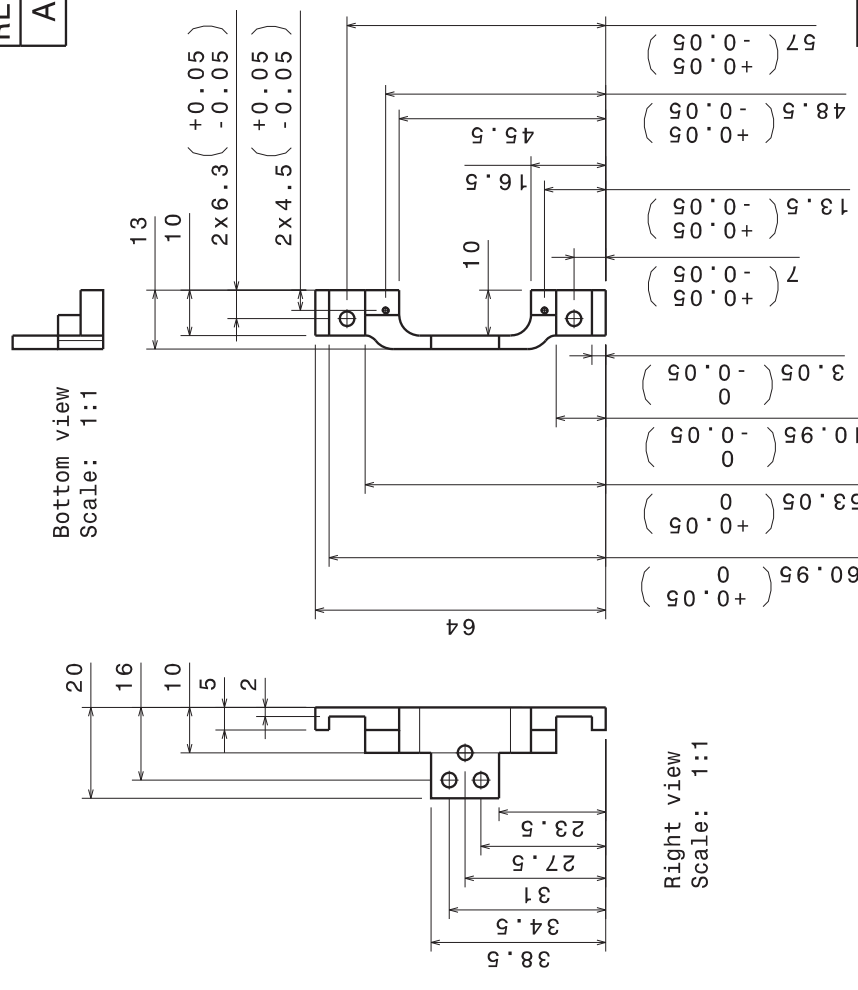
Isometric view
Scale: 2:1

General Tolerances		Roughness	Dimensions	This drawing is property of the ESA/ESTEC. It is not to be reproduced or communicated without our written agreement.
ISO 2768-fH Unless otherwise specified		max: Ra = 0.8 Unless otherwise specified	mm angles: deg Unless otherwise specified	
DESIGNED BY: F. van der Hulst		Material: Brass		
DATE: 06 Jun. 2012				
CHECKED BY: XXX		Finish: None		
DATE: XXX				
SIZE A4	ESA/ESTEC Telerobotics Lab		SHEET 1/1	
SCALE	PART NUMBER HHD-1-121-06			
WEIGHT (kg)		PART NAME GroovedPin_2m6		A dd-mm-yyyy

A

D

REV	DATE	DESCRIPTION	INIT
A	dd-mm-yyyy



Front view
Scale: 1:1

Left view
Scale: 1:1

Right view
Scale: 1:1

Bottom view
Scale: 1:1

General Tolerances	Roughness	Dimensions
ISO 2768-fH Unless otherwise specified	max: Ra = 0.8 Unless otherwise specified	mm angles: deg Unless otherwise specified

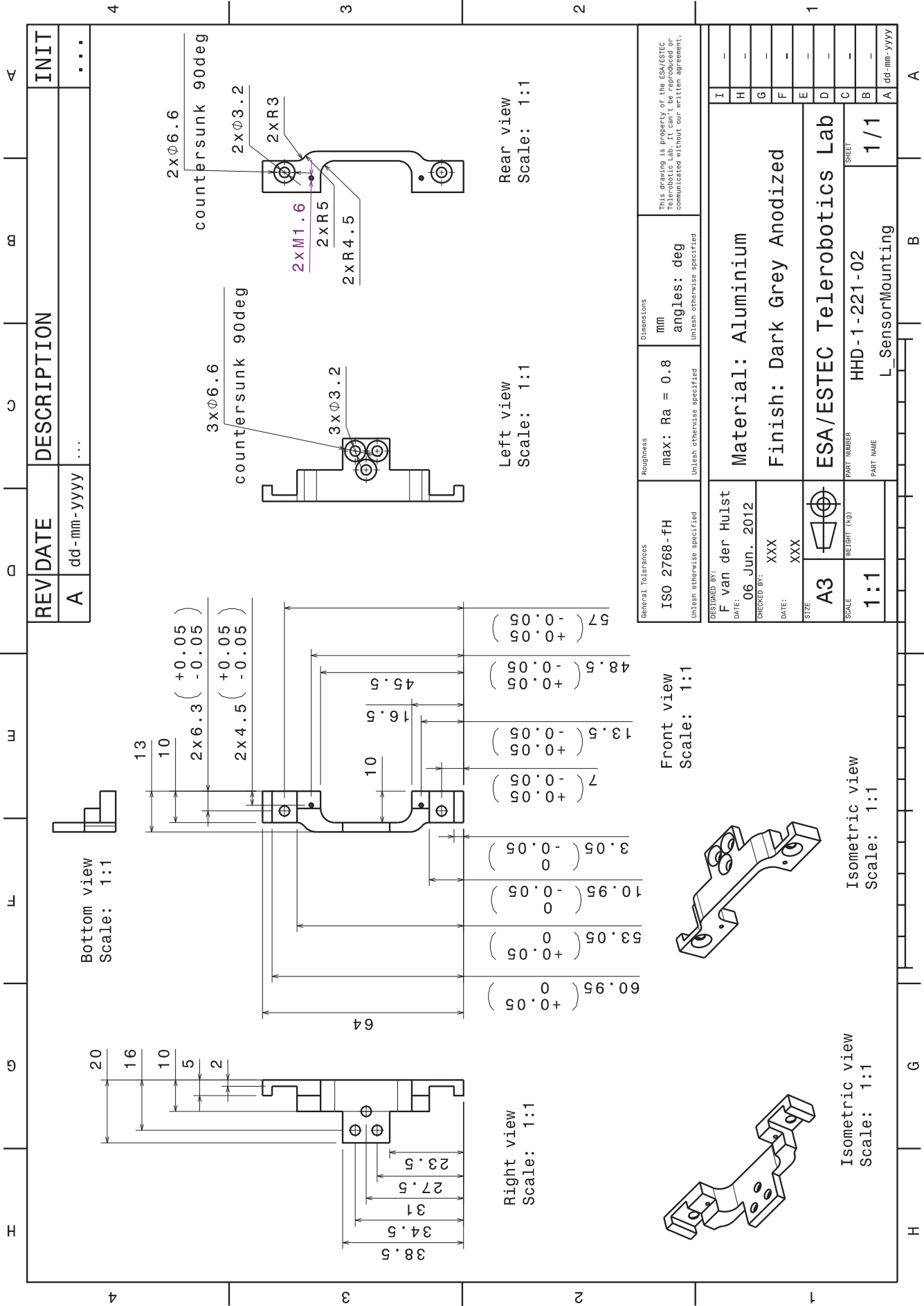
DESIGNED BY: F van der Hulst	Material: Aluminium Finish: Dark Grey Anodized ESA/ESTEC Telerobotics Lab
DATE: 06 Jun. 2012	
CHECKED BY: XXX	
DATE: XXX	HHD-1-221-02 L_SensorMounting
SIZE: A3	
SCALE: 1:1	PART NUMBER PART NAME SHEET 1/1

Front view
Scale: 1:1

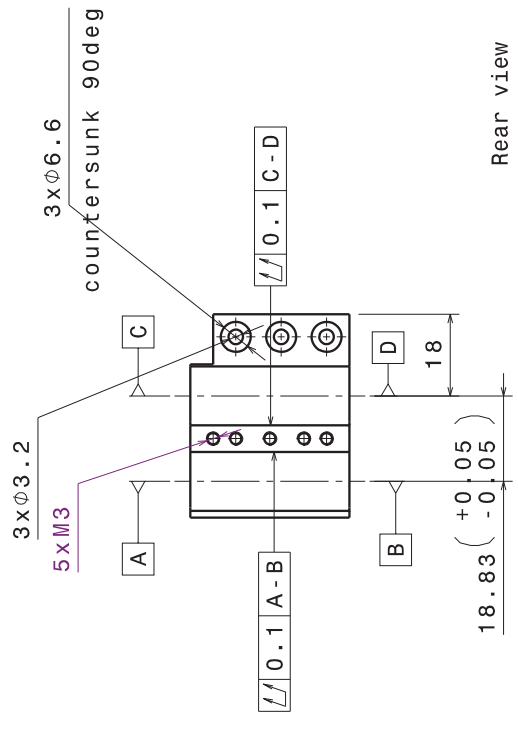
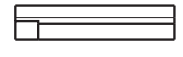
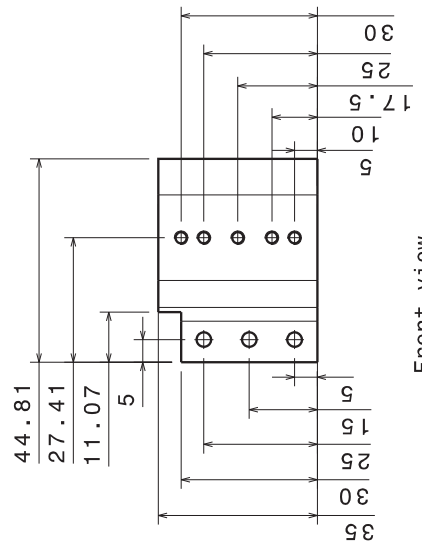
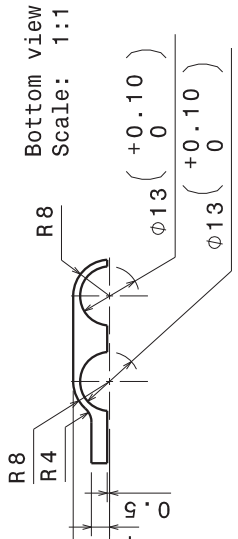
Isometric view
Scale: 1:1

Isometric view
Scale: 1:1

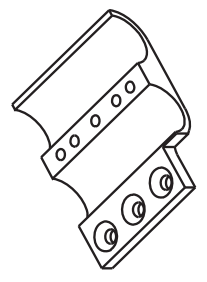
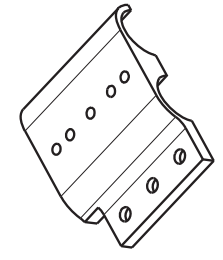
This drawing is property of the ESA/ESTEC Telerobotics Lab. It is not to be reproduced or communicated without our written agreement.



REV	DATE	DESCRIPTION	INIT
A	dd-mm-yyyy



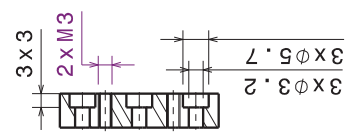
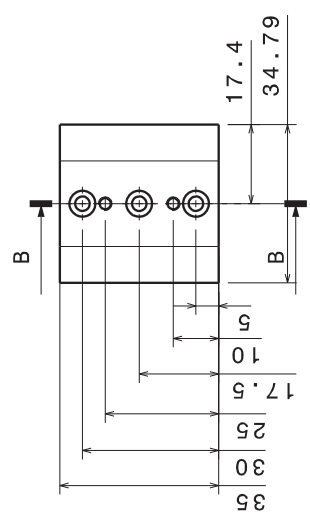
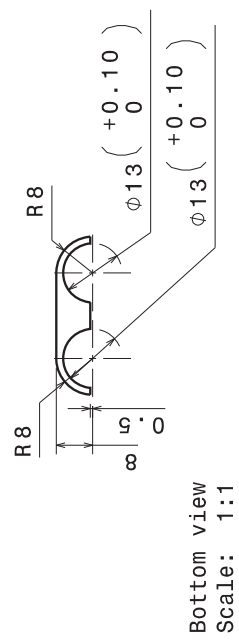
General Tolerances	ISO 2768-fH	Unless otherwise specified	Roughness	max: Ra = 0.8	Unless otherwise specified	Dimensions	mm	angles: deg	Unless otherwise specified	This drawing is property of the ESA/ESTEC. The use of this drawing for any other purpose without our written agreement.						
DESIGNED BY:	F van der Hulst									Material: Aluminium						
DATE:	06 Jun. 2012									Finish: None						
CHECKED BY:	XXX									ESA/ESTEC Telerobotics Lab						
DATE:	XXX									HHD-1-300-01						
SIZE	A3									MotorHousingFingerHalf						
SCALE	1:1									SHEET 1/1						
WEIGHT (kg)										PART NUMBER HHD-1-300-01						
										PART NAME MotorHousingFingerHalf						



Grid lines: E, F, G, H, U, W, Q, R, S, T, A, B, C, D, E, F, G, H, I

Section lines: 1, 2, 3, 4

REV	DATE	DESCRIPTION	INIT
A	dd-mm-yyyy



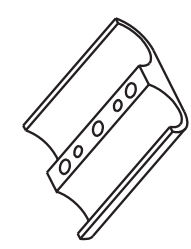
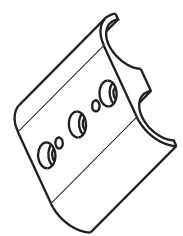
Front view
Scale: 1:1

Section view B-B
Scale: 1:1

18.83 $\left(\begin{matrix} +0.05 \\ -0.05 \end{matrix} \right)$

Rear view
Scale: 1:1

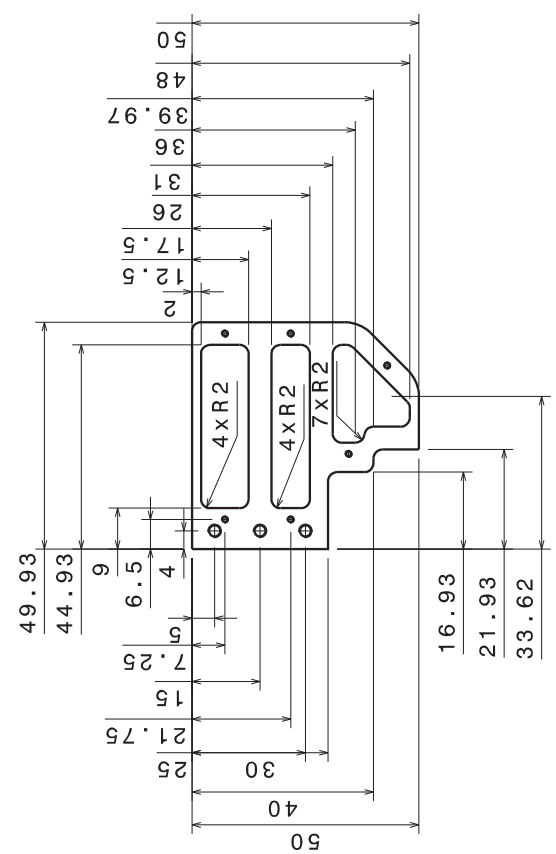
General Tolerances	Roughness	Dimensions	This drawing is property of the ESA/ESTEC Technology Centre. It is not to be reproduced or communicated without our written agreement.
ISO 2768-fH <small>Unless otherwise specified</small>	max: Ra = 0.8 <small>Unless otherwise specified</small>	mm angles: deg <small>Unless otherwise specified</small>	
DESIGNED BY: F van der Hulst	DATE: 06 Jun. 2012	Material: Aluminium Finish: None	
CHECKED BY: XXX	DATE: XXX		
SIZE A3	WEIGHT (kg)		
SCALE 1:1	PART NUMBER HHD-1-300-02	ESA/ESTEC Telerobotics Lab SHEET 1 / 1	
	PART NAME MotorHousingThumbHalf	I - H - G - F - E - D - C - B - A dd-mm-yyyy	



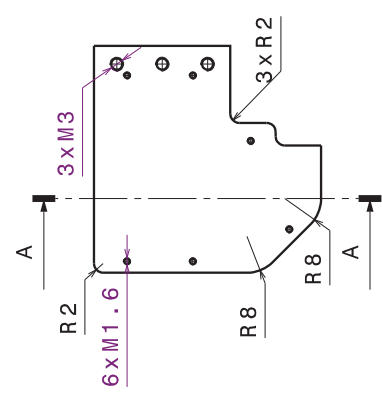
Isometric view
Scale: 1:1

Isometric view
Scale: 1:1

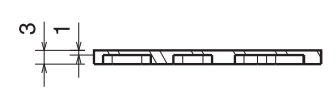
REV	DATE	DESCRIPTION	INIT
A	dd-mm-yyyy



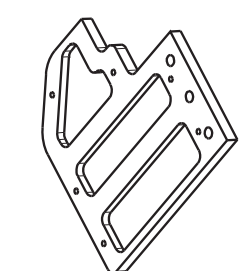
Front view
Scale: 1:1



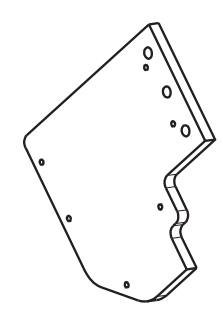
Rear view
Scale: 1:1



Section view A-A
Scale: 1:1

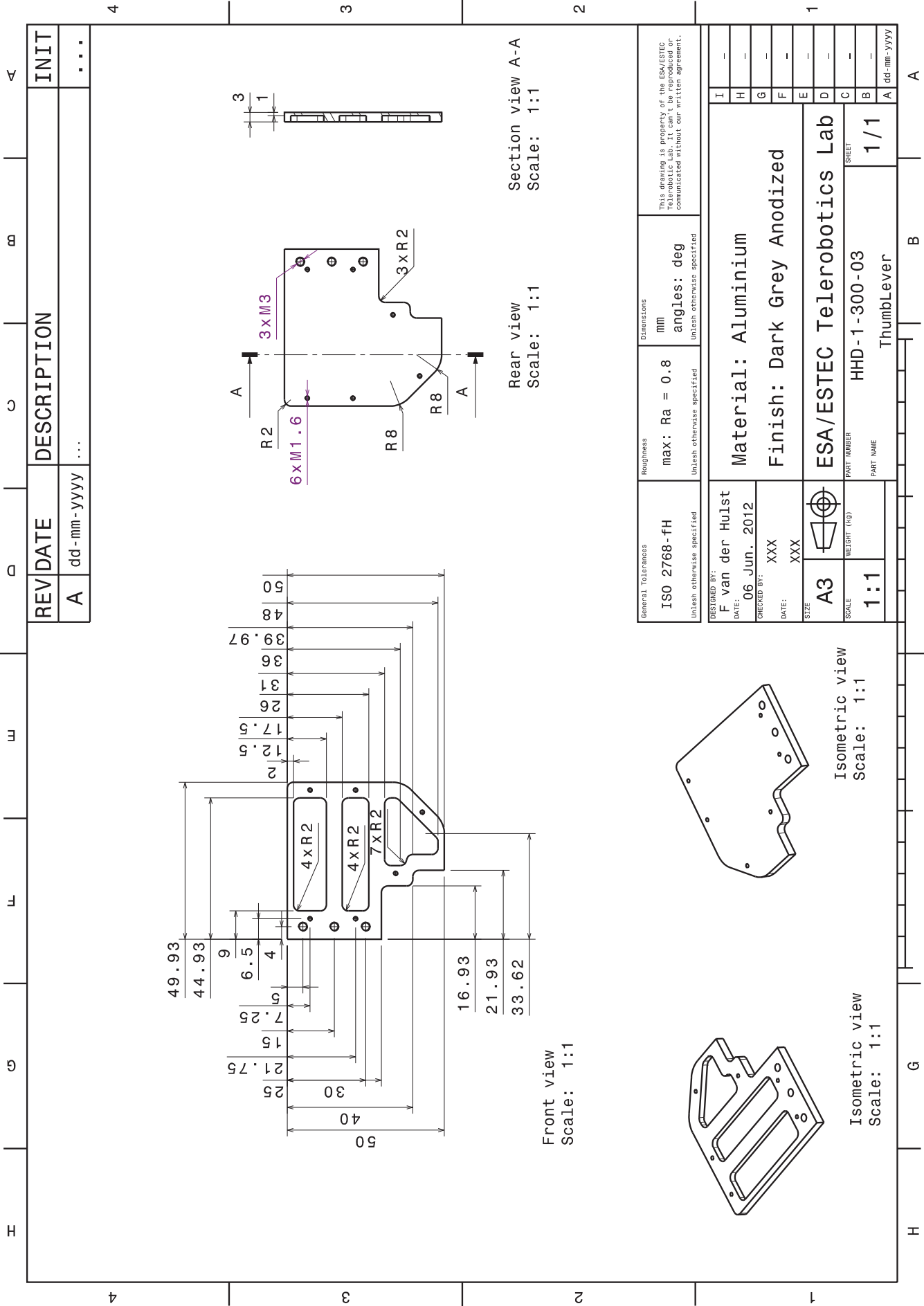


Isometric view
Scale: 1:1

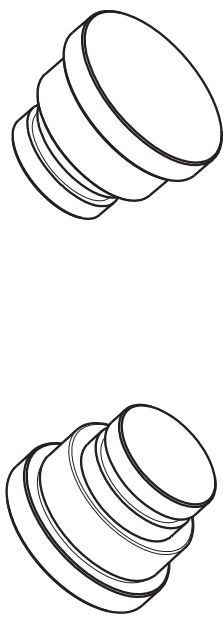
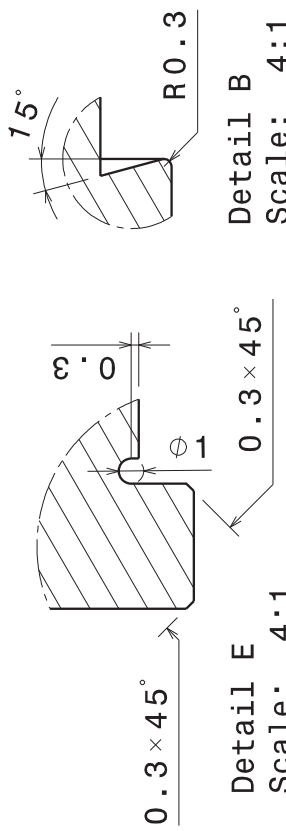
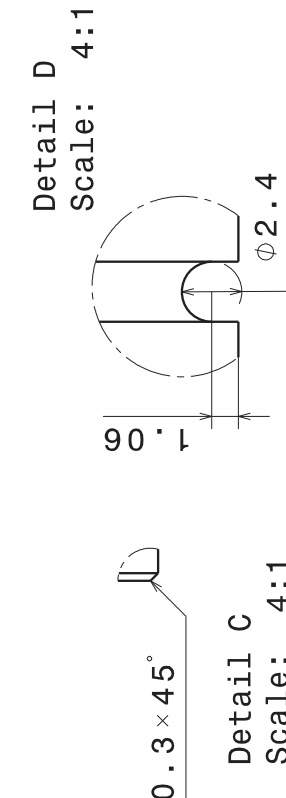
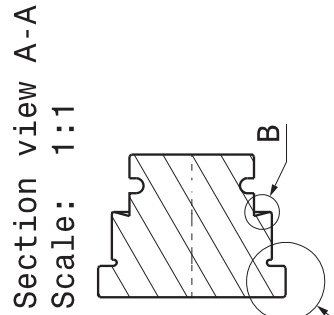
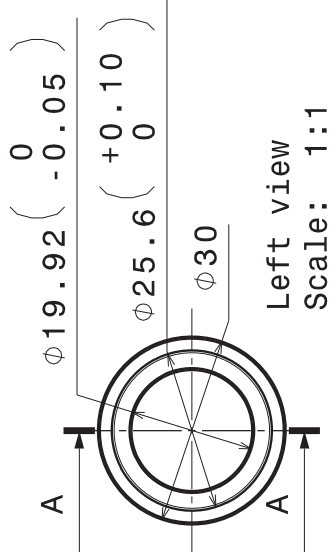
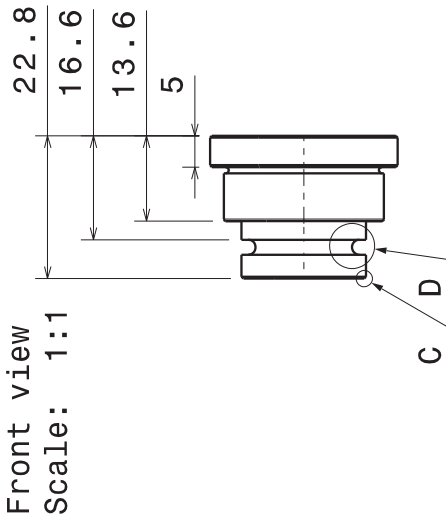


Isometric view
Scale: 1:1

General Tolerances	Roughness	Dimensions	This drawing is property of the ESA/ESTEC. The use of this drawing for other purposes is prohibited without our written agreement.
ISO 2768-fH Unless otherwise specified	max: Ra = 0.8 Unless otherwise specified	mm angles: deg Unless otherwise specified	
DESIGNED BY: F van der Hulst	Material: Aluminium Finish: Dark Grey Anodized		
DATE: 06 Jun. 2012			
CHECKED BY: XXX	ESA/ESTEC Telerobotics Lab		
DATE: XXX			
SIZE A3	PART NUMBER HHD-1-300-03		
SCALE 1:1			
WEIGHT (kg)	ThumbLever		
SHEET 1/1			



REV	DATE	DESCRIPTION	INIT
A	dd-mm-yyyy



General Tolerances	Roughness	Dimensions	angles: deg
ISO 2768-fH Unless otherwise specified	max: Ra = 0.8 Unless otherwise specified	mm Unless otherwise specified	deg Unless otherwise specified

DESIGNED BY: F. Van der Hulst	This drawing is property of the ESA/ESTEC. This object shall not be reproduced or communicated without our written agreement.
DATE: 06 Jun. 2012	
CHECKED BY: XXX	Material: Stainless Steel
DATE: XXX	
SIZE A4	Finish: None
SCALE	

ESA/ESTEC Telerobotics Lab	
PART NUMBER	HHD-4-121-01
PART NAME	NeedleBearingDolly
WEIGHT (kg)	
SHEET	1/1

A

D

Annex C

Literature Survey: Toward the Design of a Low-complexity Space Telerobotic Hand Master

Literature Survey
Nov. 15 2010 - May 10 2011

This literature survey reports on a detailed analysis of relevant operation context and gives an advice on the design of a low-complexity haptic hand master for space robotics teleoperation. The analysis includes identification of relevant space operation tasks, the grasp types required for this, requirements from human factors and possibilities to exploit psychophysical effects. This knowledge was used in the efficient hand master concept development in Chapter. 3.

Toward the Design of a Low-complexity Space Telerobotic Hand Master

Literature Survey

F.P.J. van der Hulst

Abstract—This paper presents an advice on the design of a low-complexity haptic hand master device for use in space teleoperation applications.

Methods for the reduction of the amount of degrees of freedom (DOFs) were obtained by analyzing intended tasks and required grasps, relevant slave devices, existing master devices and human factors including force coupling effects. These can be used to keep the device complexity low, resulting in good usability and high device performance.

Full slave controllability and sufficient observability can be achieved by the application of a sensor-actuator asymmetry, implemented as a separate sensing and force reflecting device. The sensing device can sense all or most DOFs of the human hand, while the force reflective device can provide feedback in a limited number of DOFs that are specifically important considering the functionality of the human hand and the capabilities of relevant slave devices.

The advised low-complexity device design with good usability and high device performance can be promising when its features are designed to specifically comply with the intended usage of the device.

Index Terms—Enslaving, Grasp Classification, Haptic Devices, Human Factors, Low-complexity Hand Master, Sensor-actuator Asymmetry, Space Robotic Teleoperation

I. INTRODUCTION

THE haptic arm exoskeleton X-Arm-2, as presented in [1], is a body grounded device that is usable by different operators without adjustments being required. It can be used to teleoperate a robotic manipulator while providing the user with haptic feedback. In order to perform dexterous manipulation and exploration, the robotic manipulator can be equipped with an end-effector. In this case, an additional interface is required to provide the user with haptic feedback to the hand.

This survey will focus on the design aspects of an easy to use haptic hand master for space telerobotic applications. A schematic system overview is shown in Fig. 1. The human operator will use a hand master device to teleoperate space environment tasks with one of several relevant slave end-effector devices. The grasping forces sensed by the slave device will be reflected onto the human hand by that hand master. The communication between master and slave device is a data stream in which a mapping defines the relation between master and slave positions and forces.

A. Problem Statement

As will be elaborated in Section. V, large variety exists in haptic hand masters described in literature. Part of the devices can be considered complex in the sense that these contain

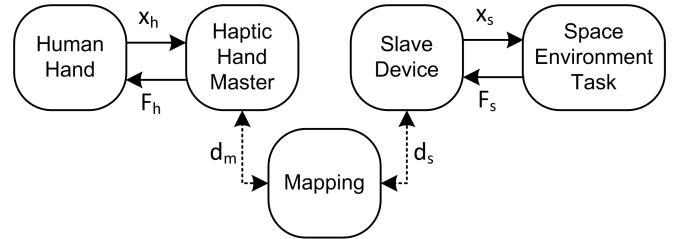


Fig. 1. Schematic haptic hand master-slave system overview. x_h : motion exerted by hand, x_s : motion exerted by slave, F_h : force reflected to hand, F_s : force sensed by the slave, d_m : data stream between master and mapping, d_s : data stream between slave and mapping.

many structural degrees of freedom (DOFs) and many components to allow natural human hand motion. By using multiple actuated DOFs in combination with inventive mechanisms, it is possible to provide force feedback with specific magnitude and orientation to specific positions on the hand and fingers. Low-complexity devices contain little degrees of freedom and considerably less components. Force feedback is provided to a limited number of positions and often the force orientation is not independently controllable.

It is important to tailor haptic interfaces to the capabilities and the limitations of the human operators, which makes usability one of the main design requirements. Usability involves effective and efficient operation to improve the user performance. It also involves comfort while wearing the device and ease of putting it on and off. Both user performance and comfort should be satisfied for operators of different stature without adjustments being required. The hand master should be compatible with other relevant devices, requiring that it does not prevent use in combination with a haptic arm master.

Device performance of haptic interfaces plays an essential role. As stressed in [2], a criterion specifically important in haptics is structural transparency that allows the operator to feel the intended force reflection without influence of the mechanical structure of the haptic device. This involves minimization of mass, inertia, friction and backlash while ensuring a high stiffness transmission. In addition to this, backdrivability should be high and both the mechanical and control bandwidths should be sufficient to provide the operator with a natural feeling.

While complex devices often provide realistic force feedback in the sense of magnitude and direction, each DOF increases the number of required components, resulting in larger size, higher mass and higher cost. This is especially true

for actuated DOFs which require an actuator and possibly a transmission. Also each DOF requires alignment to achieve good sensing and force reflecting accuracy and to prevent constraint forces that can limit the workspace. As a result, the usability and the device performance can be negatively influenced when using many DOFs. Complex devices often are fixed to the hand on multiple positions, making them difficult to put on. The placement of the structures and actuators is a challenge in these devices and as a result actuators are often located away from the hand. This reduces the size and the complexity of the structure on the hand, but can limit ease-of-use and compatibility with an arm device. Moreover, the required transmissions can reduce performance in terms of structural transparency.

B. Goal of Literature Survey

The goal of this literature survey is to investigate existing hand master and slave devices, relevant tasks to perform and the grasps required for this, and human factors in order to extract necessary features for an easy to use bi-lateral haptic hand master that improves user performance in space telerobotics applications.

A low-complexity device contains few structural DOFs and few actuators. It likely does not provide force feedback to each hand and finger segment and probably this neither will be in the natural directions. On the other hand, a simple structure can provide good usability and increased user performance as shown in [3]. Thanks to low mass and size, device handling and compatibility with other devices can be increased. The device performance can be high when short drive chains are used to obtain good structural transparency. Also it is important to note that while actuators are mass, size, cost and power expensive, sensors can be small, light, and cheap. This suggests to investigate towards a simple device design with good sensing capability.

It is hypothesized that a haptic hand master with low structural complexity, which is designed to have good usability and high device performance, can increase user performance.

C. Document Structure

Multiple related topics were studied in order to summarize requirements and techniques for the design of a haptic hand master with good usability and device performance. Chapter. II summarizes relevant tasks and the typical grasps required to perform these. In Chapter. III relevant slave devices are covered. The functional principles and human factors of the hand are summarized in Chapter. IV. In Chapter. V, a comparison of reported master devices is presented. The principles of sensor-actuator asymmetry are introduced in Chapter. VI. In Chapter. VII the content of the previous chapters is discussed. In Chapter. VIII the insights from the discussion are used to formulate advice on the design of a haptic hand device. The conclusion is drawn in Chapter. IX.

II. TASKS AND GRASPS

Distinct grasps are used depending on the object handled and the operation performed. Analysis of space environment

operations and tools, and the principles of human grasp modeling, provide insight in the relevant tasks and the grasps required to perform these.

A. Space Environment Tasks

Within the framework of ongoing research, the X-Arm-2 will be sent to the International Space Station (ISS). In this microgravity environment, teleoperation experiments will be performed wherein astronauts control complex tasks on earth. The purpose of this is to investigate how effectively human operators can use teleoperation interfaces within space.

Many practical applications of space teleoperation can be thought of. One of those is manual operation of a robotic manipulator distant from human presence, for instance in planetary investigation, satellite servicing or during extravehicular activity (EVA).

In [4], the following description and applications of EVA were reported. EVA is activity performed in an unpressurized space environment such as on the outside of the ISS. Applications of EVA include among others: inspection, maintenance, repair, assembly and experimentation. While these are all activities invaluable in operating and maintaining the space station, EVA comes with many inconveniences. The preparation, execution and the after works are cost and time intensive processes that are executed over multiple days. During EVA the pressurized space suit highly limits the astronaut's sensory perception, mobility, dexterity, strength and endurance. In addition to this, EVA imposes risks and hazards among which exposure to radiation and damage of the protective space suit due to micrometeoroids, debris and equipment.

Considering the limited and dangerous nature of EVA, assistance of, or substitution by robotic systems is desirable. Two versatile robotic platforms designed for this purpose are Eurobot [5] and Robonaut [6]. Eurobot is a non-anthropomorphic robot that is able to translate along the standard EVA interfaces and is designed to perform similar tasks as an astronaut. For this a limited set of specific purpose end-effectors is used, including: hand rail-, worksite interface-, robotic-, general purpose-, and specific operation end-effectors [5]. Also Robonaut has been designed to be able to use the hand rails and to perform the same tasks as an astronaut, but in contrast to the Eurobot, it has a human form and two dexterous hands as its end-effectors. Via teleoperation, Robonaut can hold and operate tools such as a flashlight, tweezers, wire stripper, scissors, tether hook, rock pick, and a torque drill [6].

Performing specific tasks in situations that are often unknown at beforehand requires delicate operation and situational awareness. Bilateral teleoperation can prove to be a method to take advantage from the strengths of both human and robot. This requires a haptic interface including a hand master tailored to the tasks encountered by a slave robotic device during space operation. The slave device, as well as the master, consequently should be suitable to teleoperate available (hand held) tools and equipment for EVA as defined in [7].

B. Classification of Grasps

Several classifications of human grasp types have been proposed in literature. In [8], Napier proposed a classification of prehensile grasps. These are stable grasps that hold the object securely, while it is fixed or movable. Grasp selection is influenced by the physical form of the object, but even more by the nature of the intended activity, what is the primary criterion in this classification. By considering both anatomical and functional aspects, precision grasps and power grasps were found being stable grasp types in [8]. Moreover, the following definitions and effects of the thumb were reported. Precision grasp was defined as pinching between the flexing segments of the fingers and that of the opposing thumb. Power grasp was defined as clamping the object between the flexed fingers and the palm. As formulated in [9], a power grasp is chosen when "considerations of stability and security predominate", while a precision grasp is chosen when "considerations of sensitivity and dexterity predominate". The position of the thumb determines whether stability and security or sensitivity and dexterity prevail in a grasp. When the thumb is adducted in a power grasp, the direction of the resulting force on the object can be controlled by small posture adjustments. When the thumb is abducted, the stability and security of the grasp are increased while the sensitivity and dexterity are decreased. In the extreme case, the thumb wraps over the dorsum of the digits, which reinforces the grasp.

As discussed in [9], analytic modeling of grasping and manipulation is highly complex and involves serious simplifications. This strongly limits its use for grasp choice in real-world conditions. As an useful alternative, the Cutkosky taxonomy as shown in Fig. 2 was constructed based on an extensive analysis of tool usage in manufacturing tasks. In this taxonomy, power and precision grasp concepts from Napier are further classified according to geometry and task. In this figure, fingers are numbered as follows: 1. thumb, 2. index finger, 3. middle finger, 4. ring finger, and 5. little finger. The same numbering will be used in the rest of this document.

The grasps required for the EVA tools that were introduced in [7], can be classified according to the Cutkosky Taxonomy. This was done in [11], where grasps were assigned to 242 different aids, tools and interfaces, based on size and intended usage. The category of cylindrical power grasps, as defined in this reference, consists of: small diameter grasp, medium wrap and large diameter grasp. In Table. I, the grasp use during EVA tool operation is shown. Also the Cutkosky taxonomy in Fig. 2 has been extended with this information. It should be noted that part of the EVA tools is used with multiple different grasps. From the table it can be seen that 29% of all tools is used with power grasps only, 38% is used with precision grasps only, and the remaining 33% of the tools is used with both precision and power grasps. More specifically, 52% of all tools is used with a cylindrical power grasp, 27% with a composite power grasp, ~7% with a circular power grasp, 63% with a thumb - 1/2 finger precision pinch grasp, ~6% with a circular precision grasp, and ~1% with a thumb - 3/4 finger precision pinch grasp. Looking further at the set of power grasps, it can be seen that 60% of all performed power

grasps is a cylindrical power grasp, 31% is a composite grasp, and the remaining 9% is a circular power grasp. For the set of precision grasps, it can be seen that 90% of all performed precision grasps is a thumb - 1/2 finger pinch grasp, ~8% is a circular precision grasp, and ~2% is a thumb - 3/4 finger pinch grasp.

In Section. VII-B1, the implication of the grasp type occurrence will be discussed with respect to the design goals.

C. Principles of Grasp Modeling

In [10], the drawback of the Cutkosky taxonomy was stated to be the "inability to explain all the exceptions which usually occur due to task constraints". It was noted that an absolute distinction between power- and precision grasps is not realistic since these are not mutually exclusive. The concepts of virtual fingers and oppositions were proposed in order to be able to

TABLE I
GRASP USE DURING EVA TOOL OPERATION

Tool Operation		
Grasp Nature	Occurrences	% of Tools
Power only	71	29%
Precision only	92	38%
Precision and Power	79	33%

Power Grasps		
% of all Power		
Grasp Type	Grasp Occurrences	% of Tools
<u>Cylindrical</u>	<u>60%</u>	<u>52%</u>
Small Diameter	30%	26%
Medium Wrap	23%	20%
Large Diameter	7%	6%
<u>Composite</u>	<u>31%</u>	<u>27%</u>
Lateral Pinch	11%	10%
Light Tool	12%	10%
Adducted Thumb	8%	7%
<u>Circular (Power)</u>	<u>~9%</u>	<u>~7%</u>
Disk (Power)	8%	7%
Sphere (Power)	<1%	<1%

Precision Grasps		
% of all Precision		
Grasp Type	Grasp Occurrences	% of Tools
<u>Thumb - 1/2 Finger</u>	<u>90%</u>	<u>63%</u>
Thumb - 1 Finger	36%	25%
Thumb - 2 Finger	54%	38%
<u>Circular (Precision)</u>	<u>~8%</u>	<u>~6%</u>
Disk (Precision)	8%	5%
Sphere (Precision)	<1%	<1%
<u>Thumb - 3/4 Finger</u>	<u>~2%</u>	<u>~1%</u>
Thumb - 3 Finger	1%	1%
Thumb - 4 Finger	<1%	<1%

Reworked representation of the data adapted from [11]. For each grasp is shown in which percentage of all power or precision grasps it occurs and which percentage of tools is used with this grasp.

Note: since part of the tools is used with multiple different grasps, the cumulative percentage of tools exceeds 100%.

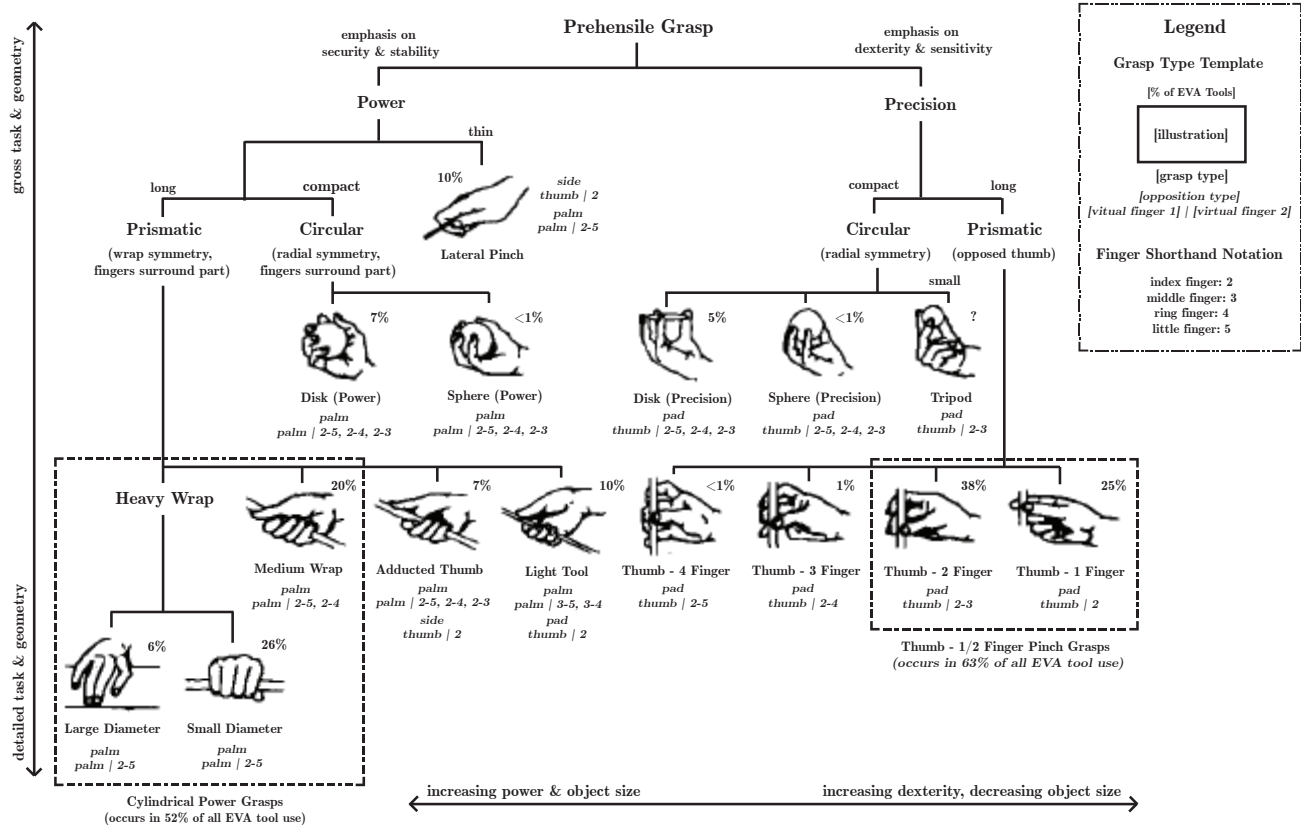


Fig. 2. Cutkosky taxonomy of manufacturing grasps, adapted from [9]. The taxonomy was reworked and extended with information from [10] on the oppositions and the composition of the virtual fingers for each grasp type. Also the percentage of EVA tools that is used with each grasp type, as reported in [11], is shown. The most occurring categories: cylindrical power grasps and thumb - 1/2 finger pinch grasps, are indicated by a dashed box. Note: since part of the tools is used with multiple different grasps, the cumulative percentage of tools exceeds 100%.

”describe prehensile postures in goal-directed terms”. Using these concepts, task constraints and hand postures can be described in terms of the size, direction and number of forces between the object and the hand.

In a task, an object is manipulated using the hand. At each moment in time, the forces applied by the five fingers combine into a limited number of resultant forces that stabilize the object in a prehensile grasp. Since the required number of stabilizing forces can be lower than the number of fingers, the concept of virtual fingers was introduced in [12]. Each virtual finger consists of one or more physical fingers and possibly the palm that work together to exert one of the stabilizing forces. This way, grasp modeling can be simplified, while keeping functional aspects of the grasp.

It was suggested in [13] that virtual fingers correspond to independently controlled contact sides, while oppositions correspond to internal grasp forces. Also it was noted that the number of virtual fingers can depend on the amount of coupling between the physical fingers.

To outline this concept, the following three types of opposition have been adapted from [14]. For each type, the method of [10] was used to indicate the virtual fingers (VF). Using the three opposition types in combination with the composition of the virtual fingers, each type of grasp can be described. This is shown in Fig. 2, where [10] was used to extend the Cutkosky

taxonomy with the concepts of oppositions and virtual fingers.

Pad opposition as shown in Fig. 3.a., is opposition between the thumb pad as virtual finger 1 (VF1) and the pads of one or more fingers (VF2), roughly parallel to the palm. It offers dexterity and sensitivity to control manipulations of the object along its translational and rotational DOFs. The stability and maximum exertable force are low.

Palm opposition as shown in Fig. 3.b., is opposition between the hand palm (VF1) and one or more fingers (VF2). It offers stability by fixing the object along an axis roughly normal to the hand palm. By placing the thumb over the fingers, the stability can be even more increased. The dexterity and sensitivity are low since the only possible motion in palm opposition is that of the wrist.

Side opposition as shown in Fig. 3.c., is opposition between the thumb pad (VF1) and the side of the index finger (VF2), or otherwise between the sides of the fingers. This type is a compromise between stability and the ability to manipulate the object. It can be further weighted by the placement of the object. Holding the object more distal increases dexterity and sensitivity, but decreases the stability.

By combining opposition types, composite oppositions are available to satisfy the task constraints. Each opposition type that is available in a grasp has its own VF1 and VF2. Composite opposition is illustrated by the example adapted from

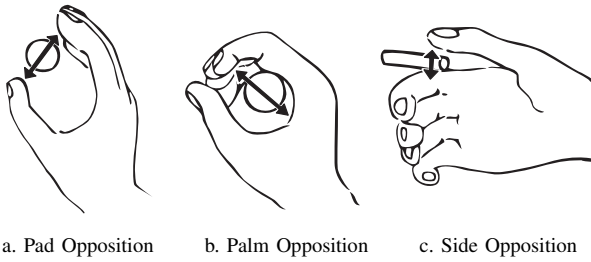


Fig. 3. Reworked illustration adapted from [10], showing the three opposition types that, together with the composition of the virtual fingers (VF1 and VF2), can be used to describe all grasp types.

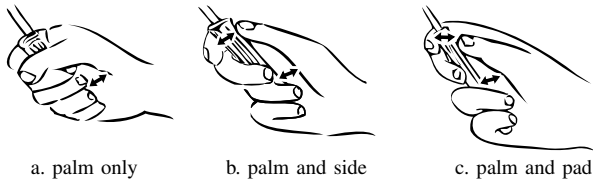


Fig. 4. Reworked illustration adapted from [14], showing how a single grasp can combine two opposition types, termed composite opposition. The combination of opposition types depends on the size of the object and the intended use.

[14], where different sized screw drivers are grasped. The large screwdriver as shown in Fig. 4.a. is held in palm opposition with the palm as VF1 and the group of all other fingers as VF2. This grasp offers power and stability but little dexterity and sensitivity. The position of the thumb helps to increase the power and stability even further. In case of the medium screwdriver as shown in Fig. 4.b., power is decreased while dexterity and sensitivity are increased by a composite form of palm and side opposition. For the palm opposition component the palm is VF1 and the group of the four other fingers is VF2. For the side opposition component the thumb is VF1 and the index finger is VF2. In case of the small screwdriver as shown in Fig. 4.c., the side opposition is replaced by pad opposition. This further increases the dexterity and sensitivity, yet decreases the power and stability. For the pad opposition the thumb is VF1 and the index finger is VF2. The virtual finger in palm opposition remains the same.

In Section. VII-B1, the implication of opposition types and virtual fingers in commonly used grasp types will be discussed with respect to the design goals.

III. SLAVE DEVICES

A haptic hand master device is desired to operate in combination with distinct end-effectors as slave devices. Relevant end-effectors for EVA operations with ESA's Eurobot were presented in [15]. These include a 1 DOF parallel jaw hand rail grasper, 1 DOF fixture grasper, actuated power tool, and a general purpose 3-fingered grasper. In [6], NASA's Robonaut was presented, which in contrast to the Eurobot has no possibility to exchange end-effectors. Its two five-fingered dexterous hands have been designed to handle tools and situations encountered during EVA. The planned use of Robonaut 2 on the ISS underlines the importance of being able to teleoperate 5-fingered dexterous robot hands.

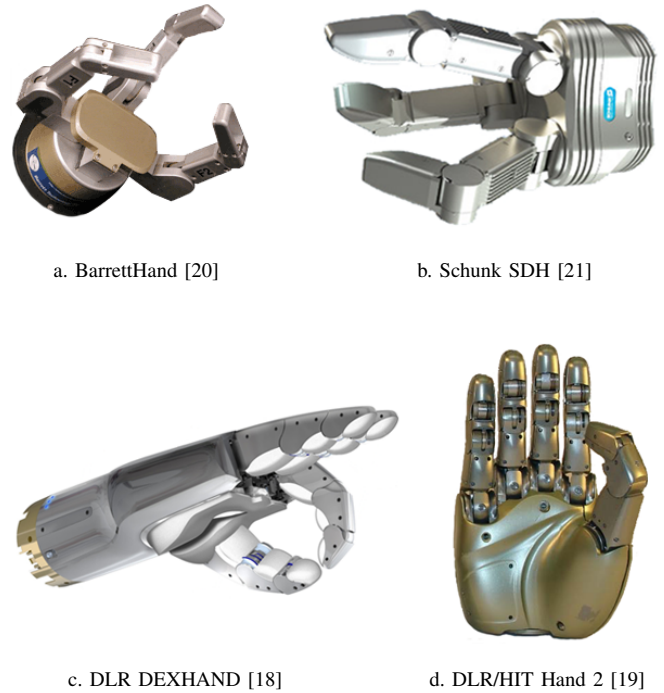


Fig. 5. Distinct slave devices with capabilities comparable to those of end-effectors for space applications. Shown are the 3-fingered graspers: BarrettHand and Schunk SDH, as well as the 4- respectively 5-fingered dexterous hands: DLR DEXHAND and DLR/HIT Hand 2.

A. Space Relevant Slave Devices

Commercially available end-effectors, having capabilities comparable to those of space devices, can be used in the design of a hand master. The hand rail and fixture graspers, in which one actuated DOF is responsible for opening and closing the jaws, resemble parallel-jaw-grippers as used in industry. Examples of general 3-fingered graspers are the BarrettHand [16] as shown in Fig. 5.a. and the Schunk Dexterous Hand (SDH) [17] as shown in Fig. 5.b. A dexterous 4-fingered hand is the DLR DEXHAND [18] as shown in Fig. 5.c. and a dexterous 5-fingered hand is the DLR/HIT Hand 2 [19] as shown in Fig. 5.d.

The BarrettHand is a 3-fingered grasper with 7 DOFs, of which 4 actuated. It is able to exert a maximum tip force at each finger of about 20 N. Its mechanical coupling between the finger digits allows compliant grasping, no matter which shape the object has. Depending on the contact, a finger digit is locked and torque is maintained until all digits are in contact. The fourth motor drives the symmetrical spread motion of the hand, being able to adjust the opposition freely from a cylindrical power grasp to a spherical power grasp. In contrast to the locking flexion motions, the spread motion is fully backdrivable in order to allow compliant spreading motion.

The SCHUNK Dexterous Hand (SDH) is a 3-fingered grasper with 7 DOFs that are all actuated. Each finger contains two independently controllable flexion-extension DOFs, the 7th DOF is the coupled symmetrical rotation of two fingers. Both the fingertips and proximal links have been equipped with a 2 dimensional tactile sensor array.

The DEXHAND is a 4-fingered space qualifiable dexterous hand. Each finger has 4 DOFs of which 3 actuated and the PIP and DIP joint coupled. The thumb has been designed to oppose each finger. The maximum exertable fingertip force is 25 N, while it can withstand 100 N passively. Joints have been equipped with joint torque sensors.

The DLR/HIT Hand 2 is a 5-fingered dexterous hand. Each finger has 4 DOFs, of which 3 actuated and the PIP and DIP joint coupled. The maximum exertable fingertip force is 10 N. Since each finger is equal, the thumb has been mounted in an orientation where it is able to reach each other finger tip. Each finger has been equipped with 3 joint torque sensors.

B. Slave Device Grasps Compared to Human Grasps

The grasps that the slave devices are able to perform can be compared to the human grasps from the Cutkosky taxonomy in Fig. 2. The parallel grasp, as performed by a parallel-jaw-gripper, can be described as pad opposition between two virtual fingers. Similar grasps from the taxonomy are the thumb - 1,2,3,4 finger precision grasps when the fingers act as a group. Since a parallel jaw grasper only features 1 DOF, the device is unable to perform precision manipulation.

Both 3-fingered end-effectors are able to perform comparable grasp types, including parallel-, cylinder-, sphere-, and disk grasps. As shown for the Schunk SDH in Fig. 6, the symmetrical finger base rotation is essential to allow this variety of grasp types. By using its symmetrical finger spread motion, the BarrettHand is able to perform similar grasps. Either device is unable to perform ab-adduction motions, and hence no precision manipulations can be performed.

When comparing the grasp types of the 3-fingered devices with the human grasp types from the Cutkosky taxonomy, the slave parallel grasp shows similarities with the human thumb - 1 finger grasp, yet with the difference that the slave device is unable to perform precision manipulations. The slave cylinder grasp is comparable to the human cylindrical power grasp. The slave sphere grasp and the slave disk grasp resemble the human sphere power grasp and the human disk power grasp respectively.

For the dexterous 4 and 5-fingered hands, many device grasps can be related to the grasps in the Cutkosky taxonomy. Because the thumb is unable to perform side opposition, the lateral pinch and the adducted thumb grasp are impossible. Also the light tool grasp might be problematic due to limitations of the thumb. The other grasps in the taxonomy match well with the capabilities of the devices. The missing 5th finger in the DEXHAND prevents from making thumb - 4 finger pinch. The other grasps either do not require the 5th finger, or can be performed without it. Thanks to the 3 independently actuated DOFs in each finger, including ab-adduction, dexterous finger motions are available. This enables to change object orientation and to simultaneously hold and manipulate a tool, like when holding and controlling a pistol grip tool.

Each device suffers from limitations concerning the functionality of the thumb and the inability to perform side opposition. As a result of this, none of the devices supports the composite grasps.



Fig. 6. Schunk SDH performing a range of distinct grasp types, adapted from [17]. In order from left to right are shown: parallel-, cylinder-, sphere-, and disk grasp.

In Section. VII-B1, the implications of the slave device capabilities will be discussed with respect to the required master device sensing and force reflecting functionality.

IV. HUMAN FACTORS

In teleoperation the human plays a central role. The system should capture human input and provide appropriate feedback to the human sensory system. To achieve realistic sensation, the entire teleoperation system should be designed considering the limitations and capabilities of the human that are termed human factors. In this section, the key characteristics necessary for the master device design are being reviewed and put into perspective.

A. Quantitative Human Factors

Many studies have been performed on the quantification of human factors. Due to the complexity of the human hand, the different studies reveal small portions of information of the complex reality. The experimental setups and methods vary largely and often small subject groups have been used. Because of these reasons, the presented values should be considered as rough indications only. Experimental details can be found in the appropriate references. The key human factors have been extracted from literature and grouped into the most prevailing performance indicators for haptic device design.

1) *Force Exertion and Perception:* Human force exertion and perception capabilities can be specified by range, resolution and bandwidth. Since the force perceived in a grasp is related to the exerted force, a combined effective range of force perception and exertion can be defined. The lower limit is the force perception threshold and the upper limit is the maximum exertable force. The minimum noticeable variation in stimulus intensity is the just noticeable difference (JND).

In [22], data from 'numerous' studies considering hand strength measurements was presented. Reported finger force in pinch grasps is shown in Table. II. Since it is unclear which exact force has been reported, it is assumed that pure pinching force without sliding force components was exerted at the level of maximum voluntary contraction (MVC). In Table. III, the force distribution among phalanges, while power grasping a cylinder, is shown. It is assumed that the reported forces are perpendicular to the phalanges and at MVC. It can be inspected that the largest force was exerted by the distal phalanges and that the ring- and little finger exerted considerably less force than the index- and middle fingers.

The maximum exertable fingertip force found during an investigation of 10 subjects as presented in [23], is 50 N for the index finger, 48 N for the middle finger and 37 N for the ring finger. As a design choice it was suggested to assume a maximum finger force of 40 N for the index and middle finger and 30 N for the ring finger. These can be maintained for flexion beyond 90 deg.

Results from experiments with 3 subjects in [24] are presented in Table. IV. These show maximum controllable fingertip forces and force control resolutions for a medium target force. In this reference it was stated that "the maximum controllable force increased from the most distal joint (PIP) to the most proximal joint (shoulder)" and the force exertion resolution in percentage tended to decrease as target force increased from PIP to shoulder joints. The resolution of force exertion as shown in Table. IV is ~ 0.30 N for MCP and PIP flexion-extension.

TABLE II
FINGER FORCE DURING PINCH GRASPS

	Tip [N]	Pad [N]	Lateral [N]
Male	65	61	109
Female	45	43	76

Data adapted from experiments using 'numerous' subjects as reported in [22], where pad- and lateral pinch grasps were termed pulp- and key pinch respectively. It is assumed that reported values are pure pinching forces at the level of maximum voluntary contraction (MVC).

TABLE III
PHALANGE FORCES DURING POWER GRASP OF A CYLINDER

	Phalange Forces		
	Distal [N]	Medial [N]	Proximal [N]
Index Finger	62	22	42
Middle Finger	68	40	24
Ring Finger	44	28	15
Little Finger	31	20	7

Data adapted from experiments using 'numerous' subjects as reported in [22]. It is assumed that reported forces are perpendicular to the phalanges and at the level of MVC.

TABLE IV
CONTROLLABLE FINGERTIP FORCE AND RESOLUTION

	Maximum Controllable Fingertip Force			
	MCP Flexion-Extension		PIP Flexion-Extension	
	Mean [N]	S.D. [N]	Mean [N]	S.D. [N]
Female	17.6	0.79	16.5	0.66
Male 1	45.1	2.02	41.9	1.88
Male 2	42.6	1.81	50.9	2.16

	Fingertip Force Control Resolution			
	MCP Flexion-Extension		PIP Flexion-Extension	
	Target [N]	Resolution [N]	Target [N]	Resolution [N]
Female	8.9	0.30	8.9	0.30
Male 1	22.2	0.28	22.2	0.22
Male 2	22.2	0.30	22.2	0.35

Data adapted from force exerting experiments using 3 subjects [24].

As summarized in [24], the JND of force perception has been found to be $\sim 7\%$ in two references presenting distinct experiments on elbow flexor muscles at high reference force and thumb-index finger pinching at low reference force. As discussed in [25], the constant JND(%) at varying force levels indicates that force perception is subject to Weber's Law, which states that the ratio between the smallest noticeable increase in stimulus intensity and the initial stimulus intensity is constant. As a result, the JND of force perception should be reported as percentage of the reference force. In a reference summarized by [26], the JND was reported to be 0.5 N for the human fingers, yet since the reference force has not been mentioned, the JND(%) is unknown.

In [27] the JND of force direction was reported. A JND of 25.6 deg was found when a force was reflected to the distal phalange of the index finger that was mounted in a thimble. It changed to 18.4 deg when visual feedback congruent to the force direction was provided in addition. The JND seemed to be independent of the reference force direction.

The data reported in the various sources can be combined into an estimate of the maximum exertable finger force. To summarize: three sources report fingertip or finger pad forces. Maximum exertable index fingertip force of 50 N was reported in [23], data of male pinch grasp force up to 65 N was reported in [22] (Table. II) and male controllable fingertip force up to 50.9 N was reported in [24] (Table. IV). The only source that reports finger pad force during a cylindrical power grasp, shows 62 N exerted by a male with the distal phalanges of the index finger (Table. III). Considering this data, the maximum exertable fingertip force for the index finger is in the range of about 50-65 N. For the middle-, ring- and little fingers, this force likely is lower, yet less data is available. Considering the maximum exertable tip force from [23] and the distal phalange force from Table. III, the maximum exertable middle finger force is 48-68 N, which is comparable to that of the index finger. For the ring finger it is 37-44 N and for the little finger it is even less and about 31 N as indicated by Table. III only.

As summarized in [28], force exertion over longer time can result in muscle fatigue. this affects sensing and motor control and can lead to discomfort and pain. It was found that the percentage of discomfort tolerance is correlated with the force magnitude and the task duration. For large levels of force exertion, the work-to-rest ratio must be chosen appropriately. At 15% maximum voluntary contraction (MVC) moderate levels of discomfort were reported after 103 minutes. At 25% MVC, significant levels of discomfort were reached in 10 minutes. Experiments showed that the perceived force magnitude increases with muscle fatigue. As also summarized in [28], others found that force perception shifts over time during force exertion above 15% MVC.

2) *Pressure Perception*: As addressed in [24], a body grounded device can create the illusion of a true ground when "the pressure distribution and its changes at the grounding location are below the absolute detection and discrimination threshold respectively". During experiments with 3 subjects, pressure perception was found to be dependent on the perimeter, but independent of the contact area. The JND ranged from 0.06 to 0.09 N/cm. In [26] a pressure perception threshold of

0.2 N/cm² was summarized.

As presented in [29], an optimal interface pressure for upper-arm and forearm air-cuffs in arm exoskeleton use was found to be 0.29 N/cm² during both subjective and objective investigation. This value was not below the pressure perception threshold.

3) *Motion Perception and Exertion*: In Table. V, active joint movement range, as summarized in [30], is shown. Movements caused by an external force can exceed the reported limits.

As summarized in [24], a position JND of ~ 2.5 deg was found for the PIP and MCP joints. Proximal joints were found to be more accurate in sensing joint angles than distal joints.

4) *Bandwidth of Motion Exertion and Force Perception*: As summarized in [34], the human can produce a motion output

TABLE V
RANGE OF MOVEMENT OF THE HAND AND FINGER JOINTS

Joint	Motion	Thumb Range of Movement [deg]	Source
CMC	ante-position	25 - 35	[31]
	retro-position	15 - 25	[31]
	flexion	20 - 35	[31]
	extension	30 - 45	[31]
MCP	flexion	60 - 70	[31]
	extension	0	[31]
	ab-adduction	5 (medial displacement)	[31]
		20 (lateral displacement)	[31]
	supination	5 - 7	[31]
	pronation	20 - 24	[31]
IP	flexion	75 - 80	[31]
	extension	5 - 10	[31]

Joint	Motion	Fingers Range of Movement [deg]				Source
		Index	Middle	Ring	Little	
CMC	flexion	~ 0	~ 0	10	20	[32]
		~ 0	~ 0	15	30	[32]
	extension	83	90	88	90	[33]
MCP	flexion	70			95	[32]
			20 - 30			[32]
PIP	extension		30 - 40			[31]
			22 - 23		34	[33]
		60	45	45	50	[32]
	flexion	increasing from index finger >90 up to little finger 135				[31]
					100 - 105	[33]
DIP	flexion		100 - 110			[32]
			0			[31]
		<90			up to 90	[31]
	extension		73 - 80			[33]
			60 - 70			[32]
	0 - 5				[31]	

Reworked table with data adapted from [30].
CMC: carpometacarpal joint, MCP: metacarpophalangeal joint, PIP: proximal interphalangeal joint, DIP: distal interphalangeal joint, IP: interphalangeal joint.

of 5-10 Hz with the hands and fingers. The output frequency is dependent on the nature of the movement. From lower to higher frequency this is: response to unexpected signals, response to periodic signals, internally-generated signals and reflexive actions.

As presented in [34], the minimal required frequency of force feedback is determined by the proprioceptive and kinesthetic sensing and was found to be 20-30 Hz. Using tactile perception, force signals up to 320 Hz can be discriminated. Vibrations up to 10 kHz can be perceived by skin vibration, but discrimination between signals is not possible.

In [28], different results and suggestions have been summarized. One source recommends a force feedback bandwidth of at least 50 Hz, yet by another source good results were obtained at 15 Hz. Also it was reported that no significant advantages were observed when increasing from 8 Hz to 32 Hz. When the force feedback bandwidth is assumed to be the control bandwidth, the mechanical bandwidth has to be at least as high. This because structural effects otherwise limit the achievable force feedback bandwidth.

5) *Stiffness*: Experiments using 3 subjects as presented in [24] show the minimum required stiffness to simulate a rigid object to be 15.3-41.5 kN/m. The height of these values underlines that a force reflective device should have a high mechanical stiffness in order to simulate stiff objects and contacts. As noted in [35] a low mechanical stiffness can result in position estimation errors when sensors are located at the joints and thus cannot sense the device deformation.

B. Design Requirements

The capabilities and limitations of the human hand as described by the human factors, impose requirements on the design of the haptic interface.

In [24] the following force requirements on a master device have been summarized. The force display resolution and the maximum exertable force of the device should meet or exceed the human sensing resolution, respectively the maximum force that the human can exert. The force exerted by the device should at least be controllable in the motion exertion and perception bandwidths of the human. Also the bandwidth of the backdriven device should at least match the motion exertion bandwidth of the human.

Based on the bandwidth of motion exertion and perception as summarized in Section. IV-A4, it was suggested in [34] that a hand master device must be able to sense motions at a maximum of 5-10 Hz, while it should be able to provide force feedback up to 30 Hz and possible vibrational information at a maximum of 320 Hz. Higher frequencies can be sensed but can not be discriminated and thus it makes sense to map these to the frequency of 320 Hz.

Factors that influence the bandwidth of the system, as summarized in [34], include: stiffness, inertia, damping, friction, backlash, gains, and operator impedance. From this, design requirements result. The interface should have low inertia by mechanical design to allow high position and force error gains at stable operation. As also stated in [34], the stiffness of the haptic interface should be equal or exceed the expected

task stiffness because the task completion time, accuracy and dexterity are negatively influenced otherwise. Also it was stated that a minimum sampling rate of 10-20 times the bandwidth is required to guarantee good performance. While in this reference it was suggested that sensors should be located as close to the actuators as possible, it would make sense to locate actuators as close to the joint outputs as possible. This way the sensed data, for use in the control loop, does not need compensation for mechanical effects and losses in the transmission chain from the actuator output to the actuated joint.

A haptic device produces reaction force at the position where it is mounted, called the grounding position. For body grounded devices this can result in an unnatural sensation. As suggested in [24], the contact area at the attachment points of the device should be minimized, while the perimeter should be maximized in order to obtain a pressure distribution below the absolute detection and discrimination thresholds.

As presented in [29], a physical human-robot interaction experiment was performed with 14 subjects wearing an arm exoskeleton device. The influence of the human-device joint alignment and attachment stiffness on the comfort, mental load, interface force, tracking error and workspace was investigated. Results showed that offsets between human and device joints easily arose during operation and led to large interaction forces and torques that limited the range of motion. In order to decrease interface forces and to enlarge the range of motion, passive joints were successfully adapted.

C. Finger Force Coupling Effects

In many studies, effects of finger force coupling have been observed. While the exact mechanisms of the couplings are complex, it was found in [36] that index finger force is more accurately perceived than little finger force during multi-finger force production. Independent of the number of simultaneously activated fingers during force matching tasks, the index finger force was not significantly different from its reference force. The little finger did produce significantly different forces than its reference force when three (middle-, ring-, and little finger) or four fingers (index-, middle-, ring-, and little finger) were activated.

Force production with an explicitly instructed finger tends to result in force production in adjacent uninstructed fingers during both sub-maximal and maximal voluntary contraction. This effect has been termed enslaving in [36] and will provide an interesting option for the hand master design as will be discussed in Section. VII-B2. As summarized from multiple references in [37], enslaving effects were more evident during ring and little finger tasks, while the index finger was the least affected. Furthermore, it was found that enslaving effects increase with the level of force production by the instructed finger. In the finger directly adjacent to the instructed finger, the effect was stronger compared to that in the other fingers. In [38] the same effects were found since it was observed that coactivation of muscles varied with force intensity, 'distance' between digits, angular displacement and angular velocity.

Enslaving is likely to have effect on the perception of finger forces. As reported in [39], the perceived heaviness of a con-

stant weight lifted by one digit progressively increased when the weight lifted by an adjacent digit increased. This suggests that finger force perception can be altered by simultaneous activation of adjacent fingers.

In [37], experiments with force matching tasks showed evidence that the absolute magnitude of the forces exerted by all fingers, both instructed and uninstructed, is perceived. Matching errors were significantly minimized when the sum of finger forces was compared. Also results from force matching tasks as reported in [40] support the notion that the absolute, rather than the individual, finger force is perceived and reproduced during force matching tasks within the same hand, as well as between the two hands. The effect that the absolute magnitude of the total finger force is perceived and reproduced was been termed 'absolute force matching'.

Effects of Enslaving are also likely to influence the direction of the exerted force. In [41] it was found that in multi-finger tasks, individual fingers can exert force in the flexion-extension plane in directions significantly different from the target direction, while the resultant of the forces is in the target direction. The direction of the force exerted by the enslaved fingers was found to depend on the target direction. On average, the direction of the force exerted by a non-instructed finger differed more from the target direction if the distance from this finger to the instructed finger was larger.

As will be discussed in VII-B2, knowledge of enslaving effects proves essential in the identification of the important features of a low-complexity haptic hand device.

V. MASTER DEVICES

In order to provide insight in the existing devices and their features, a survey of 24 reported master devices was made. In addition to the features presented in this section, the complete device comparison has been included in Annex. A.

A. Device Appearance and Mounting

A force reflective hand device can be of palmar, dorsal or end-point type. Palmar and dorsal type devices reside in the palm, respectively on the back of the hand. These are body grounded and reflect forces to one or multiple positions on the hand. An end-point type device is only connected to the hand in the force-feedback positions and it is grounded to the environment. This device ground can also be a supporting structure like a table-top setup or a robotic/haptic arm. In body grounded devices, body coverage ranging from only the fingers, up to the total of fingers, hand, wrist, and forearm is encountered. For most body grounded devices, actuators are mounted on the worn structure, while some have the actuators placed externally in order to reduce mass and volume on the body. In each of the reported end-point devices, the actuators have been directly mounted on the device. Device type, device ground, body coverage and actuator placement of the compared devices are shown in Table. VI.

Inspection shows large variety in the reported devices. The only palmar device is the compact, low mass, Rutgers Master as presented in [42]. Due to its placement in the palm, the workspace of the human hand is limited.

Five end-point devices have been reported, of which three have been attached to a robotic or haptic arm. The device in [63] is a robotic arm with a dexterous hand opposing the human hand and connected at the fingertips only. In [61] and [60], devices mounted on an external haptic arm were presented. The latter is a device that is only in contact with the hand at the moment force feedback is provided. A table-top device connecting to the thumb and index finger pad was presented in [64] and a table-top device with many actuated DOFs, including 2 in the wrist, was reported in [62].

Both the table-top and robotic/haptic arm end-point type devices are large in size and heavy in weight, yet little weight

TABLE VI
DEVICE APPEARANCE AND MOUNTING

Property	Number of Devices ¹	Percentage	Sources
<u>Device Type</u>			
palmar	1	4%	[42]
dorsal	18	75%	[43][44][45][46][47][48][49][50][51][52][53][54][55][56][57][58][59]
end-point	5	21%	[60][61][62][63][64]
<u>Number of Supported Fingers</u>			
1	8	33%	[43][44][47][48][49][51][52]
2	5	21%	[61][50][64][55][59]
3	0	0%	
4	2	8%	[42][56]
5	9	38%	[45][46][60][62][63][53][54][57][58]
<u>Device Ground</u>			
body	19	79%	[43][44][45][46][42][47][48][49][50][51][52][53][54][55][56][57][58][59]
environment	5	21%	[60][61][62][63][64]
<u>Body Coverage</u>			
excluding forearm	12	50%	[43][46][42][60][61][63][64][53][55][57][58][59]
including forearm	12	50%	[44][45][47][62][48][49][50][51][52][54][56]
<u>Actuator Placement</u>			
body	15	63%	[44][45][42][47][48][49][50][51][52][53][54][55][56][59]
external	4	17%	[43][46][57][58]
on end-point device	5	21%	[60][61][62][63][64]

¹In total of 24 devices have been compared (of which 2 presented in [52]).

resides on the human hand since the device is grounded on the environment.

Half of all compared devices not only cover the fingers, hand and wrist, but parts of the arm as well. The reasons for this are device fixation and actuator placement. A drawback is that compatibility with other devices, like an arm master, is severely limited. To reduce size and mass on the body 5 end-point devices and 4 body mounted devices have externally placed actuators. This lowers size and mass on the hand and arm, increasing comfort and compatibility. Yet, the placement of actuators on an external setup, requires long transmissions that might limit workspace and can decrease device performance due to parasitic effects. In all 4 devices with external actuator setups, cable transmissions have been used.

Information on finger workspace has been reported for few devices only. The index finger extension-flexion range has been specified for four devices as shown in Table. VII. The natural motion range was estimated using the most extreme upper and lower limits as reported by multiple sources summarized in Table. V. Since there exists variation in reported data, it should be noted that this motion range might be too large to represent the average human operator. Although natural finger workspace is important for comfortable and unconstrained use, it can be inspected from the table that natural flexion is limited for nearly all cases. Natural extension is only limited for the MCP joint. The device from [42] is of the palmar type, what clarifies the relatively small motion range.

B. Force Reflection

From the number of supported fingers, as shown in Table. VI, it seems that hand masters most often have been designed for either 1, 2 or 5 fingers (8, 5 and 9 devices respectively). All one-finger devices have been designed to support the index finger and all two-finger devices to support both the thumb and index finger. Only 2 of the devices support 4 fingers and none supports 3 fingers. 3 of the reported devices have a modular design, enabling to extend the number of involved fingers [48], [49], [64].

In 3 of the 24 devices, fingers have been grouped and move as one entity. In the device presented in [45], the middle-, ring- and little finger move as a group, actuated

TABLE VII
MASTER DEVICE INDEX FINGER EXTENSION-FLEXION RANGE

MCP [deg]	PIP [deg]	DIP [deg]	Source
<u>natural index finger motion range</u>			
-40 - 83	0 - 110	0 - 90	Table. V
<u>master device finger motion range</u>			
0 - 73	0 - 80	0 - 65	[43]
-15 - 75	0 - 90	0 - 75	[51]
0 - 90	0 - 110	0 - 70	[49] ^{1,2}
	0 - 45	0 - 45	[42] ¹

¹Only flexion angles were reported. ²Simulated values. Note: only for 4 of the 24 reported devices a clear definition of motion range has been given.

by a single cable that flexes the middle finger's PIP, DIP and MCP joints simultaneously. In the device in [54], the same fingers have been grouped, but here 3 actuators are used to flex the PIP, DIP and MCP joints. One extra joint offers ab-adduction between the index finger and the grouped fingers. The device as presented in [56], was designed for hand assistance when wearing a spacesuit glove. The ring and little finger are grouped together and this structure is actuated by 1 DOF via a mechanical coupling.

As shown in Table. VIII, the positions where feedback is applied differ per device. 9 of the 24 devices apply force to one position per finger. In one case this is the medial phalange, in all other cases this is the fingertip or finger pad, which are grouped as 'distal phalanges' in the table. 2 devices apply feedback to both distal and medial phalanges, while 10 devices apply force feedback to each phalange. Remaining devices have multiple distinct feedback positions as a result of finger grouping.

In Section. IV human properties including range, resolution and bandwidth of force perception and exertion were addressed. For 10 out of the 24 reported master devices, the maximum feedback force has been given. In 2 of those cases this is the force from the actuator [44], [46], in the other 8, this is the tip/-pad force as shown in Table. VIII. The force control resolution was only specified for 2 devices [46], [42], being 12-bit for both. Considering the maximum force of 12 N and 16 N respectively, the force resolution would be 3 mN and 4 mN respectively. It should be noted that this is the theoretical value only, more relevant would be the actual force resolution as measured at the device-body interface. The actuator control rate was given for 3 devices [46], [42], [59], being 1000 Hz, 300 Hz and 100 Hz respectively.

The number of actuators encountered on hand master devices ranges from 1 up to 20. Since the number of fingers supported by the devices vary, the average number of actuators per finger is shown in Table. VIII.

Some of the master devices have been specifically designed to provide force feedback perpendicular to the phalanges. For many devices the actual direction of force reflection has not been specified or the direction depends on the hand size and the posture. Since the exact kinematics are rarely reported, it is unclear for many devices if perpendicular force reflection is provided over the whole range of movement and for varying hand sizes.

Although increased performance can be obtained using non-perpendicular force reflection as shown in [3], multiple techniques have been reported to achieve perpendicular force reflection. In [43] and [49], sliding mechanisms were used to change the center of rotation during finger motion. This allows for perpendicular force exertion over the full motion range and for some hand size variation. Similar functionality is provided by the rolling joints as presented in [52]. Other special joint types that can provide perpendicular force reflection are: parallel joints in [60] and [56], and circuitous (simultaneously sliding and translating) joints in [53]. These devices are optimal for one hand size only. Devices reported in [51] and [48] offer hand size variation support by mechanical adjustments. Force feedback in any direction and good hand

size variation support is offered by devices reported in [64], [55] and [63]. These provide at least 3 actuated DOFs per finger of which 2 in the flexion-extension plane and 1 in the ab-adduction direction, while, force is only applied to the fingertip or finger pad.

Low-complexity devices without many actuators or complex mechanisms can take advantage of structural optimization as adopted in the device presented in [50]. This technique to optimize link length and actuator placement in order to achieve perpendicular force exertion and sufficient workspace was reported in [65].

C. Master Device Performance

In [66], performance measures for haptic interfaces were defined in order to provide a standard that is useful in comparison and analysis of haptic devices. The measures include among others: number and nature of DOFs, motion range, peak force, inertia, mechanical bandwidth, acceleration, resolution, precision, and safety.

None of the reported devices has been defined in terms of this complete set of properties. Moreover, most properties have not been reported at all and when they are, different measurement and simulation techniques can prevent comparison with other devices.

TABLE VIII
MASTER DEVICE FORCE REFLECTION PROPERTIES

Property	Number of Devices ¹	Sources
<u>Feedback Positions</u>		
distal phalanges	8	[46][42][60][61][63][64][53][55]
distal & medial phalanges	2	[62][56]
medial phalanges	1	[50]
multiple positions	3	[45][47][54]
all phalanges	10	[43][44][48][49][51][52][57][58][59]
<u>Average Number of Actuators per Finger</u>		
> 0 - 1	9	[45][46][42][60][61][48][50][53][56]
> 1 - 2	4	[44][47][49][54]
> 2 - 3	5	[63][64][55][57][59]
> 3 - 4	5	[43][62][52][58]
> 4	1	[51]
<u>Max. Tip/pad Force²</u>		
3.3 N	1	[47]
3.6 N	1	[63]
5 N	1	[54]
8 N	3	[45][60][53]
16 N	1	[42]
45 N	1	[50]

¹In total of 24 devices have been compared (of which 2 presented in [52]).

²Fingertip/-pad force has been reported for 8 devices only.

The lack of reported properties makes it difficult to compare device performance. An important property of haptic device is transparency, a result of low inertia, low friction and low backlash. Inertia has only been defined for 1 device [51], friction for 3 [47], [63], [52], and backlash for 1 [63]. The important property of backdrivability has not been defined for these devices at all.

VI. SENSOR-ACTUATOR ASYMMETRY

As described in [67], controllability and observability can be used to express the controlling and reflecting capabilities of a haptic master. A sensed DOF in the master device can be used to control an actuated DOF in the slave device. An actuated DOF in the master device can be used to observe a sensed DOF in the slave device. When the number of sensed DOFs of the master device matches the number of actuated DOFs of the slave device, the master offers full controllability over the slave. When the number of actuated DOFs of the master device matches the number of sensed DOFs of the slave device, the master offers full observability of the slave.

A drawback of low-complexity masters is the limited number of actuated DOFs that restricts the observability if the slave has more DOFs. When only the actuated master DOFs are sensed, the controllability is limited as well. In this case the system is symmetric and the interaction is realistic, which means that each sensed movement results in realistic force reflection in the same DOF. Unfortunately, when no full controllability and observability is available, a number of DOFs of the slave are both uncontrollable and unobservable.

Unlike actuators, sensors nearly do not influence the transparency and thus more sensed DOFs can be used in the master to increase the controllability of the slave. When the number of sensed DOFs is unequal to the number of actuated DOFs, the system is having a sensor-actuator asymmetry. In Section. VII-B1, this effect will be exploited in a novel way for the design of the hand master.

As described in [27], perceptual issues can arise in devices with a sensor-actuator asymmetry. When available sensors perceive a movement along a certain direction, the lower number of actuators might prevent from reflecting the force in this exact direction. In this case, the force perceived by the user is in a different direction than the movement exerted by the user. In order to keep the feeling natural, the mismatch in force direction should remain below the JND of force direction perception as summarized in Section. IV-A.

VII. DISCUSSION

A haptic hand master for space teleoperation in combination with the X-Arm-2 is desired. Ease of use and device performance are important requirements that should result in a low-complexity device that improves user performance. It should be usable by different operators without device adjustments and extensive mounting procedures. Full controllability over the slave device is required at all times. High device transparency should ensure that the forces experienced by the user are those as intended, without negative influence from the structure and transmissions. The device should be designed to

have a natural feel during operation. This involves that the motions and forces are compatible with the human factors in the sense of range, resolution and bandwidth.

A. Reported Master Devices

In Section. V, the master device comparison gave insight in the properties of existing devices. Considering this it can be discussed which device types have potential for usage in the intended space telerobotic situation.

1) *Device Compatibility*: For compatibility with an arm master, it is important that the hand device makes efficient use of space. When parts are mounted on the arm, the use of an arm master is likely limited or prohibited. As shown in Section. V-A, this is the case for 50% of the reported devices. Among the 12 devices without arm coverage are 4 devices that are grounded on the environment instead of the user. These devices are large and heavy, yet do not place mass on the hand and provide a good workspace. This is especially true for devices mounted on a robotic or haptic arm and that allow movement of the wrist and arm. These large and heavy environment grounded devices are limited considering portable use. 4 of the 12 devices without arm coverage have external actuator placement. In Section. V-A, this was shown to lower size and mass on the hand and arm to increase comfort and compatibility. It should be noted that still the actuator setup and transmission to the hand part need to be placed such that the workspace is not obstructed. The required transmissions potentially introduce undesired effects like friction and backlash.

From the total set of 24 devices, 4 devices have no external actuator placement and do not cover the arm. These are the devices reported in: [42], [53], [55], and [59]. From these devices, the Rutgers Master as presented in [42] is interesting for its small size and low mass, while able to provide 4 finger with force feedback. It would be suitable without adaptation for portable usage in combination with a haptic arm. A drawback of this device is the limited workspace due to the palmar device placement. It should be noted that the air pressure supply, that powers the actuators, is located externally. Since the actuators are located on the hand and are having their force ground on the hand, the connection to the air supply is a flexible connection rather than a drive transmission. The three other devices have large structures on the back of the hand that might limit the range of movement when used in combination with a haptic arm device.

2) *index finger support*: As shown in Section. V-B, all reported devices that support one or two fingers have been designed for the index finger and thumb. This indicates that these fingers are considered being the most useful to provide with force feedback. This is supported by the important function of the index finger in the most occurring grasp types in EVA tool use, as presented in Section. II-B. Not only is the index finger involved in each grasp type, also it offers dexterity in grasps and the ability to actuate or manipulate a tool while holding it. This will also be discussed in Section. VII-B1, where the importance of the middle finger will be indicated as well. Yet, no three finger devices have been reported, except

for the devices with a grouped third finger. The importance of the index finger is also stressed by the knowledge that the index finger force is the most accurately perceived and that the index finger is the least affected by enslaving, as addressed in Section. IV-C.

3) Master Device Performance and Device Comparison:

Considering the device performance, the actuation bandwidth and force resolution have only been specified in two cases. Also the inertia, friction and backlash, relevant for structural transparency, have been reported for few devices. This lack of reported properties makes it difficult to compare device performance. Since each part in the transmission introduces parasitic effects, the highest transparency likely can be obtained in devices with a low number of actuators and transmissions as short as possible. As much as 9 out of the 24 reported devices have only one or less actuators per finger.

Since comparison of devices remains difficult due to distinct designs for specific tasks, small numbers of test subjects in reported experiments, and distinct device evaluation tests, no clear preference for a specific device type can be defined. Important design requirements on device properties were addressed in [24] and attempts were made to provide a list of standard performance measures in [66]. While these are important indicators of device performance and usability, in practice information about devices is not specified in a standard way or even unknown.

Another approach might be to use performance criteria to evaluate devices and to provide comparable measures. An investigation using performance criteria was executed in [3], where an experimental approach was used to determine user performance in terms of grasp completion time, grasp quality assessment, and perceived grasp difficulty while using a haptic hand master with and without force feedback.

B. Toward Low-complexity Device Design

In the following sections, the design of a low-complexity device is discussed. Having only few DOFs increases the importance of well considered design choices that take into account the intended usage of the device, the intended tasks and required grasps, the intended slave devices to interact with, and the human factors. Also experience on earlier reported devices can provide valuable information.

1) *Considering Tasks, Grasps and Slave Devices:* In Section. II the intended tasks to perform and the grasps required for this were analyzed for typical EVA tasks. As shown in Table. I and presented in Section. II-B, the percentages of EVA tools requiring only power grasps, only precision grasps, or both do not show large differences. This indicates that the hand master should be usable when performing both power and precision grasps.

As presented in Section. II-B, grasps can be grouped according to the percentage of EVA tools used with it. The most occurring grasps are the cylindrical power grasps and the thumb - 1/2 finger pinch grasps. Less occurring grasps are the composite grasps and the least occurring grasps are the power and precision circular grasps (including disk-, sphere- and tripod grasp) and the thumb - 3/4 finger pinch grasps.

The opposition types in the different groups of grasp occurrence were determined and are shown in Table. IX. It can be seen which fingers operate separately from other fingers and which operate in a group. For each finger and finger group, the type of opposition and the opposed fingers are shown. The table gives an indication of the most important finger motions that a hand master should support for the set of EVA tasks.

The only fingers that should be able to operate separately are the thumb and the index finger. Considering the most occurring grasps, the index finger, as well as the grouped index and middle finger, should be able to make pad opposition with the thumb. Together with the little and/or ring finger, the index and middle finger also should be able to make palm opposition. During thumb-index pad opposition, the remaining three fingers should be able to perform palm opposition in a group excluding the index finger. Using the same 3 finger group in palm opposition, while the index finger is able to perform pad and palm opposition separately, adds the possibility to hold and to manipulate/control a tool at the same moment, as in pistol grip tool operation. Only the less occurring composite grasps require side opposition between thumb and index finger. The least occurring grasps add the requirement that the index finger is able to perform grouped pad opposition to the thumb. This only requires a larger abduction of the thumb.

Implementing sensor-actuator asymmetry, as introduced in Section. VI, results in a device with a number of sensors that is unequal to the number of actuators. It is proposed to decouple the sensing and reflecting functionalities even

TABLE IX
GRASPING MOTIONS PER FINGER FOR EVA TOOL HANDLING

Most Occurring Grasps ¹		
Finger	Opposition Type	Opposed Fingers/palm
1	pad	2, 2-3
2	pad	1
2-3	pad	1
2-4, 2-5	palm	palm
Composite Grasps ²		
Finger	Opposition Type	Opposed Fingers/palm
1	pad	2
1	side	2
2	pad	1
2	side	1
2-3, 2-4, 2-5, 3-4, 3-5	palm	palm
Least Occurring Grasps ³		
Finger	Opposition Type	Opposed Fingers/palm
1	pad	2-3, 2-4, 2-5
2-3, 2-4, 2-5	pad	1
2-3, 2-4, 2-5	palm	palm

The grasps from the Cutkosky taxonomy are divided into three groups according to the frequency of occurrence.

¹*Most occurring:* cylindrical power grasp (large diameter grasp, medium wrap and small diameter wrap) and thumb-1 or thumb-2 finger precision pinch.

²*Composite grasps:* lateral pinch, adducted thumb, light tool.

³*Least occurring:* circular power and precision grasps (disk and sphere), thumb-3 and thumb-4 finger precision pinch and tripod grasp.

more by providing separate unconnected devices of which one offers full controllability and the other offers little but sufficient observability. From now on these devices, that together function as master device, will be called the sensing device, respectively the force reflective device. The previous analysis of required finger functionality for EVA tasks, can be used to define the force reflection requirements for the observability that is provided by the force reflecting device.

Working toward a minimum number of actuated DOFs, force reflection to grouped fingers is preferred when possible. A proposed solution for the force reflecting device is to provide separate force feedback to thumb and index finger, while grouping middle, ring and little finger. This takes into account the importance of the index finger as discussed in Section. VII-A2. The thumb should be supported in palm opposition with at least the index and possibly the middle finger. Also side opposition with the index finger could be supported considering the task and grasp analysis, yet the importance of this motion diminishes since slave devices do not support it as shown in Section. III-B. The index finger should be supported in palm and thumb pad opposition, what also should allow tool manipulation/control. The grouped fingers (3-5) should be supported in at least palm opposition, while thumb pad opposition is usable, but less important.

The resulting set of desired force reflective motions is: index finger - palm opposition (Fig. 7.a), grouped fingers (3-5) - palm opposition (Fig. 7.b), index finger - thumb pad opposition (Fig. 7.c), and possibly grouped fingers (3-5) - thumb pad opposition (Fig. 7.d). With this set, it is possible to provide the user with force feedback from slave devices when performing the most occurring grasp types. To implement these four force reflective motions, only a limited number of actuated DOFs is required.

The sensing device should offer full controllability of the relevant slaves in order to allow dexterous motions and use of the full slave workspace. No dexterous finger motions are required to perform a cylindrical power grasp, yet for the thumb - 1 finger and thumb - 2 finger pinch grasps, dexterous finger motions are of fundamental importance to reorientate and to manipulate the object or tool. This also requires ab-adduction of the thumb in order to oppose the index and the middle finger. In the least occurring grasps, like the disk and sphere grasps, independent finger motion is required to position the fingers around the object. When handling a pistol grip tool, dexterity is required to both position the fingers and to manipulate the tool.

Due to the difference between the human hand and slave devices, a kinematic mapping from human hand grasps to slave device grasps is required. The Cutkosky taxonomy was used in Section. III-B to select human grasps that have close similarity to the slave device grasps. These can be used to provide intuitive human-slave grasp mapping. This way natural human grasps can be used to perform slave grasps.

The hand master preferably offers equal workspace as the operated slave devices. In this case no scaling of motions between the master and slave is required and negative effects like decreased stability and decreased resolution are avoided.

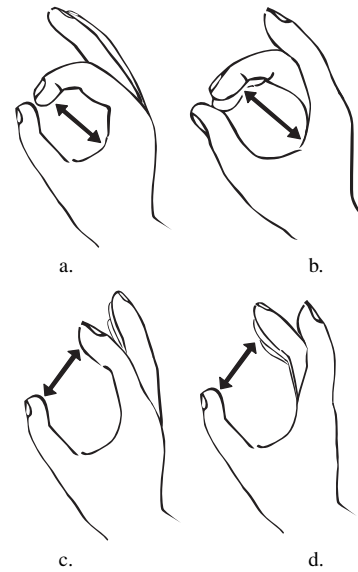


Fig. 7. The four force reflective motions that should be supported by the force reflective device: a. index finger - palm opposition, b. grouped fingers (3-5) - palm opposition, c. index finger - thumb pad opposition, d. grouped fingers (3-5) - thumb pad opposition.

2) *Considering Finger Force Coupling Effects:* As addressed in Section. IV-C, fingers are subject to force- and motion coupling effects, termed enslaving. These effects can be accounted for in the design of a hand master device, especially with regard to coupling finger feedback in the master device in order to reduce complexity by limiting actuated DOFs. The ring and little finger show the most coupling, while the index finger is the least affected. During multi-finger force production, the index finger force is the most accurately estimated, while the little finger force is the least. Furthermore the effect of absolute force perception has been reported, describing that the absolute magnitude of the total finger force in both instructed and uninstructed fingers is perceived. The reported enslaving effects advocate that some force reflective DOFs in a master device can be coupled.

Since the index finger shows the least enslaving effects and since its force is the most accurately estimated, it makes sense to provide this finger with independent force feedback. This supports the high requirements on the index finger in precision grasps. As discussed before, considering tasks and grasps, fingers 3-5 can be handled as a group. The concept of absolute force perception suggests that the force applied to the fingers 3-5, can be applied as an absolute force to the group of the three fingers. Since adjacent finger activation increases force perception, it might as well be possible to not provide the ring- and little finger with force feedback at all, while an increased force is reflected to the middle finger. This also is supported by the large influence of enslaving effects on the ring- and little fingers, which means that force exerted by the middle finger can generate forces and force perception in the ring and little fingers. The approach of grouped feedback would require a separation between sensor and actuator paths to allow the middle-, ring-, and little finger to make independent motions

to control the slave device. Thus, the group of fingers 3-5 might be provided with coupled force feedback motion as long as individual controllability can be maintained. The operator then has the freedom to use the fingers either as a group or separately.

C. Detailed Sensor and Actuator Performance

After the discussion on the general layout, remains the discussion on sensor and actuator performances. In order to obtain good usability, the hand master should be tailored to the human capabilities and limitations. In Section. IV, reported human factors were summarized. The requirements on force perception and exertion, as well as the position perception and control were defined in terms of range, resolution, JND and bandwidth.

The upper boundary of the range can be defined as the maximum exertable fingertip force which was found to be 50-65 N in Section. IV-A1. As addressed in the same section, the maximal continuous fingertip force should remain below 15% MVC to avoid muscle fatigue, discomfort and shifting of force perception. When assuming that the maximal exertable index fingertip force of 50-65 N is comparable to the MVC, a range of exertable fingertip force of 8-10 N is required. The reported force levels of existing devices, as presented in Table. VIII, match this value quite well. It can be advised to design the master device to be able to exert this index finger force as maximum force during continuous operation. Using the maximum exertable forces for the other fingers as presented in Section. IV-A1, the level of 15% MVC that is advised as maximum force during continuous operation is: 7-10 N for the middle finger, 6-7 N for the ring finger, and 5 N for the little finger. The grouped fingers (3-5) work together in force exertion and thus the device should be able to reflect this group with a force higher than that of the separate fingers. Simply summing the forces to the middle-, ring-, and little finger results in 18-22 N.

As summarized in Section. IV-A1, the resolution of force exertion, as reported in one experiment with a small subject group, is ~ 0.30 N. Considering force perception, a JND of $\sim 7\%$ was reported. This percentage applies to Weber's Law since it remains constant at different levels of target force exerted by different muscle groups. 7% of the 8-10 N maximum exertable fingertip force results in a JND of 0.5-0.7 N. When exerting a lower force, the JND expressed in force level decreases. As design guideline for a hand master device a force display resolution better than 7% of the minimum force level can be advised. To have an indication of realistic low force levels in object handling, soft objects can be considered. In [35] various soft objects were used, including a sponge and a foam ball with a stiffness of 0.18 N/mm, respectively 0.33 N/mm. For a 5 mm deformation of the sponge, 0.9 N should be exerted. At this force level, 7% JND is about 0.06 N.

The JND for motion perception was found in [24], where ~ 2.5 deg for the MCP and PIP joints was reported. These results were gathered from 3 subjects only. Since likely the force and position performance for bilateral control will have higher demands, achieving both force and position resolution for human operation should not pose problems.

The ranges of active motion for all hand and finger joints are shown in Table. V. This data can be used to define the desired workspace of the sensing device and to design the actuated motions in the force reflecting device.

As addressed in Section. IV-B, the device should be able to perceive motion with a frequency up to 10 Hz and to exert force with a frequency up to 30 Hz. When display of vibrations is desired, a force feedback frequency up to 320 Hz is required. In the same section, it was noted that the bandwidth of the backdriven device should at least match the human motion exertion bandwidth of 10 Hz.

D. Device Optimization

As mentioned in Section. I-A, an important criterion concerning device performance is structural transparency. In [68] a design methodology to maximize structural transparency was presented. A multivariable optimization approach was used to optimize the mechanical structure (base location, link lengths, inertia, and balancing weights), transmission ratio, and motor characteristics (rotor inertia and motor torque) when moving along a set of possible paths. This method was demonstrated on a 5 DOF device and was found "suitable for any actuated mechanism that must be optimized along a given path". Since the desired low-complexity hand master has a low number of DOFs and a simple structure, this optimization method can prove useful to optimize device performance in terms of structural transparency.

As shown in Section. V-B, reported devices use multiple actuators or complex structures in order to provide perpendicular force reflection over the whole movement range. Low-complexity devices are limited in this sense. The commercial success of the CyberGrasp[®] and the experiments performed with this device as reported by [3], are indications that a simple hand master without full range perpendicular force exertion can increase user performance. As addressed in the same section, structural optimization might be used to optimize the reflected force direction, workspace, and hand size variation support.

VIII. SYNTHESIS AND FORMULATION OF FUTURE RESEARCH

In Section. VII-B1, it was discussed that a large sensor-actuator asymmetry can be obtained by separation of sensor and actuator paths. It was proposed to handle motion sensing and force reflection by separate devices to achieve full controllability while keeping observability limited but sufficient. This architecture is shown in Fig. 8 and can lead to a compact and high performance device solution.

As the sensing device, a sensor glove like the CyberGlove[®] [69] might be used. When the motion of the glove is unconstrained by the force reflective device, this offers great advantages like unconstrained finger motion, full finger workspace, full controllability, comfortable usage, and hand size variation support. When the sensing and the force reflecting device are unconnected to each other, interaction forces caused by misalignment between human joints and device joints, as presented in Section. IV-B, are avoided. The positions of the

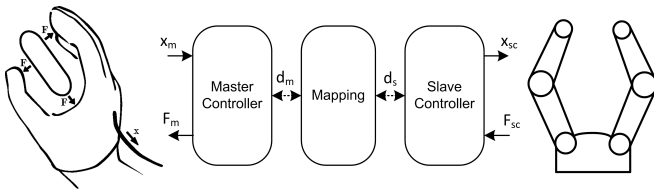


Fig. 8. Separated sensor and actuator paths implemented by a sensing glove offering full slave controllability and a force reflective device offering limited but sufficient slave observability.

x_m : sensed motion from sensing master device, x_{sc} : motion exerted by slave, F_m : force reflected to hand by the force reflecting master device, F_{sc} : force sensed by the slave, d_m : data stream between master controller and mapping, d_s : data stream between slave controller and mapping.

contact points between the two devices, however, need to be known in order to calculate the required force feedback. To investigate the feasibility of this end-point estimation, an exploratory experiment may be performed.

The force reflective device should be able to provide force feedback in a limited set of fundamental motions, as discussed in VII-B1. The four required force reflective motions are: a) index finger - palm opposition, b) grouped fingers (3-5) - palm opposition, c) index finger - thumb pad opposition, and possibly d) grouped fingers (3-5) - thumb pad opposition. This set was selected to support the most occurring grasps in EVA tool use and takes the operation of distinct relevant slave devices into account.

The set of force reflective motions will be provided using a minimum number of actuated DOFs. It may be sufficient to provide force feedback only along the direction normal between the two opposing virtual fingers. It should be considered that the orientation of the normal depends on the exact finger postures and thus the low number of actuated DOFs might limit the possibility to exert force specifically along the desired direction. In this case, it might be sufficient to display the projection of the force along the direction normal. This is supported considering the JND of force direction, as addressed in Section. IV-A, that allows variation of force direction which the operator is unable to perceive. Optimization techniques as presented in Section. VII-D might be usable to keep the variation of force direction below the JND for the whole movement range and for a range of hand sizes. It might be possible to combine this with optimization of structural transparency as addressed in the same section.

As discussed in Section. IV-B, a haptic device produces reaction force at the grounding position, what can result in an unnatural sensation. In order to turn this disadvantage into an advantage, it is proposed to place the grounding position such that the reaction force is exploited for useful force reflection. For all force reflective motions, forces can be exerted on the index and grouped fingers (3-5), while the force ground can be positioned on the thumb for the motions with pad opposition and on the palm for the motions with palm opposition. In this approach, force feedback is provided to the virtual fingers in opposition, rather than to all physical fingers. This lowers the required number of actuated DOFs since not all fingers, but only the four distinct force reflective motions require actuation.

Since only few actuators are required, they can be placed close to the position of force exertion. This keeps the transmissions short and simple, and undesired mechanical effects to a minimum. A simple structure can have high stiffness to enable display of stiff object interactions with good resolution. A stiff structure can also have a high mechanical bandwidth that does not limit the control bandwidth and allows for display of soft object interactions.

IX. CONCLUSION

It was hypothesized that a haptic hand master with low structural complexity, which is designed for good usability and high device performance, can increase user performance.

While the hypothesis can not yet be answered, a low-complexity device design with good usability and high device performance is promising when its features have been designed to specifically apply to the intended usage of the device.

The following conclusions can be drawn: 1) Analysis of intended tasks and required grasps, relevant slave devices, existing master devices and human factors, provides guidelines for the reduction of DOFs in a haptic hand master device. 2) Force coupling effects in the human fingers, termed enslaving effects, should be taken into account when considering the essential motions to provide with force feedback. 3) Sensor-actuator asymmetry, implemented as separate unconnected sensing and force reflecting devices, can provide full controllability and limited but sufficient observability. 4) Feedback forces may be reflected using a limited number of actuated DOFs that are optimized for workspace and direction of force reflection.

REFERENCES

- [1] A. Schiele and G. Hirzinger, "A new generation of ergonomic exoskeletons - the high-performance x-arm-2 for space robotics telepresence," in *IEEE/RSJ Int. Conf. Intelligent Robots and Systems*, San Francisco, California, Sept 2011, pp. 25–30, (to appear).
- [2] R. Hui, A. Ouellet, A. Wang, P. Kry, S. Williams, G. Vukovich, and W. Peruzzini, "Mechanisms for haptic feedback," in *IEEE Int. Conf. Robotics and Automation*, vol. 2, May 1995, pp. 2138–2143.
- [3] N. Lii, Z. Chen, B. Pleintinger, C. Borst, G. Hirzinger, and A. Schiele, "Exploratory investigations of the effects of visual and low performance force feedback on robotic hand grasping performance for space teleoperations," *IEEE/RSJ Int. Conf. Intelligent Robots and Systems.*, 2010.
- [4] *Man-Systems Integration Standards, Volume I*, NASA-STD-3000, Rev. B, Jul 1995.
- [5] F. Didot, P. Schoonejans, E. Pensavalle, G. Battistoni, S. Ferraris, S. Estable, T. Huesling, and EADS-Astrium, "Eurobot underwater model: System overview, test results & outlook," in *i-SAIRAS 02*, 2008.
- [6] R. Ambrose, S. Askew, W. Bluethmann, and M. Diftler, "Humanoids designed to do work," in *IEEE/RAS Int. Conf. Humanoid Robots*, 2001, pp. 173–180.
- [7] *EVA Tools and Equipment Reference Book*, NASA-TM-109350, Rev. B, Nov 1993.
- [8] J. R. Napier, "The prehensile movements of the human hand," *The Journal of Bone and Joint Surgery*, vol. 38-B, no. 4, pp. 902–913, 1956.
- [9] M. Cutkosky, "On grasp choice, grasp models, and the design of hands for manufacturing tasks," *IEEE Transactions on Robotics and Automation*, vol. 5, no. 3, pp. 269–279, 1989.
- [10] T. Iberall, "The nature of human prehension: Three dextrous hands in one," in *IEEE Int. Conf. Robotics and Automation.*, vol. 4, 1987, pp. 396–401.
- [11] D. Akin, C. Carignan, and A. Foster, "Development of a four-fingered dexterous robot end effector for space operations," in *IEEE Int. Conf. Robotics and Automation ICRA*, vol. 3, 2002, pp. 2302–2308.

- [12] M. Arbib, T. Iberall, and D. Lyons, "Coordinated control program for movements of the hand," *Experimental Brain Research*, 1985.
- [13] M. R. Cutkosky and R. D. Howe, *Human grasp choice and robotic grasp analysis*. New York, NY, USA: Springer-Verlag New York, Inc., 1990, pp. 5–31.
- [14] T. Iberall, G. Bingham, and M. A. Arbib, "Opposition space as a structuring concept for the analysis of skilled hand movements," *Experimental Brain Research Series*, vol. 15, pp. 158–173, 1986.
- [15] S. Michaud, M. Dominguez, U. Nguyen, L. Zago, and S. Droz, "Eurobot end-effectors," in *8th ESA Workshop on Advanced Space Technologies for Robotics and Automation ASTRA*. ESTEC, Nov 2004.
- [16] W. T. Townsend, "The barretthand grasper programmably flexible part handling and assembly," *Industrial Robot*, vol. 27, no. 3, pp. 181–188, 2000.
- [17] *SDH - Gripping Hands - 3-Finger Gripping Hand*, SCHUNK.
- [18] A. Wedler, M. Chalon, A. Baumann, W. Bertleff, A. Beyer, R. Burger, J. Butterfass, M. Grebenstein, R. Bruber, F. Hacker, E. Kraemer, K. Landzettel, M. Maier, H. Sedlmayr, N. Seitz, F. Wappler, B. Willberg, T. Wimboeck, F. Didot, and G. Hirzinger, "Dlrs space qualifiable multi-fingered dexhand," in *Symp. Advanced Space Technologies in Robotics and Automation ASTRA*, 2011, (to appear).
- [19] H. Liu, K. Wu, P. Meusel, N. Seitz, G. Hirzinger, M. Jin, Y. Liu, S. Fan, T. Lan, and Z. Chen, "Multisensory five-finger dexterous hand: The dlr/hit hand ii," in *IEEE/RSJ Int. Conf. Intelligent Robots and Systems IROS*, 2008, pp. 3692–3697.
- [20] Barretthand. Barrett Technology Inc. (retrieved: 24-04-2011).
- [21] Schunk dexterous hand. SCHUNK. (checked: 24-04-2011).
- [22] K. An, L. Askew, and E. Chao, "Biomechanics and functional assessment of upper extremities," *Trends in Ergonomics/Human Factors III*, Elsevier Science Publishers, B.V., 1986.
- [23] P. Sutter, J. Iatridis, and N. Thakor, "Response to reflected-force feedback to fingers in teleoperations," in *Proc. NASA Conf. Space Telerobotics*, 1989.
- [24] H. Tan, M. Srinivasan, B. Eberman, and B. Cheng, "Human factors for the design of force-reflecting haptic interfaces," in *Proc. Haptic Interfaces for Virtual Environment and Teleoperator Systems, ASME/IMECE, DSC:55-1, Design of Haptic Icons 363*, 1994.
- [25] X. Pang, H. Tan, and N. Durlach, "Manual discrimination of force using active finger motion," *Attention, Perception, and Psychophysics*, vol. 49, pp. 531–540, 1991.
- [26] K. B. Shimoga, "A survey of perceptual feedback issues in dexterous telemanipulation. i. finger force feedback," in *Proc. IEEE Virtual Reality Annual International Symposium*, 1993, pp. 263–270.
- [27] F. Barbagli, K. Salisbury, C. Ho, C. Spence, and H. Z. Tan, "Haptic discrimination of force direction and the influence of visual information," *ACM Trans. Applied Perception*, vol. 3, Apr 2006.
- [28] G. Burdea, *Force and Touch Feedback for Virtual Reality*. New York, NY, USA: John Wiley & Sons, Inc., 1996.
- [29] A. Schiele and F. van der Helm, "Influence of attachment pressure and kinematic configuration on phri with wearable robots," in *Applied Bionics and Biomechanics*, vol. 6, 2009, pp. 157–173.
- [30] G. Gil-Gómez and A. Schiele, "A kinematic model of the human hand truly based on its functional anatomy," ESA/ESTEC, ESA Internal Report, 2006.
- [31] I. Kapandji, *The Physiology of the Joints. Volume I: Upper Limb*. Churchill Livingstone, 1982.
- [32] A. Freivalds, *Biomechanics of the Upper Limbs: Mechanics, Modeling and Musculoskeletal Injuries*. CRC Press, 2004.
- [33] E. Chao, K. An, W. Cooney, and R. Linscheid, *Biomechanics of the Hand: A Basic Research Study*. World Scientific, 1989.
- [34] T. Brooks, "Telerobotic response requirements," in *IEEE Int. Conf. Systems, Man and Cybernetics*, Nov 1990, pp. 113–120.
- [35] S. Jeon and S. Choi, "Stiffness modulation for haptic augmented reality: Extension to 3d interaction," in *Proc. IEEE Haptics Symposium*, 2010, pp. 273–280.
- [36] S. Li, "Perception of individual finger forces during multi-finger force production tasks," *Neuroscience Letters*, vol. 409, no. 3, pp. 239–243, 2006.
- [37] S. Li and C. Leonard, "The effect of enslaving on perception of finger forces," *Experimental Brain Research*, vol. 172, pp. 301–309, 2006.
- [38] S. L. Kilbreath and S. C. Gandevia, "Limited independent flexion of the thumb and fingers in human subjects," *The Journal of Physiology*, vol. 479, no. Pt 3, pp. 487–497, 1994.
- [39] —, "Independent digit control: Failure to partition perceived heaviness of weights lifted by digits of the human hand," *The Journal of Physiology*, vol. 442, no. 1, pp. 585–599, 1991.
- [40] W.-H. Park, C. Leonard, and S. Li, "Finger force perception during ipsilateral and contralateral force matching tasks," *Experimental Brain Research*, vol. 189, pp. 301–310, 2008.
- [41] F. Gao, M. L. Latash, and V. M. Zatsiorsky, "Control of finger force direction in the flexion-extension plane," *Experimental Brain Research*, vol. 161, pp. 307–315, 2005.
- [42] M. Bouzit, G. Burdea, G. Popescu, and R. Boian, "The rutgers master ii - new design force-feedback glove," *IEEE/ASME Transactions on Mechatronics*, vol. 7, no. 2, pp. 256–263, 2002.
- [43] J. Wang, J. Li, Y. Zhang, and S. Wang, "Design of an exoskeleton for index finger rehabilitation," in *Proc. IEEE Annual Int. Conf. Engineering in Medicine and Biology Society EMBC*, 2009, pp. 5957–5960.
- [44] M. DiCiccio, L. Lucas, and Y. Matsuoka, "Comparison of control strategies for an emg controlled orthotic exoskeleton for the hand," in *Proc. IEEE Int. Conf. Robotics and Automation ICRA*, vol. 2, 2004, pp. 1622–1627.
- [45] M. F. Rotella, K. E. Reuther, C. L. Hofmann, E. B. Hage, and B. F. BuSha, "An orthotic hand-assistive exoskeleton for actuated pinch and grasp," in *IEEE 35th Annual Northeast Bioengineering Conference*, 2009, pp. 1–2.
- [46] M. Turner, R. Findley, W. Griffin, and M. Cutkosky, "Development and testing of a telemanipulation system with arm and hand motion," in *Proc. ASME Int. Mechanical Engineering Congress and Exposition, Dynamic Systems and Controls*, vol. 69, 2000, pp. 1057–1063.
- [47] B. Eberman and B. An, "Exos research on force reflecting controllers," *SPIE Telemanipulator Technology*, vol. 1833, pp. 9–19, 1992.
- [48] A. Chiri, F. Giovacchini, N. Vitiello, E. Cattin, S. Roccella, F. Vecchi, and M. C. Carrozza, "Handexos: Towards an exoskeleton device for the rehabilitation of the hand," in *Proc. IEEE/RSJ Int. Conf. Intelligent Robots and Systems IROS*, 2009, pp. 1106–1111.
- [49] Y. Fu, P. Wang, S. Wang, H. Liu, and F. Zhang, "Design and development of a portable exoskeleton based cpm machine for rehabilitation of hand injuries," in *Proc. IEEE Int. Conf. Robotics and Biomimetics ROBIO*, 2007, pp. 1476–1481.
- [50] J. Iqbal, N. Tsagarakis, A. Fiorilla, and D. Caldwell, "A portable rehabilitation device for the hand," in *IEEE Int. Conf. Engineering in Medicine and Biology Society EMBC*, Sept 2010, pp. 3694–3697.
- [51] T. T. Worsnopp, M. A. Peshkin, J. E. Colgate, and D. G. Kamper, "An actuated finger exoskeleton for hand rehabilitation following stroke," in *Proc. IEEE 10th Int. Conf. Rehabilitation Robotics ICORR*, 2007, pp. 896–901.
- [52] M. Lelieveld, T. Maeno, and T. Tomiyama, "Design and development of two concepts for a 4 dof portable haptic interface with active and passive multi-point force feedback for the index finger," in *ASME International Design Engineering Technical Conference & Computers and Information in Engineering Conference*, 2006.
- [53] S. Nakagawara, H. Kajimoto, N. Kawakami, S. Tachi, and I. Kawabuchi, "An encounter-type multi-fingered master hand using circuitous joints," in *IEEE Int. Conf. Robotics and Automation ICRA*, Apr 2005, pp. 2667–2672.
- [54] Y. Hasegawa, Y. Mikami, K. Watanabe, and Y. Sankai, "Five-fingered assistive hand with mechanical compliance of human finger," in *IEEE Int. Conf. Robotics and Automation ICRA*, 2008, pp. 718–724.
- [55] M. Fontana, A. Dettori, F. Salsedo, and M. Bergamasco, "Mechanical design of a novel hand exoskeleton for accurate force displaying," in *Proc. IEEE Int. Conf. Robotics and Automation ICRA*. Piscataway, NJ, USA: IEEE Press, 2009, pp. 2599–2604.
- [56] B. L. Shields, J. A. Main, S. W. Peterson, and A. M. Strauss, "An anthropomorphic hand exoskeleton to prevent astronaut hand fatigue during extravehicular activities," *IEEE Transactions on Systems, Man and Cybernetics, Part A: Systems and Humans*, vol. 27, no. 5, pp. 668–673, 1997.
- [57] C. Tzafestas and P. Coiffet, "Computing optimal forces for generalised kinesthetic feedback on the human hand during virtual grasping and manipulation," in *Proc. IEEE Int. Conf. Robotics and Automation*, vol. 1, 1997, pp. 118–123.
- [58] A. Wege and A. Zimmermann, "Electromyography sensor based control for a hand exoskeleton," in *Proc. IEEE Int. Conf. Robotics and Biomimetics ROBIO*, 2007, pp. 1470–1475.
- [59] B. Choi and H. Choi, "Skk hand master-hand exoskeleton driven by ultrasonic motors," in *IEEE/RSJ Int. Conf. Intelligent Robots and Systems IROS*, vol. 2, 2000, pp. 1131–1136 vol.2.
- [60] H. Fang, Z. Xie, and H. Liu, "An exoskeleton master hand for controlling dlr/hit hand," in *IEEE/RSJ Int. Conf. Intelligent Robots and Systems IROS*, 2009, pp. 3703–3708.

- [61] P. Stergiopoulos, P. Fuchs, and C. Lurgeau, "Design of a 2-finger hand exoskeleton for vr grasping simulation," in *EuroHaptics, Trinity College, Dublin and Media Lab Europe*, 2003.
- [62] S. Ito, H. Kawasaki, Y. Ishigure, M. Natsume, T. Mouri, and Y. Nishimoto, "A design of fine motion assist equipment for disabled hand in robotic rehabilitation system," *Journal of the Franklin Institute*, vol. 348, no. 1, pp. 79 – 89, 2011, mechatronics and its Applications.
- [63] T. Endo, H. Kawasaki, T. Mouri, Y. Doi, T. Yoshida, Y. Ishigure, H. Shimomura, M. Matsumura, and K. Koketsu, "Five-fingered haptic interface robot: Hiro iii," in *Proc. and Symp. EuroHaptics conf. Haptic Interfaces for Virtual Environment and Teleoperator Systems. World Haptics 2009. Third Joint*, 2009, pp. 458–463.
- [64] M. Monroy, M. Oyarzabal, M. Ferre, A. Campos, and J. Barrio, "Masterfinger: Multi-finger haptic interface for collaborative environments," in *Proc. 6th Int. Conf. Haptics: Perception, Devices and Scenarios EuroHaptics '08*. Berlin, Heidelberg: Springer-Verlag, 2008, pp. 411–419.
- [65] J. Iqbal, N. Tsagarakis, A. Fiorilla, and D. Caldwell, "Design requirements of a hand exoskeleton robotic device," in *14th IASTED Int. Conf. Robotics and Applications RA*, Cambridge, Massachusetts, 2009, p. 4451.
- [66] V. Hayward and O. Astley, "Performance measures for haptic interfaces," in *7th Int. Symp. Robotics Research*. Springer Verlag, 1996, pp. 195–207.
- [67] F. Barbagli and K. Salisbury, "The effect of sensor/actuator asymmetries in haptic interfaces," in *Proc. 11th Symp. Haptic Interfaces for Virtual Environment and Teleoperator Systems HAPTICS*, 2003, pp. 140–147.
- [68] K. Vlachos and E. Papadopoulos, "Transparency maximization methodology for haptic devices," *IEEE/ASME Transactions on Mechatronics*, vol. 11, no. 3, pp. 249–255, 2006.
- [69] *CyberGlove*[®], Immersion Corporation, Sep 2001, datasheet.

ANNEX A - MASTER DEVICE COMPARISON

This annex contains the data gathered during a comparison of 24 hand master devices. Part of this data is presented and explained into more detail in Section. V.

A. Device Appearance and Functionality

The following properties concerning the appearance and the basic functionalities of devices are shown in Table. X.

1) *Device Type*: {palmar, dorsal, end-point} The palmar and dorsal devices reside in the palm, respectively on the back of the hand and are body grounded. An end-point type device is only connected to the hand in the force-feedback positions and it is grounded to the environment.

2) *Device Ground*: {body, environment} A device is body grounded when the reaction force is exerted onto the human operator. A device is environment grounded when the reaction force is exerted on the environment, possibly via a mechanical structure.

3) *Body Coverage*: {fingertips, fingers, hand, forearm} A device can cover or enclose one or multiple parts of the human body, making these parts inaccessible and/or unusable for other devices.

4) *Actuator Placement*: {body, external, on end-point device} Actuators can be mounted on the body of the human operator, on external setups, or on end-point devices.

5) *Feedback Positions*: {all phalanges, distal phalanges, medial phalanges, multiple positions} Force can be fed-back at one or multiple positions per finger. For many devices each finger is treated equally in the sense that force is fed-back to the same phalange(s) of each finger. In some devices forces are fed-back at distinct positions per finger or finger group, this is termed 'multiple positions'.

6) *Actuated Motions*: {flexion, extension, abduction, adduction} The motions of each hand and finger joint can be actuated in either one or two directions. Depending on the joint, motion is in the flexion-extension plane or ab-adduction plane.

B. Finger Force Feedback

The following properties concerning force feedback to the fingers are shown in Table. XI.

1) *Nr. of Supported Fingers*: The number of fingers to which one or multiple forces are fed-back.

2) *Expandable up to*: Some devices are modular, allowing to expand the number of supported fingers.

3) *Separated Fingers*: The fingers that are separately provided with force feedback.

4) *Grouped Fingers*: The fingers that are grouped and thus are provided with force feedback as a group.

5) *Nr. of Actuated DOFs*: The number of DOFs that are actuated to provided force feedback.

6) *Nr. of Actuators*: The number of actuators that is used to provide all DOFs with force feedback. There are cases in which two actuators were used in order to actuate either direction of a single DOF.

7) *Average Number of Actuators per Supported Finger*: The ratio between the number of actuators and the number of supported fingers.

8) *Actuator Type*: The reported actuator type.

9) *Actuator Series*: More specific actuator series information.

C. Device Performance

The following properties concerning device performance are shown in Table. XII.

1) *Finger Joint Workspace*: The joint workspace per finger DOF has been specified via two different methods: 1. as a range with upper and lower limits of extension-flexion and ab-adduction, and 2. as a range without absolute limits.

2) *Maximal Force*: The maximal feedback force to the fingertip or the maximal (cable) force from the actuator.

3) *Force Resolution*: The resolution of the feedback force. It should be noted that the reported values are force sampling resolutions, which might not represent the actual force feedback resolution at the device tip.

4) *Control Bandwidth*: The control loop bandwidth.

D. Device Performance Continued

Device performance properties as presented in Table. XII are relevant, yet rarely reported.

1) *Reflected Inertia*: The reflected motor inertia as experienced at each joint.

2) *Mechanical Bandwidth at Fingertip*: The bandwidth of the feedback force at the fingertip.

3) *Static Friction Torque*: The static friction torque as experienced at each joint.

4) *Resonance Frequency*: System resonance frequency.

TABLE X
DEVICE APPEARANCE AND FUNCTIONALITY

Source	Device Type	Device Ground	Body Coverage	Actuator Placement	Feedback Positions	Actuated Motions
[43]	dorsal	body	fingers, hand	external	all phalanges	flex-extension
[44]	dorsal	body	fingers, hand, forearm	body	all phalanges	flexion
[45]	dorsal	body	fingers, hand, forearm	body	multiple positions	flexion
[46]	dorsal	body	fingers, hand	external	distal phalanges	extension
[42]	palmar	body	fingers, palm	body	distal phalanges	flexion (-extension?)
[60]	end-point	environment	fingers, hand	on end-point device	distal phalanges	flex-extension
[61]	end-point	environment	fingers, hand	on end-point device	distal phalanges	flex-extension
[47]	dorsal	body	fingers, hand, forearm	body	multiple positions	flex-extension
[62]	end-point	environment	fingers, hand, forearm	on end-point device	distal & medial phalanges	flex-extension, ab-adduction
[48]	dorsal	body	fingers, hand, forearm	body	all phalanges	flex-extension
[49]	dorsal	body	fingers, hand, forearm	body	all phalanges	flex-extension, ab-adduction
[63]	end-point	environment	fingertips	on end-point device	distal phalanges	flex-extension, ab-adduction
[50]	dorsal	body	fingers, hand, forearm	body	medial phalanges	flex-extension
[64]	end-point	environment	fingertips	on end-point device	distal phalanges	flex-extension, ab-adduction
[51]	dorsal	body	fingers, hand, forearm	body	all phalanges	flex-extension
[52] a.	dorsal	body	fingers, hand, forearm	body	all phalanges	extension
[52] b.	dorsal	body	fingers, hand, forearm	body	all phalanges	braking ¹
[53]	dorsal	body	fingers, hand	body	distal phalanges	extension
[54]	dorsal	body	fingers, hand, forearm	body	?multiple positions	flexion
[55]	dorsal	body	fingers, hand	body	distal phalanges	flex-extension, ab-adduction
[56]	dorsal	body	fingers, hand, forearm	body	distal & medial phalanges	flexion
[57]	dorsal	body	fingers, hand	external	all phalanges	?
[58]	dorsal	body	fingers, hand	external	all phalanges	flex-extension, ab-adduction
[59]	dorsal	body	fingers, hand	body	all phalanges	flex-extension

¹This device uses actuators to prevent motion rather than to actuate motion.

TABLE XI
FINGER FORCE FEEDBACK

Source	Nr. of Supported Fingers	Expandable up to	Separate Fingers	Grouped Fingers	Nr. of Actuated DOFs	Nr. of Actuators	Average Nr. of Actuators per Supported Finger	Actuator Type	Actuator Series
[43]	1	—	{2}	—	4	4	4	DC-motor	—
[44]	1	—	{2}	—	2	2	2	pneumatic	—
[45]	5	—	{1,2}	{3-5}	4	4	0.8	motor	—
[46]	5	—	{1-5}	—	5	5	1	motor	—
[42]	4	—	{1-4}	—	4	4	1	pneumatic	—
[60]	5	—	{1-5}	—	5	5	1	BLDC motor	Maxon EC-20
[61]	2	—	{1,2}	—	2	2	1	DC-motor	—
[47]	1	—	{2}	—	2	2	2	DC-motor	—
[62]	5	—	{1-5}	—	16	16	3.2	motor	—
[48]	1	5	{2}	—	1	1	1	DC-motor	—
[49]	1	5	{2}	—	2	2	2	DC-motor	—
[63]	5	—	{1-5}	—	15	15	3	DC-servomotor	—
[50]	2	—	{1,2}	—	2	2	1	DC-motor	Maxon RE-25
[64]	2	3	{1,2}	—	6	6	3	DC-motor	Maxon RE-25
[51]	1	—	{2}	—	3	6	6	brushless DC-motor	—
[52] a.	1	—	{2}	—	4	4	4	brushless DC-motor	Maxon EC-22
[52] b.	1	—	{2}	—	4	4	4	brushless DC-motor	Maxon EC-22
[53]	5	—	{1-5}	—	5	5	1	DC-motor	Faulhaber 1724 SR
[54]	5	—	{1,2}	{3-5}	8	8	1.6	DC-motor	—
[55]	2	—	{1,2}	—	6	6	3	DC-motor	—
[56]	4	—	{2,3}	{4,5}	3	3	0.75	DC-motor	—
[57]	5	—	{1-5}	—	14?	14?	2.8?	DC disk motor	—
[58]	5	—	{1-5}	—	20	20	4	DC-motor	—
[59]	2	—	{1,2}	—	5?	5?	2.5?	ultrasonic motor	—

Sets of fingers are defined using the following format: {x,y} meaning finger x and y. {x-z} meaning finger x up to z including every finger in between.

TABLE XII
DEVICE PERFORMANCE

Source	Finger Joint Workspace [deg]				Maximal Force [N]		Force	Control
	MCP1	MCP2	PIP	DIP	Fingertip	Actuator	Resolution	Bandwidth [Hz]
[43]	0 - 65	—	0 - 80	0 - 73	—	—	—	—
[44]	—	—	—	—	—	44.5	—	—
[45]	—	—	—	—	8	—	—	—
[46]	—	—	—	—	—	12	12 bit	1000
[42]	—	—	45	45	16	—	12 bit	300
[60]	—	—	—	—	8	—	—	—
[61]	—	—	—	—	—	—	—	—
[47]	—	90 deg flexion	—	—	3.3	—	—	—
[62]	—	—	—	—	—	—	—	—
[48]	—	—	—	—	—	—	—	—
[49]	90	20	110	70	—	—	—	—
[63]	—	—	—	—	3.6	—	—	—
[50]	—	—	—	—	45	—	—	—
[64]	—	—	—	—	—	—	—	—
[51]	-15 - 75	—	0 - 90	0 - 75	—	—	—	—
[52] a.	—	—	—	—	—	—	—	—
[52] b.	—	—	—	—	—	—	—	—
[53]	—	—	—	—	8	—	—	—
[54]	—	—	—	—	5	—	—	—
[55]	—	—	—	—	—	—	—	—
[56]	—	—	—	—	—	—	—	—
[57]	—	—	—	—	—	—	—	—
[58]	—	—	—	—	—	—	—	—
[59]	—	—	—	—	—	—	—	100

TABLE XIII
DEVICE PERFORMANCE CONTINUED

Source	Property
	<u>Reflected Inertia [$kg\ m^2$]</u>
[51]	MCP1 0.783 PIP 0.039 DIP 0.006
	<u>Mechanical Bandwidth at Fingertip</u>
[46]	~40 Hz
[42]	10 Hz
	<u>Static Friction Torque</u>
[47]	7 mNm at index finger MCP and PIP
	<u>Resonance Frequency</u>
[46]	~20 Hz

